



TECHNISCHE
UNIVERSITÄT
WIEN

DISSERTATION

**First Fuel Tests at a Novel 100 kW_{th}
Dual Fluidized Bed Steam Gasification Pilot Plant**

ausgeführt zum Zwecke der Erlangung des akademischen Grades eines Doktors der
technischen Wissenschaften unter der Leitung von

Univ. Prof. Dipl.-Ing. Dr. techn. Hermann Hofbauer
und der Mitbetreuung von
Ing. Dipl.-Ing. Dr. techn. Stefan Müller

am

Institut für Verfahrenstechnik,
Umwelttechnik und Technischen Biowissenschaften
der Technischen Universität Wien

eingereicht an der Technischen Universität Wien,
Fakultät für Maschinenwesen und Betriebswissenschaften

von

Dipl.-Ing. Maximilian Kolbitsch
Matrikelnummer 0527147

Wien, am 13.06.2016

.....
Maximilian Kolbitsch

Imprint

© Maximilian Kolbitsch, 2016
maximilian.kolbitsch@tuwien.ac.at,
Institute of Chemical Engineering,
Vienna University of Technology,
Getreidemarkt 9/166,
1060 Vienna,
Austria,

Dissertation:
"First Fuel Tests at a Novel
100 kW_{th} Dual Fluidized Bed
Steam Gasification Pilot Plant"

ISBN: 978-3-9503671-0-2

Printed by: Institute of Chemical Engineering in Vienna, Mai 15th, 2016

Reproduction requires color print

Distributed by:

Vienna University of Technology,
Institute of Chemical Engineering,
Getreidemarkt 9/166,
1060 Vienna
Austria
+43 1 58801 166335
www.vt.tuwien.ac.at

Doctoral Committee

Supervisor:	Univ.Prof. Dipl.-Ing. Dr.techn. Hermann Hofbauer Institut für Verfahrenstechnik, Technische Universität Wien
External reviewer:	Ao.Univ.Prof. Dipl.-Ing. Dr.techn. Andreas Werner Institut für Energietechnik und Thermodynamik, Technische Universität Wien
Chairman:	Ao.Univ.Prof. Dipl.-Ing. Dr.techn. Franz Winter Institut für Verfahrenstechnik, Technische Universität Wien
Date of oral defense:	13.06.2016

Abstract

The dual fluidized bed (DFB) steam gasification technology presents a promising technology to produce electricity, heat, and fuels out of biogenic feedstock materials. The state of the art of DFB steam gasification, as implemented in a pilot plant at the TU Wien, showed a number of shortcomings. These include an inflexibility in gasifying different feedstock materials, limited carbon and water conversion, limited tar reduction in the product gas, limited cold gas efficiencies, and slow fuel power changes.

In this thesis, we describe a novel pilot plant that was designed and assembled at the TU Wien to address these shortcomings. To evaluate the novel pilot plant, we conduct experiments with different feedstock and bed materials at various operating parameters. To interpret the measurements and produce key figures, we use the simulation tool IPSEpro.

The evaluation section discusses experiments conducted for this thesis using variations of feedstock materials (wood pellets, sugarcane bagasse pellets, and exhausted olive pomace pellets), gasification temperature, steam to fuel ratio, fuel power, and bed material (fresh olivine as well as a mixture of fresh olivine and limestone).

Additionally, we examine the performance of tar reforming and tar cracking processes along the counter-current column of the novel gasification reactor. To estimate the improvements of the novel pilot plant, we provide a detailed discussion of a comparative experiment conducted on the novel and classical DFB plant.

One of the main contributions of this thesis is that the novel DFB pilot plant is able to gasify all evaluated feedstock materials successfully. This includes problematic feedstock materials, such as exhausted olive pomace that results in GC-MS tar contents comparable to those of wood pellets.

When comparing the two DFB pilot plants, we measure similar product gas compositions and tar contents while reaching significantly higher water conversion rates, carbon conversion rates as well as cold gas efficiencies on the novel plant. Furthermore, we measure similar overall cold gas efficiencies (up to 61%), despite significantly higher heat losses

at the novel DFB pilot plant influencing the overall cold gas efficiency negatively.

Another contribution of the thesis is that we show that the counter-current column of the novel gasification reactor reforms tar species successfully at even low gasification temperatures. Mainly heterocyclic and light aromatics with functional groups (such as oxygen or methane) show significant reductions along the column. We examine heavy PAHs and show that they are very stable and show only slight reductions.

Kurzfassung

Die Zweibett-Wirbelschicht-Dampfvergasungstechnologie stellt eine vielversprechende Technologie dar, um Strom, Wärme und Treibstoffe aus biogenen Brennstoffen zu erzeugen. Die konventionelle Zweibett-Wirbelschicht-Dampfvergasungsversuchsanlage, die an der TU Wien errichtet wurde, zeigte eine Anzahl an Mängeln. Dabei handelt es sich um eine begrenzte Brennstoffflexibilität, einen geringen Kohlenstoffumsatz, einen geringen Wasserumsatz, einer begrenzten Teerreduktion im Produktgas, geringen Kaltgaswirkungsgrade, sowie eines trägen Verhaltens bei Brennstofflastwechsel.

Um eine Verbesserung der Performance in diesen Bereichen zu realisieren wurde eine neuartige Zweibett-Wirbelschicht-Dampfvergasungsversuchsanlage ausgelegt, konstruiert und im Technikum der TU Wien gebaut. Um die neue Versuchsanlage zu bewerten wurden Versuche mit unterschiedlichen Brennstoffen und Bettmaterialien bei variablen Versuchsparametern durchgeführt. Unterstützend zur Versuchsauswertung wurde das Simulationstool IPSEpro herangezogen um Messwerte zu evaluieren und relevante Kennzahlen zu berechnen.

Im Versuchsteil werden Variationen des Brennstoffes (Holzpellets, Zuckerrohrbagassepellets und Oliventresterpellets), des Dampf/Brennstoffverhältnis, der Vergasungstemperatur, der Brennstoffleistung und des Bettmaterials (frisches Olivin und eine Mischung aus frischem Olivin und Kalkstein) untersucht.

Zusätzlich wurde die neuartige Gegenstromkolonne des Vergasungsreaktors im Zuge eines Versuches mit Holzpellets auf Teerabbauprozesse untersucht. Um das Potential der neuen Versuchsanlage abschätzen zu können wurden die Ergebnisse vergleichbarer Versuchsläufe beider Versuchsanlagen miteinander verglichen und im Detail diskutiert.

Im Zuge dieser Dissertation konnte gezeigt werden, dass die neue Versuchsanlage alle untersuchten Brennstoffe erfolgreich vergasen konnte. Sogar Oliventrester als problematischer Brennstoff konnte geringe GC-MS Teerwerte, im Bereich von Holzpellets, erreichen.

Beim Vergleich beider Versuchsanlagen wurden keine relevanten Unterschiede in der

Produktgaszusammensetzung, wie auch im Teergehalt des Produktgases gemessen. Ein deutlich höherer Wasserumsatz, Kohlenstoffumsatz, wie auch Kaltgaswirkungsgrad konnte bei der neuen Versuchsanlage erreicht werden. Ähnliche Kaltgaswirkungsgrade im Bereich von 61% konnten erreicht werden, obwohl die neue Versuchsanlage signifikant höhere Wärmeverluste aufweist.

Des Weiteren konnte gezeigt werden, dass die Gegenstromkolonne des neuen Vergasungsreaktors den Gehalt spezieller Teerbestandteile, sogar bei geringen Vergasungstemperaturen, erfolgreich reduzieren konnte. Speziell heterozyklische und leichte aromatische Verbindungen mit funktionellen Gruppen (wie z.B. Sauerstoff oder Methan) zeigten signifikante Reduktionen. Schwere polyaromatische Kohlenwasserstoffe (PAH) konnten hingegen kaum gespalten werden und zeigten daher nur minimale Reduktionen.

Acknowledgements

In course of this work main contents of following research projects were summarized:

- G-Volution II: "Zweibettwirbelschicht Biomasse-Dampfvergaser der zweiten Generation - II".
- ERBA: "Erzeugung eines Produktgases aus Biomassereformierung mit selektiver CO₂-Abtrennung zur Einspeisung in das Koks- oder Hüttengasnetz eines integrierten Hüttenwerkes".
- ERBA II: "Optimierung von Sorption Enhanced Reforming" zur Verbesserung der CO₂-Bilanz in der Roheisenerzeugung mittels Biomasse".
- Phenolive: "Revalorization of wet olive pomace through polyphenol extraction and subsequent steam gasification".
- SCB2GAS: "Vergasungsversuche mit Zuckerrohrbagasse (Sugar cane bagasse)".

The results have been reached with financial support from the Austrian "Klima & Energiefonds" supported by the Austrian "Forschungsförderungsgesellschaft" (FFG).

"The research leading to the results of the project "Phenolive" has received funding from the European Union's Seventh Framework Programme managed by REA Research Executive Agency under grant agreement nr FP7-SME-2013-605357".

Special thanks are also given to all project partners listed below:

- Voestalpine Stahl GmbH, Linz,
- Voestalpine Stahl Donawitz GmbH,
- Fitroleum Biochemicals GmbH,
- Tecon Engineering GmbH, and
- all industrial partners of the project "Phenolive".

Danksagung

Ich möchte mich auf diesem Weg bei meinem Betreuer Hermann Hofbauer bedanken, eine Dissertation am Institut für Verfahrenstechnik, Umwelttechnik und Technische Biowissenschaften verfassen zu dürfen.

Ein besonderer Dank für die regelmäßige und konstruktive Kritik meiner Dissertation gilt auch meinem Zweitbetreuer Stefan Müller.

Dankbar für technisch relevante Diskussionen bin ich besonders Johannes Schmid und Fritz Kirnbauer, die mir stets mit Rat und Tat zur Seite standen und so neue Aspekte in meine Arbeit einfließen ließen. Danke Johannes, dass du dir auch während des Anlagenbaus und der Projekteinreichungen stets Zeit für mich genommen hast.

Ein herzliches Dankeschön an meine Arbeitskollegen Mario Schmalzl, Michi Weitzer, Martin Hammerschmidt, Florian Benedikt, Josef Fuchs, Dalibor Martinovic, Matthias Kuba, Stefan Hemetsberger, Stephan Kraft und Roland Diem für eine tolle Zeit in und außerhalb der Arbeit.

Daneben gilt mein Dank auch Michael Kraussler, Philipp und Clemens Kolbitsch, für das Korrekturlesen dieser Arbeit.

Nicht zuletzt gebührt meinen Eltern Dank. Meinem Papa, mit dem ich über fachspezifische Inhalte diskutieren konnte und meiner Mama, die mich bei Notwendigkeit stets in allen Belangen, besonders auch emotional, unterstützt hat.

Auch meiner Freundin Karin will ich für ihre ruhige und verständnisvolle Art während den zeitintensiven Monaten meiner Dissertationabgabe danken.

List of Publications

Conference paper

- Kolbitsch, M., Schmid, J.C., Diem, R., Müller, S., Hofbauer, H., 2014, "Influence of Fuel Feeding Position on Sorption Enhanced Reforming in a Dual Fluid Gasifier" in: Proceedings of the 11th International Conference on Circulating Fluidized Bed Technology (CFB11), 14-17 May 2014, Beijing, China

Conference abstract

- Kolbitsch, M., Müller, S., Hofbauer, H., 2014, "State of the Art Measurement Methods for the Evaluation of Experiments with Dual Fluid Gasification Systems", in: Proc. of the 4th International Symposium on Gasification and its Applications (iSGA-4), 2-5 Sept. 2014, Vienna, Austria

Final reports

- Schmid, J.C., Müller, S., Kolbitsch, M., Tesch, W., Hofbauer, H., 2015, "G-VOLUTION II: Zweibettwirbelschicht Biomasse-Dampfvergaser der zweiten Generation - II", Neue Energien 2020, publizierbarer Endbericht, Klima und Energiefonds managed by FFG, TU Wien, 30.01.2015
- Schmid, J.C., Kolbitsch, M., Fuchs, J., Benedikt, F., Müller, S., Hofbauer, H., 2016, "Steam gasification of exhausted olive pomace with a dual fluidized bed pilot plant at TU Wien", technical report for the EU-project PHENOLIVE, Institute of Chemical Engineering, TU Wien, 29.02.2016

Contents

Imprint	ii
Doctoral Committee	iii
Abstract	iv
Kurzfassung	vi
Acknowledgements	viii
Danksagung	ix
List of Publications	x
1 Introduction	1
1.1 Background	1
1.2 Aim and Scope of this Work	3
2 Theoretical Background	4
2.1 Gasification of Biomass	4
2.1.1 Processes and Sub-Processes of Steam Gasification of Biomass	4
2.1.2 The Process of Dual Fluidized Bed Steam Gasification	6
2.1.3 Basic Chemical Reactions	7
2.1.4 Ash Related Challenges	9
2.2 Tar - Definition and Classification	11
2.3 Fundamentals of Fluidization Technology	14
2.3.1 Characterization of Particles	18
2.3.2 Basic Fluiddynamic Equations for Fluidized Bed Systems	19
2.3.3 Mapping of Fluidization Regimes	23

3	Classical Dual Fluidized Bed Steam Gasification System	25
3.1	Assembly and Functionality of the Classical Dual Fluidized Bed Steam Gasification Pilot Plant	25
3.2	Experimental Results of the Classical DFB Pilot Plant	29
3.3	Overview of Key Findings of the Classical DFB Pilot Plant	33
4	Methodology - Novel Dual Fluidized Bed Steam Gasification Pilot Plant	35
4.1	Cold Flow Model of the Novel DFB Pilot Plant	35
4.2	IPSEpro - Simulation Software for Modelling and Calculation of Processes .	40
4.3	Novel Dual Fluidized Bed Steam Gasification Pilot Plant	42
4.4	Measuring Equipment of the Novel DFB Pilot Plant	51
4.5	Solid Sampling	57
5	Experimental Results at the Novel DFB Pilot Plant	59
5.1	Evaluation of the Fluid Dynamics of the Novel DFB Pilot Plant	64
5.2	Commissioning Test Run at the Novel DFB Pilot Plant	67
5.3	Temperature Variation	70
5.4	Fuel Power Variation	75
5.5	Bed Material Variation	78
5.6	Steam to Fuel Ratio Variation	81
5.7	Tar Reduction and Change of the Product Gas Composition along the Counter-Current Column of the Novel DFB Pilot Plant	84
5.8	Feedstock Variation	91
5.8.1	Wood Pellets	92
5.8.2	Sugarcane Bagasse	94
5.8.3	Exhausted Olive Pomace	98
5.9	Evaluation of the Performance of the Novel DFB Test Plant	103
5.10	Overview of Experimental Results	106
6	Conclusion and Outlook	111
	Nomenclature	XIII
	List of Figures	XIX
	List of Tables	XXIV
	References	XXVII
	Appendix A	XXXVIII

1 Introduction

1.1 Background

Growing prosperity in society leads to rising consumption of commodities and energy. The combustion of fossil fuels influences the amount of greenhouse gases released into the atmosphere. Figure 1.1 depicts the persistent increase of emitted carbon dioxide that has taken place in the last 150 years. The United Nations Framework Convention on

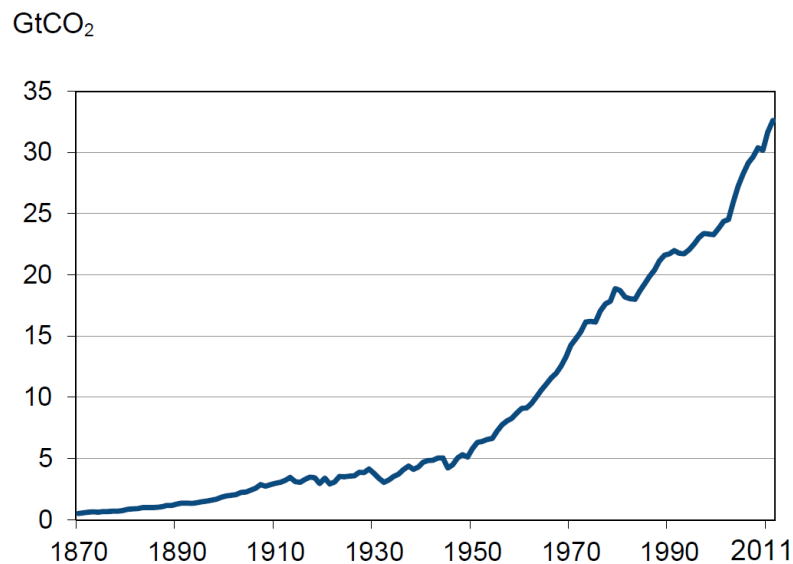


Figure 1.1: Progress of emitted carbon dioxide has increased exponentially in the last 70 years [8]

Climate Change, 21st Conference of the Parties (COP21) was held in Paris in 2015 with the objective to reduce greenhouse gases (GHG). The agreement of all United Nation members includes a commitment "to keep the rise in global temperatures well below 2°C to pre-industrial times, while striving to limit them even more, to 1.5°C" [104]. To do so, the energy system has to be changed dramatically towards sustainable energy technologies.

Already today, renewable energy resources like wind, sun, and water show great potential

to compensate a relevant share of fossil fuels as primary energy source. Biomass as an unique resource is the only renewable carbon carrier which allows to produce carbon based fuels via synthesis to substitute oil and gas. The use of biogenic fuels shows further advantages in order to reduce GHG, since biomass fuels can be classified as carbon dioxide neutral [61]. To substantiate the change in energy systems over the last 170 years, Figure 1.2 illustrates the history of primary energy sources.

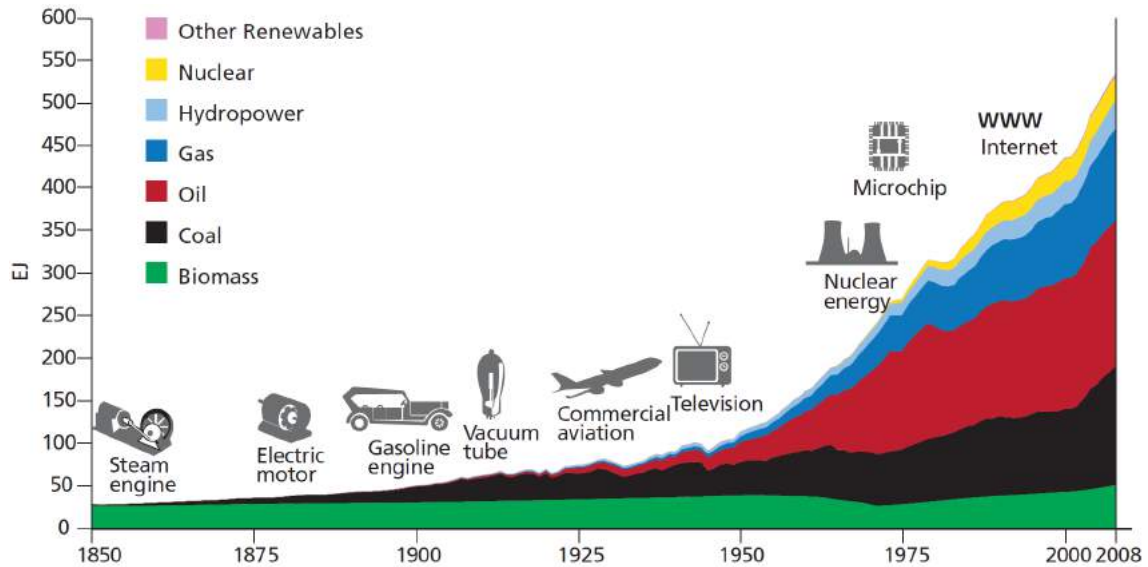


Figure 1.2: History of primary energy use along the last 170 years until now [61]

The gasification process presents a promising technology to generate a medium calorific product gas using a wide range of feedstock. The utilization of biogenic fuels and biogenic residues allow to provide a carbon dioxide neutral energy source. The TU Wien (TUW) is doing researches in the field of dual fluidized bed steam gasification since 1993 [45]. This process is able to convert a solid feedstock into storable, secondary energy carriers. However, recent research activities focus on limitations in terms of tar reduction, especially for challenging feedstock like biogenic residues. Therefore, a novel Dual Fluidized Bed (DFB) steam gasification pilot plant was designed and assembled to improve the performance of the gasifier. A better performance should aim the follows:

- a better feedstock flexibility,
- an increased carbon and water conversion,
- a better conversion of tar components,
- increased cold gas efficiencies, and

- a better product gas quality in terms of unconverted carbon, tar and ash contents.

The generated product gas, which mainly consist of hydrogen, carbon monoxide, carbon dioxide, and methane can further be used for either the operation of gas engines or for further processing to synthesis products [43].

The question "does the new concept of the novel DFB pilot plant show a better performance compared to prior pilot plant" has not been answered and will be done throughout this work.

1.2 Aim and Scope of this Work

The main aim of the present work is to find an answer on the described research question. Therefore, a detailed literature research of the fundamentals of gasification were conducted. While the classical DFB steam gasification pilot plant was dismantled, the novel DFB steam gasification pilot plant was constructed and assembled. Furthermore, first fuel test have been conducted at the novel DFB pilot plant, discussed and published throughout this thesis.

In the first part of this work a theoretical background of the fundamentals of gasification is described. Furthermore, the prior DFB steam gasification pilot plant is briefly explained to clarify main differences in the design and assembly. A detailed explanation of the novel DFB steam gasification pilot plant is included. In the last step, carried out experiments are described and results presented to find an answer to the key question asked at the beginning.

2 Theoretical Background

2.1 Gasification of Biomass

In this section an overview of the fundamental principles of gasification is presented. This involves a brief overview of the process of gasification itself, the stages of conversion as well as basic chemical reactions occurring during the process.

2.1.1 Processes and Sub-Processes of Steam Gasification of Biomass

A gasification process can be defined as the conversion of solid feedstock into product gases. The aim is to convert carbonaceous materials into a high-value gas for further utilizations like for example the combustion in a gas engine or for further synthesis applications. A detailed overview of the utilization of the product gas can be found in Bridgwater et al. [6]. Since steam was used as gasification agent for all test runs conducted, only the process of steam gasification will be discussed in detail. Figure 2.1 presents the thermo-chemical process a solid particle has to go through while being gasified. This process can be divided into three phases, depending on the temperature level and the presence of oxygen. Phase one describes the process of heating up and drying of the biomass, where temperatures up to 150 - 200°C are reached. The second phase is defined as pyrolytic decomposition/devolatilization taking place at temperatures up to 500°C. In this step irreversible changes in structure of biomass occur where the volatiles (H_2 , CO , CO_2 , CH_4 , H_2O and hydrocarbons¹) and solid residues (mainly consisting of char and ash²) are released. The amount of volatile matters reaches values in the range of 80wt.-% and only 20wt.-% remain as char. The ratio of volatiles and solids is very important regarding the design of a gasifier [6]. During the third phase volatiles and residual char get converted in the presence of steam, at temperatures between 800 - 900°C. All these steps are mainly endothermic and ,therefore, require heat [28, 43]. Depending on the favourable

¹Hydrocarbons occurring during devolatilization are referred to as primary tar

²Solid residues remaining after pyrolysis are referred to as pyrolytic char or residual char

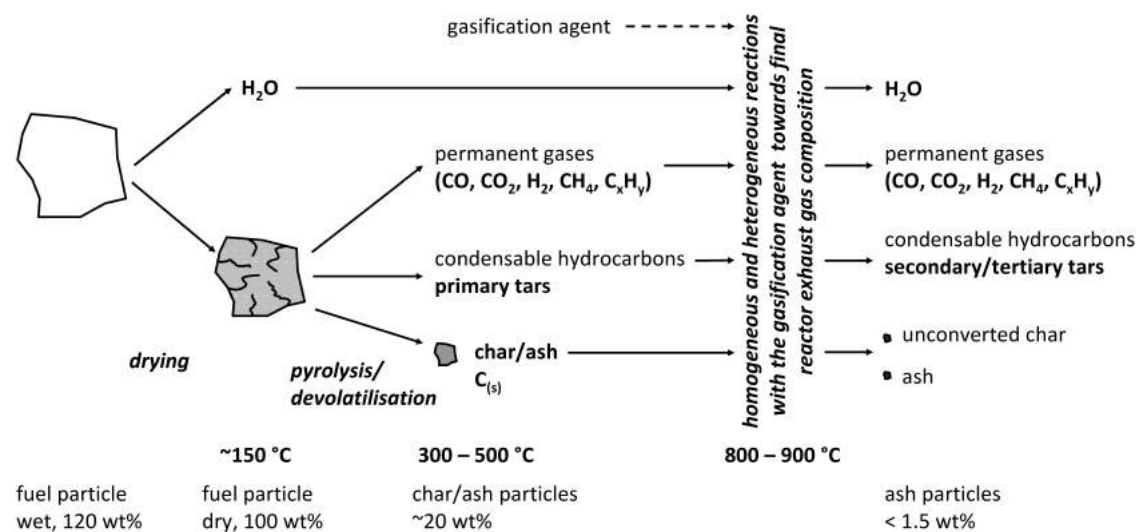


Figure 2.1: Overview of conversion steps for a single particle, adopted from [43]

product gas composition and the design of the gasifier, air, steam, oxygen, carbon dioxide or a mixture of these agents can be used as gasification agents [28]. Figure 2.2 pictures a simple overview of biomass gasification processes linked with ranges for product gas compositions and ranges of heating values achieved with different gasification agents. Air is a very common gasification agent due to its availability and low complexity in gasifier designs. However, it has to be taken into account that using air leads to dilution of the product gas with nitrogen, resulting in a low calorific heating value of the product gas of around $4 - 6\text{ MJ}/\text{Nm}^3_{db}$ [25]. In this case an **autothermal** gasification is realized, where the heat for the overall endothermic gasification reaction is provided by the partial oxidation of the biomass with oxygen in the gasification reactor itself. To avoid a dilution of the product gas with nitrogen a mixture of oxygen and steam as gasification agent can be used to realize a nitrogen free product gas, but requires an air separation unit which ends up in higher plant costs. Heating values up to $10 - 12\text{ MJ}/\text{Nm}^3_{db}$ can be realized. On the contrary, the heat can be produced indirectly and provided by an **allothermal** process. This means that the energy for the endothermic gasification reaction is supplied by a (circulating) heat carrier or a heat exchanger. Both require a more extensive design. As gasification agent, steam or carbon dioxide is typically used. Steam as gasification agent can lead to product gas heating values up to $12 - 14\text{ MJ}/\text{Nm}^3_{db}$ [74]. Further information about the basics of gasification processes were published by [6, 28, 40, 74].

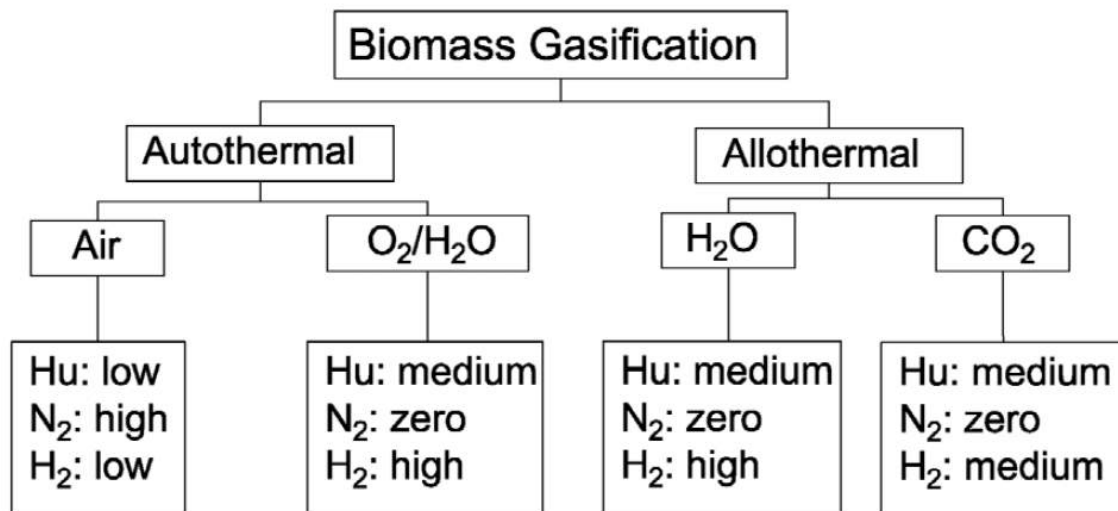


Figure 2.2: Schematic description of gasification processes using different gasification agents from [11] based on data from [6]

2.1.2 The Process of Dual Fluidized Bed Steam Gasification

The Dual Fluidized Bed steam gasification process is based on an allothermal gasification process where a circulating bed material provides energy for the overall endothermic gasification process. The system itself consists of two reactors, the gasification reactor (GR) and the combustion reactor (CR) as shown in Figure 2.3. The gasification takes place

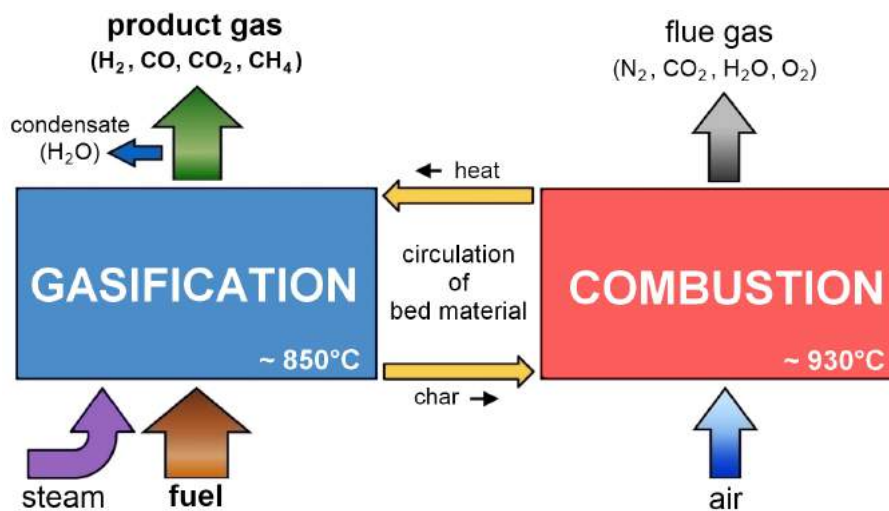


Figure 2.3: Illustration of the basic principle of a Dual Fluidized Bed steam gasification System, modified from [84]

at temperatures of about 850°C, whereas the combustion occurs at higher temperatures of about 930°C. The feedstock is conveyed into the gasification reactor where drying, de-

volatilization and gasification of the feedstock occurs. The product gas is formed by the aid of steam as gasification agent and circulating hot bed material. Hot bed material (e.g. olivine, dolomite, limestone) provides energy for the gasification process and is fed together with residual matter (char) back into the combustion reactor. Since combustion using air as combustion agent occurs at higher temperatures, the bed material gets heated up and transported along the combustion reactor back into the gasification reactor.

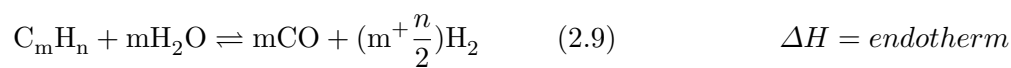
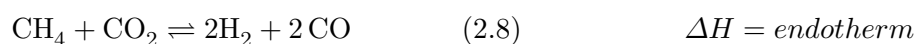
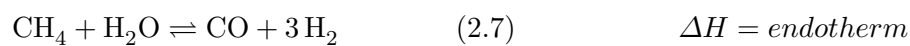
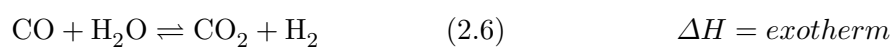
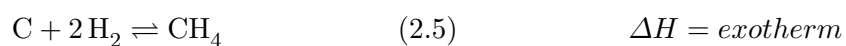
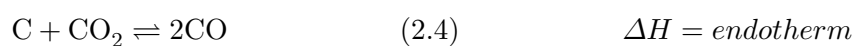
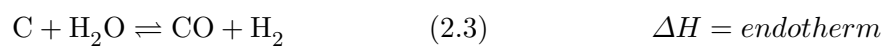
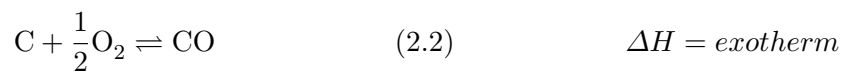
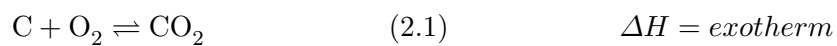
A DFB steam gasifier produces two separate gas streams. A flue gas and a product gas stream, where the product gas consists of a high hydrogen content. DFB steam gasification is mainly applied due its benefits listed below:

- good intermixing of particles (carbonaceous and inorganic matter) and the gas phase,
- excellent heat transfer,
- use of catalytic active bed material,
- production of nitrogen free product gas, and
- good preconditions for the utilization of a wide range of different feedstock types.

2.1.3 Basic Chemical Reactions

The overall process of gasification is dominated by several homogeneous and heterogeneous reactions occurring in a gasification reactor simultaneously. Pyrolysis char remaining after devolatilisation is gasified by using a gaseous agent according to Eq.(2.1) to (2.5). Main solid-gas (heterogeneous) reactions are listed, where Eq.(2.1) shows the reaction for the oxidation of carbon, Eq.(2.2) the partial oxidation of carbon, Eq.(2.3) the heterogeneous water-gas reaction, Eq.(2.4) the Boudouard reaction and Eq.(2.5) the methanation reaction.

Gaseous substances mainly resulting from pyrolysis can be converted by gas-gas reactions according to Eq.(2.6) to (2.9). Eq.(2.6) shows the water-gas-shift reaction, Eq.(2.7) the methane reforming reaction, Eq.(2.8) the dry reforming reaction and Eq.(2.9) the reaction for the general reaction for steam gasification (reforming of hydrocarbons) [28, 29, 36]. All equations are listed below:



To describe the direction of a reaction, an equilibrium constant (K_p) can be introduced as

$$K_p = \frac{(p_C)^{\nu_C} \cdot (p_D)^{\nu_D}}{(p_A)^{\nu_A} \cdot (p_B)^{\nu_B}} \quad (2.10)$$

, when a reaction is described as shown in Eq. 2.11 [43].



Values for K_p greater 1 indicate a reaction towards the side of products, lower 1 towards the side of the reactants. In the case the equilibrium constant reaches a value of 1 the reaction is in an equilibrium state, where equal forth and back reactions occur. Further information about the meaning of K_p and its calculation can be found in Stephan [93]. Depending on the dominating conditions of pressure and temperature, different positions of equilibrium can be reached. Typical values for equilibriums during biomass steam gasification over temperatures at 1 bar can be found in Koppatz [43]. Kaltschmitt et al. [28] present values for K_p for rising temperatures at 1 and 20 bar. Since equilibrium conditions can not be expected during gasification, catalytic substances are used to enhance equilibrium conditions [36]. The novel Dual Fluidized Bed steam gasifier is operated at atmospheric conditions. Basics of the behaviour of reactions at pressurized atmosphere can be found in [40].

2.1.4 Ash Related Challenges

The elemental composition of the feedstock, especially inorganic matter in its ash can lead to technological challenges, like deposit formation and bed material agglomeration in gasification and combustion processes. Generally, two different types of deposit formation can be named. These are fouling and slagging. Fouling occurs in cooler sections of boilers due to the formation of ash deposits, whereas slagging takes place in high temperature boiler sections due to molten ash. Both phenomena inhibit the heat transfer, reduce the efficiency and can lead to mechanical damage of the boiler. Bed material agglomeration in fluidized bed systems can deteriorate the heat transfer in the bubbling bed. The agglomeration of sticky ash particles and sand/bed materials may even lead to defluidization and total collapse of the bubbling bed [7, 13, 55, 65, 94]. For more detailed information about ash-related challenges, the author refers to [27, 94].

Main ash-forming elements are described by Bostroem et al. [5] as to be silicon (Si), calcium (Ca), magnesium (Mg), potassium (K), sodium (Na), phosphor (P), sulphur (S), chlorine (Cl), and aluminium (Al) in a certain degree of simplification. Ash components mainly consist of alkali and alkali earth sulphates, silicates, chlorides, phosphates, and

carbonates.

Bostroem et al. divided ash-related reactions into two categories, primary and secondary ash transformation reactions. Thus, primary reactions were split into basic and acidic compounds as listed in Table 2.1 with its reactivity descending from top to bottom. A schematic overview of main secondary ash-forming reactions for combustion of biomass are shown in Table 2.2. These reactions may vary for gasification processes but also for different physical conditions, such as temperature, residence time, and flue gas speed [5].

Table 2.1: Basic and acidic compounds of primary ash transformation reactions by Bostroem et al. [5]

basic compounds	acidic compounds
KOH (l,g) (K ₂ O)	P ₂ O ₅ (g)
NaOH (l,g) (Na ₂ O)	SO ₂ (g)/SO ₃ (g)
CaO (s)	SiO ₂ (s)
MgO (s)	HCl (g) (Cl ₂)
H ₂ O (g)	CO ₂ (g)
	H ₂ O (g)

s...solid, l...liquid, g...gaseous

Table 2.2: Survey of secondary ash-forming reactions modified from Bostroem et al. [5]

reaction	comments
$P_2O_5(g) + 2KOH(g) \longleftrightarrow 2KPO_3(l,g) + H_2O(g)$	fast reaction
$SO_3(g) + 2KOH(g) \longleftrightarrow K_2SO_4(l,g) + H_2O(g)$	fast reaction
$HCl(g) + KOH(g) \longleftrightarrow KCl(g,l) + H_2O(g)$	fast reaction
$SiO_2(s) + 2KOH(g) \longleftrightarrow K_2SiO_3(l) + H_2O(g)$	medium fast reaction
$CO_2(g) + 2KOH(g) \longleftrightarrow K_2CO_3(l,g) + H_2O(g)$	fast reaction
$P_2O_5(g) + 3CaO(s) \longleftrightarrow Ca_3P_2O_8(s)$	medium fast reaction
$SO_3(g) + CaO(s) \longleftrightarrow CaSO_4(s,l)$	medium fast reaction
$2HCl(g) + CaO(s) \longleftrightarrow CaCl_2(g,l) + H_2O(g)$	medium fast reaction
$SiO_2(s) + CaO(s) \longleftrightarrow CaSiO_3(s)$	slow reaction
$CO_2(g) + CaO(s) \longleftrightarrow CaCO_3(s)$	medium fast reaction
$K_2SiO_3(l) + CaO(s) \longleftrightarrow K-Ca-silicate(l)$	rather slow reaction

s...solid, l...liquid, g...gaseous

Results of Bostroem et al. [5] demonstrate forming of K-silicate systems with eutectic temperatures as low as 600°C. Thus, these systems form larger agglomerated particles that may promote slag formation and result in bed agglomeration. However, reducing slagging tendencies can be gained by adding specific amounts of Ca, Mg, and alkali silicates, since K can be driven out of the melt and melting temperatures can be increased.

Results obtained from Teixeira et al. [94] showed appearing sintering phenomena, when ash with high amounts of K and Si occurs. The presence of Ca forms potassium-calcium-silicates increasing the sintering temperature and decreasing the unwanted property of the feedstocks tendency to cause bed agglomeration. Research was made adding several additives to investigate the melting behavior of the ash during combustion of woody fuels. Oehman et al. [64] showed great influence adding additives like limestone and kaolin. The addition of limestone showed to have a distinct effect on slag formation, showing significant lower formation phenomena, whereas kaolin showed only slight reduced impacts. Hupa [27] published low impact of alkali sulphates such as Na_2SO_4 and K_2SO_4 on corrosion. The addition of alkali chlorides, however, changed melting temperatures of fly ashes dramatically [94]. As described in literature, phosphor influences bed agglomeration phenomena. Since woody biomass is low in phosphor concentration the influence of phosphor can be considered to be low. Phosphor enhances the adhesion of potassium and therefore increases the tendency to cause bed agglomeration of sticky ash particles and material [21, 22]. Further studies regarding deposit formation using coal and biomass as feedstock were conducted and can be found in [10, 15, 57, 63, 69, 72].

2.2 Tar - Definition and Classification

Numerous publications report definitions for the term tar. According to the tar guideline tar is defined as follows: "Generic (unspecific) term of entity of all organic compounds present in the producer gas excluding hydrocarbons (C1 through C6). Benzene is not included in this definition" [62]. Figure 2.4 shows representative GC-MS tar compounds typically occurring from biomass gasification with increasing molar mass from small to large. Since melting point and boiling point are essential properties of tar compounds, both are listed there. Figure 2.5 demonstrates gravimetric tar compounds.

Beside the number of different definitions, several classifications exist in literature. In the course of this work, two major classifications are named. Milne et al. [58] suggested to classify tar as primary, secondary and tertiary tar (according to rising temperature and residence time), whereas the latter is divided into alkyl tertiary products and condensed tertiary products.

- Primary tar: mainly consists of oxygenated compounds
- Secondary tar: characterized by phenolics and olefins

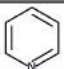
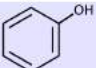
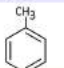
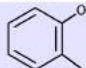
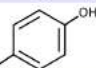
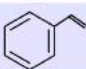
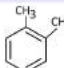
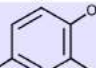
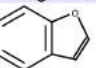
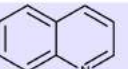
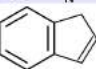

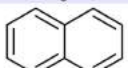
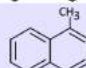
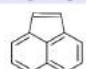

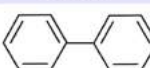

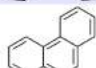
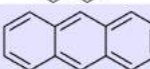
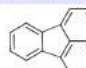
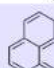
Species	Structure	Chemical formula	Molar mass [g/mol]	Melting point [°C]	Boiling point [°C]
Pyridine		C ₅ H ₅ N	79.10	-	116
Phenol		C ₆ H ₆ O	94.11	43	182
Toluene		C ₇ H ₈	92.14	-	111
2-Methylphenol		C ₇ H ₈ O	108.18	31	191
4-Methylphenol		C ₇ H ₈ O	108.18	35	202
Styrene		C ₈ H ₈	104.15	-30.63	145.2
Xylene		C ₈ H ₁₀	106.16	-	144
2,4-Dimethylphenol		C ₈ H ₁₀ O	122.17	26	211.5
Benzofuran		C ₈ H ₆ O	118.14	-	173-174
Quinoline		C ₉ H ₇ N	129.16	-	238
1H-indene		C ₉ H ₈	116.16	-1.8	182.6
Dibenzofuran		C ₁₂ H ₈ O	168.19	86-87	287
Naphthalene		C ₁₀ H ₈	128.17	80.2	218
1-Methylnaphthalene		C ₁₁ H ₁₀	142.20	-30.5	245
Acenaphthylene		C ₁₂ H ₈	152.20	92	265
Acenaphthene		C ₁₂ H ₁₀	154.21	96.2	279
Biphenyl		C ₁₂ H ₁₀	154.21	70.72	255
Fluorene		C ₁₃ H ₁₀	166.22	115	298
Phenanthrene		C ₁₄ H ₁₀	178.23	101	340
Anthracene		C ₁₄ H ₁₀	178.23	218	340
Fluoranthene		C ₁₆ H ₁₀	202.26	110	384
Pyrene		C ₁₆ H ₁₀	202.26	150	393

Figure 2.4: Typical GC-MS tar compounds in product gas of biomass gasification, modified from Koppatz [43]

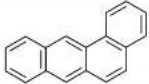
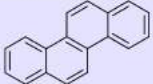
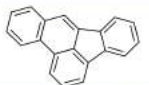
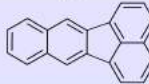
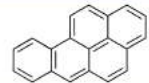

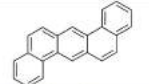
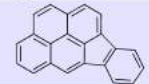
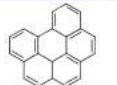
Species	Structure	Chemical formula	Molar mass [g/mol]	Boiling point [$^{\circ}$ C]
Benzo[a]anthracene		$C_{18}H_{12}$	228	438
Chrysene		$C_{18}H_{12}$	228	448
Benzo[e]acephenanthrylene		$C_{20}H_{12}$	252	357
Benzo[k]fluoranthene		$C_{20}H_{12}$	252	480
Benzo[a]pyrene		$C_{20}H_{12}$	252	495
Perylene		$C_{20}H_{12}$	252	497
Dibenzo[a,h]anthracene		$C_{22}H_{14}$	278	524
Indeno[1,2,3-cd]pyrene		$C_{22}H_{14}$	276	536
Benzo[g,h,i]perylene		$C_{22}H_{12}$	276	542

Figure 2.5: Illustration of main properties of gravimetric tar, from [59]

- Alkyl tertiary tar: methyl derivatives of aromatics
- Condensed tertiary tar: Polyaromatic hydrocarbons (PAH) including benzene, naphthalene, acenaphylen, anthracene/phenanthrene, pyrene

A further classification for a better evaluation of tar compounds was conducted by the Energy Research Centre of the Netherlands (ECN) as well as Li and Suzuki. The classification of ECN is demonstrated in Table 2.3. Tar is distinguished into gravimetric and GC-MS tar. A detailed description of both terms can be found in Chapter 4.4.

Table 2.3: Tar classification from the Energy Research Centre of the Netherlands (ECN) [12]

Tar class	Class name	Property	Representative compounds
1	GC-undetectable	very heavy tars cannot be detected by GC	gravimetric tar
2	heterocyclic aromatics	tar containing hetero atoms, highly water soluble compounds	pyridine, phenol, cresol, quinoline
3	light aromatic (1 ring)	usually light hydrocarbons with single ring; do not pose a problem regarding condensability and solubility	toluene, xylene, styrene
4	light PAH compounds (2-3 rings)	two and three rings compounds, condense at low temperature even at very low concentration	naphthalene, methylnaphthalene, biphenyl, acenaphthylene, fluorene, acenaphthene phenanthrene, anthracene
5	heavy PAH compounds (4-7 rings)	larger than three rings, these components condense at high-temperature at low concentration	fluoranthene, pyrene, benzoanthracene, perylene chrysene, dibenzoanthracene, benzoperylene benzofluoranthene, benzopyrene, indenopyrene

2.3 Fundamentals of Fluidization Technology

This chapter should give a brief overview about the fundamentals of fluidized bed technologies referring to numerous publications by Bi and Grace [4], Fan and Zhu [14], Geldart [17], Hofbauer [24], Knowlton [41], Kuuni and Levenspiel [52], Lim et al. [54], Saxena and Vogel [76], and Schmid [78]. Besides the definition of hydrodynamic regimes occurring in fluidized beds and main equations for the calculation of fluiddynamic numbers a classification of particles will be presented. Figure 2.6 presents main regimes occurring.

A fixed bed occurs when an upward gas stream below the minimum fluidization velocity (U_{mf}) passes a bulk of solid particles. Therefore, the bulk of solid inventory remains in a "solid-like" state.

When increasing the velocity of the gas stream slightly above U_{mf} , solid particles get transferred from a "solid-like" state into a "fluid-like" state and bubbles begin to occur. In this case the upward flow and the frictional forces between particles counterbalance the weight of the particles and the bed slightly expands.

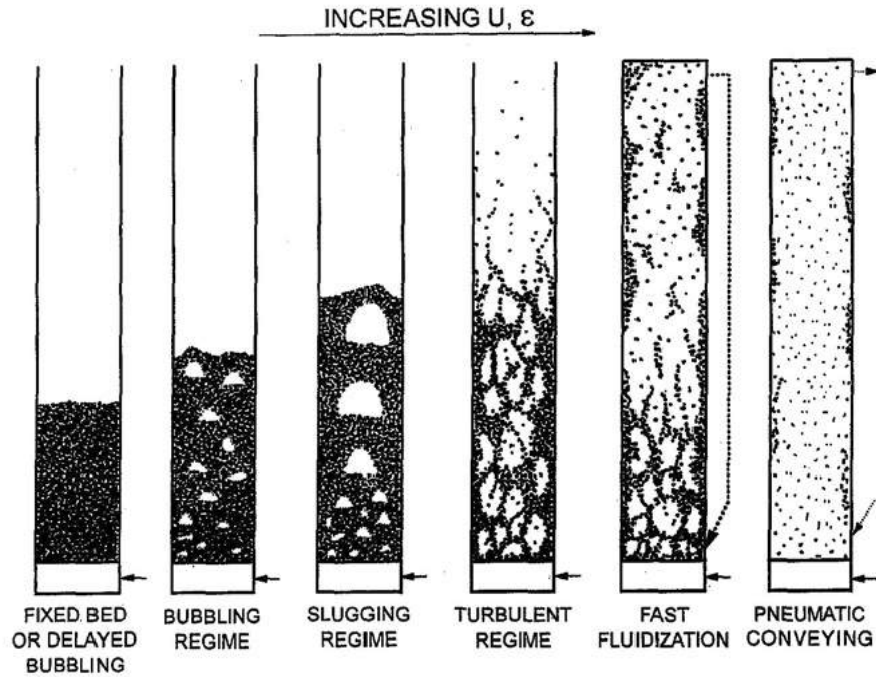


Figure 2.6: Scheme of hydrodynamic regimes in a fluidized bed, adapted from [54]

By a further increase of the velocity below the terminal velocity (U_t), a more extensive expansion of the bed and a significant higher hold up of solids can be observed. This turbulent regime shows turbulent motions of solid clusters instead of bubbles at lower velocities. U_t is the terminal velocity of a single particle. In contrast to U_t , the critical velocity (U_c) defines the onset of turbulent fluidization of a bulk of particles.

When increasing the velocity to U_{se} solids start to move upwards and are carried out of the column. This state where entrainment of particles occurs is called fast fluidization.

At an even higher gas velocity clearly above U_{se} pneumatic conveying takes place. Columns showing the two last-mentioned regimes have to be equipped with separator units to feed the solids back into the bed in order to obtain a steady state operation.

Slugging represents a fluidizing regime indicated by bubbles with a diameter nearly equal to diameters of the vessel moving upwards along the column. Slugging mainly appears when a good intermixing of solids can not be realized. This regime can mainly be observed at a small column diameter and should be prevented.

In Figure 2.7 the distribution of the fraction of solids ε_S along the height at different regimes of fluidized beds is shown. ε_f presents the void particle volume fraction. All regimes show a different distribution of solids along the height. Bubbling beds have a dense

fraction distribution in the bed and a lean distribution in the area above the bubbling bed, the so called freeboard. Only very small particles can reach the freeboard at a bubbling bed regime. At higher velocities more and more particles are carried out from the bed to the freeboard by the gas stream showing a turbulent fluidization. The higher the velocity, the more solids are spread over the height.

At pneumatic conveying the fraction of solids is very low along the height due to very high velocities in the column. Further literature was published by Avidan and Yerushalmi [3].

The onset of fluidization regimes are dependent on several particle properties [43] and gas properties such as:

- particle density,
- particle diameter,
- particle shape,
- particle distribution,
- gas temperature,
- gas density, and
- gas viscosity

To give proper statements about fluidization regimes occurring, fluidization numbers and ratios are inevitable. The **ratios** U/U_{mf} and U/U_t are key figures for a first classification of the fluidization regime, where U_t classifies the terminal velocity of a single particle. The following statements about fluidization ratios and velocities can be made where all statements depend on a defined particle size and Ar-number, respectively:

- if the ratio U/U_{mf} is below one a fixed bed is present; if it is above one, fluidization commences,
- $U_{mf} < U < U_c \rightarrow$ a bubbling fluidization regime is present,
- $U_c < U < U_{se} \rightarrow$ a turbulent fluidization regime is present and
- $U > U_{se} \rightarrow$ a fast fluidization regime is present.

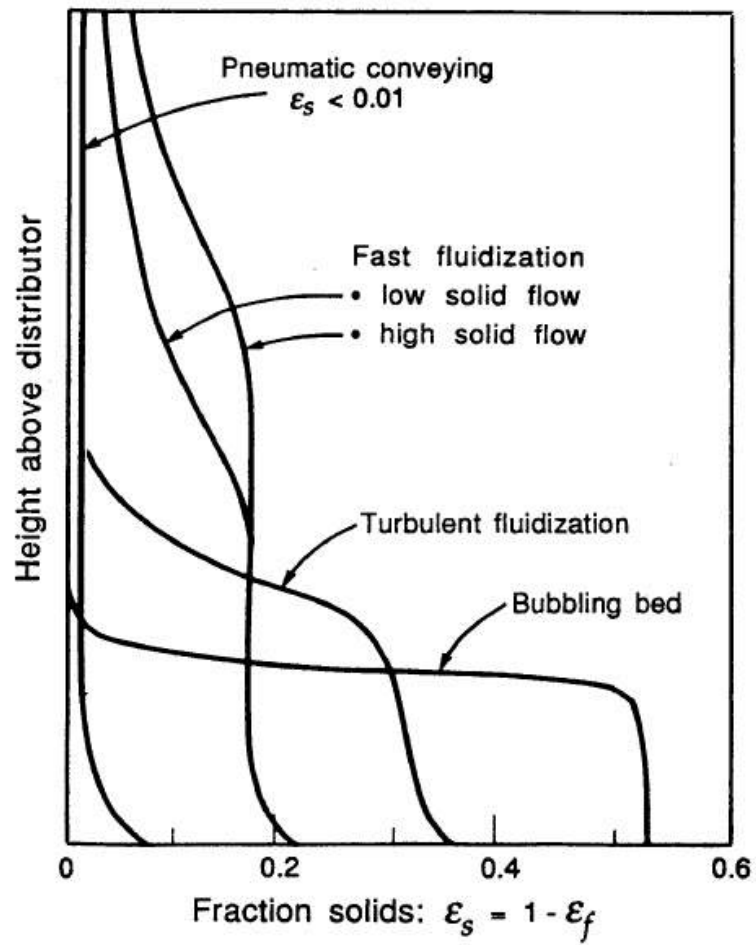


Figure 2.7: Profile of the fraction of solids along the height of the distributor, adapted from [52]

2.3.1 Characterization of Particles

Solid particles fluidized by gases can be distinguished and classified in four different groups. Geldart showed that particles can be characterized by density difference of particles and fluid stream ($\rho_p - \rho_f$) as well as mean particle size d_p . However, it should be noted that other variables beside the ones mentioned above can influence the particle properties and therefore the Geldart classification: 1) different gas species, 2) process temperature, and 3) pressure just to name some examples [14]. The groups can be classified as follows, with respect to the size of particles from small to large [17]:

- Group C: Powders belonging to group C, such as flour and face powder, are extremely difficult to fluidize due to interparticle forces. Particle mixing and heat transfer of the particle surface and the bubbling bed is much poorer than particles of group A and B.
- Group A: Bubbling beds considering particles of group A expand before bubbling commences and collapse slowly when gas supply gets shut off. Group A particles show small mean particle sizes and/or low particle densities.
- Group B: In contrast to Group A particles, Group B contains of materials with greater particle sizes and densities. Furthermore, bubbles get formed at gas velocities slightly above minimum fluidization velocity (U_{mf}). Sand can be cited as a typical example.
- Group D: Materials of group D consist of large and/or very dense particles and are difficult to fluidize.

The characterization of Geldart is based on standard conditions. The behavior of the materials of each group are likely to change at different pressure conditions and/or gas viscosities. Investigations with dual fluidized bed gasification systems were conducted at ambient pressure conditions. Therefore, the effects of pressure on a fluidized bed reactor will not be discussed in detail. Several authors published further information about this [41, 76]. In Figure 2.8 the Geldart classification for air fluidization at ambient conditions is shown. More detailed information about characterization and classification of particles in fluidized beds can be found in [17, 52].

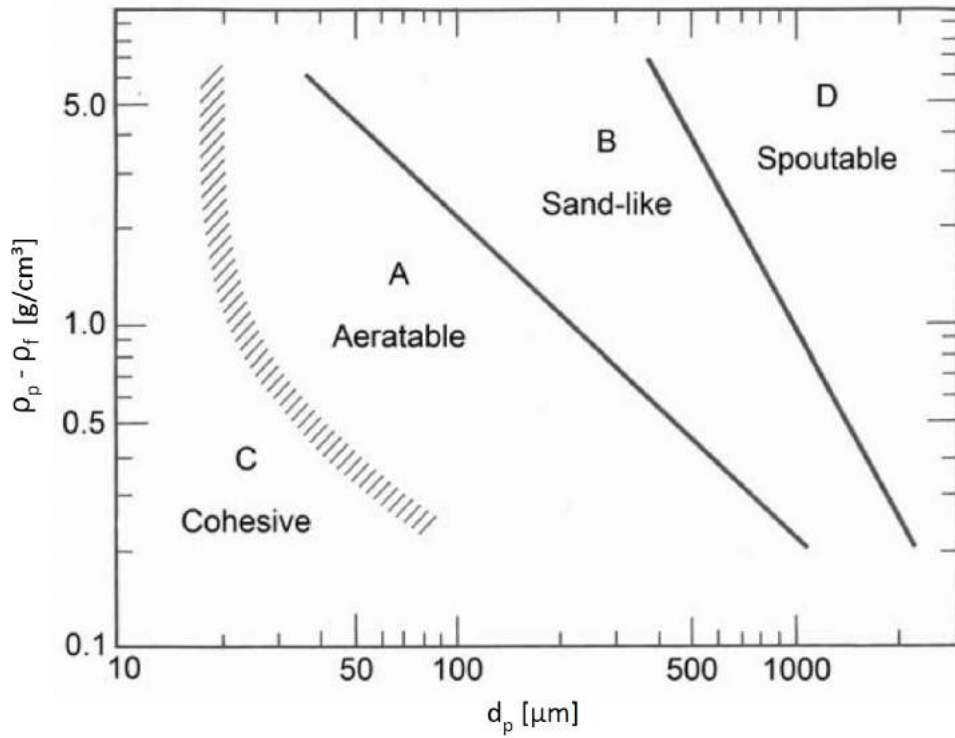


Figure 2.8: Geldart classification of particles A - D for air at ambient conditions, modified from [52]

2.3.2 Basic Fluiddynamic Equations for Fluidized Bed Systems

In this subsection basic equations for a "first" calculation of a fluidized bed for the determination of particle diameters, gas velocities, and pressure drop are described. The influence of the particle shape is described by the sphericity. Several authors use the sphericity ϕ to describe the real diameters. ϕ is defined as follows [24, 52, 54]:

$$\phi = \frac{\text{surface of sphere at the same volume}}{\text{surface of the particle}} = \left(\frac{d_v}{d_s}\right)^2 \quad (2.12)$$

where ϕ equals 1 for sphere and is in a range of $0 < \phi < 1$ for all other particles. Values for ϕ have been published by several authors mentioned in Section 2.3. Using Eq. 2.12 a diameter for all particles called Sauter diameter d_{sv} can be calculated. The Sauter diameter is defined as the diameter of a sphere having the same ratio of surface to volume as the particle of interest (see Eq. 2.13):

$$d_{sv} = \frac{6V}{S} = \phi \cdot d_v \quad (2.13)$$

where S is the particle surface area and V is the particle volume [14, 24]. Depending on the spericity of particles the following simplifications can be made:

- for particles nearly spherical

$$d_{sv} \approx \phi \cdot d_p \quad (2.14)$$

- for particles with a length ratio not greater than 2:1

$$d_{sv} \approx d_p \quad (2.15)$$

- for particles with a length ratio not less than 1:2

$$d_{sv} \approx \phi^2 \cdot d_p \quad (2.16)$$

To clarify the indices of diameter and to avoid misunderstandings, Table 2.4 gives a short summary of the diameters used in this work.

Table 2.4: Overview of the diameters used for calculation in this work, adapted from [24]

d_v	diameter of a sphere with same volume as the particle
d_s	diameter of sphere with same surface as the particle
d_{sv}	diameter of a sphere with same ratio of surface/volume as the particle
d_p	mean sieve diameter, characterized by the length of the sieve opening

The pressure drop in a fixed bed can be characterized by the Carmen-Kozeny equation and the Ergun equation, depending on the Reynolds number. For $Re < 1$ the Carmen-Kozeny equation (Eq. 2.17) shows a good correlation, whereas the Ergun equation (Eq. 2.18) is used for $Re > 1$. Both equations are displayed below:

$$\frac{\Delta p}{H} = 180 \cdot \frac{(1 - \varepsilon)^2}{\varepsilon^3} \cdot \frac{\mu \cdot U}{d_{sv}^2}, \quad (2.17)$$

$$\frac{\Delta p}{H} = 150 \cdot \frac{(1 - \varepsilon)^2}{\varepsilon^3} \cdot \frac{\mu \cdot U}{d_{sv}^2} + 1.75 \cdot \frac{(1 - \varepsilon)}{\varepsilon^3} \cdot \frac{\rho_g \cdot U^2}{d_{sv}}. \quad (2.18)$$

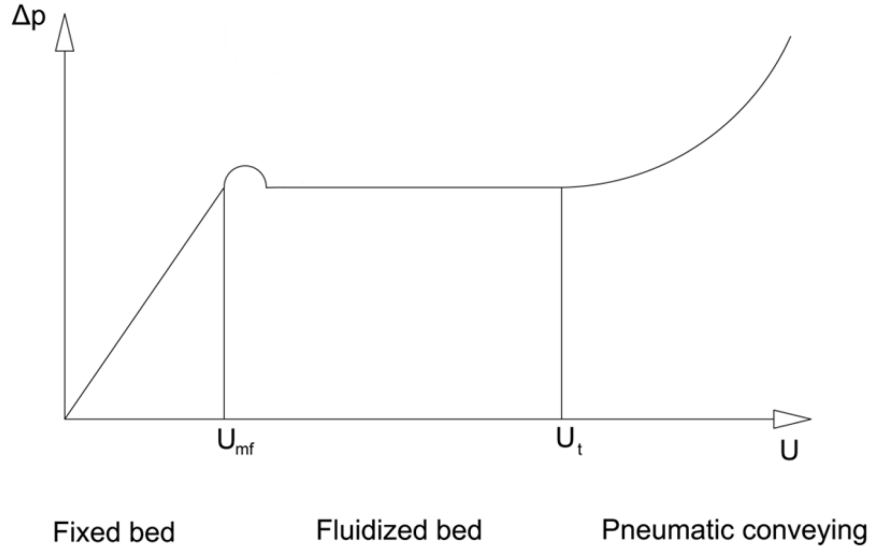


Figure 2.9: The relation of the pressure drop and the velocity of the fluidization agent [75]

The pressure drop in a fluidized bed can be calculated according to Eq. 2.19:

$$\Delta p = (1 - \varepsilon)(\rho_p - \rho_g) \cdot g \cdot H \quad (2.19)$$

Since the pressure drop at the transition from fixed bed to fluidized bed is equal, the Ergun equation (Eq. 2.18) can be combined with the formula for pressure drop in a fluidized bed (Eq. 2.19). Figure 2.9 shows the relation of the pressure drop versus the velocity of the fluidization agent [75].

Equalization and transformation of the two equations for the pressure drops the following equation can be displaced:

$$\frac{\rho_g \cdot d_{sv}^3 \cdot (\rho_p - \rho_g) \cdot g}{\mu^2} = \frac{150 \cdot (1 - \varepsilon_{mf})}{\varepsilon_{mf}^3} \cdot \frac{\rho_g \cdot d_{sv} \cdot U_{mf}}{\mu} + \frac{1.75}{\varepsilon_{mf}^3} \cdot \frac{\rho_g^2 \cdot d_{sv}^2 \cdot U_{mf}^2}{\mu^2} \quad (2.20)$$

Eq. 2.20 includes both dimensionless number, the Reynolds number and the Archimedes number. Therefore, Eq. 2.20 can be displayed as follows:

$$Re_{mf} = \sqrt{K_1^2 + K_2 \cdot Ar} - K_1, \quad (2.21)$$

where Re_{mf} and Ar are the Reynolds and Archimedes number given as:

$$Ar = \frac{\rho_g \cdot d_{sv}^3 \cdot (\rho_p - \rho_g) \cdot g}{\mu^2} \quad (2.22)$$

$$Re_{mf} = \frac{\rho_g \cdot d_{sv} \cdot U_{mf}}{\mu} \quad (2.23)$$

The empirical parameters K_1 and K_2 are nearly constant for different particles for a wide range of Reynolds numbers (0.001 to 4000) according to Wen and Yu [95]. Values for K_1 and K_2 have been published by several authors [19, 76, 95] and have been used to form Eq. 2.24 for the velocity of minimum fluidization (U_{mf}) :

$$U_{mf} = \frac{\mu}{\rho_g \cdot d_{sv}} \left[\sqrt{27.2^2 + 0.0408 \cdot Ar} - 27.2 \right] \quad (2.24)$$

$U_{c(AV)}$ (Eq. 2.25) shows an average critical velocity based on data from literature (cf. [78]) is calculated as follows:

$$U_{c(AV)} = \frac{\nu}{d_{sv}} \cdot Re_{c(AV)}, \quad (2.25)$$

where

$$Re_{c(AV)} = \frac{Ar^{(19/30)}}{0.85 + 0.85Ar^{(1/5)}} \quad (2.26)$$

$U_{c(AV)}$ is applicable for a wide range of Archimedes number ($0.6 < Ar < 10^5$).

The velocity U_{se} where entrainment of solids occur can be calculated according to Eq. 2.27 [4]:

$$U_{se} = \frac{\nu}{d_{sv}} \cdot Re_{se}, \quad (2.27)$$

where

$$Re_{se} = 1.53Re^{0.5} \quad (2.28)$$

2.3.3 Mapping of Fluidization Regimes

Several authors such as Reh [73], Grace and Bi [4, 20], and Avidan and Yerushalmi [3] compiled charts and basic parameters to map fluidization regimes. Reh published the well-known Reh-diagram in his PhD-thesis in 1961. He displayed a regime map with the abscissa as the dimensionless Reynold's number along a modified, dimensionless Froude-number as ordinate. Later on Grace published the Grace-digram (Figure 2.10) where the axes are labeled with a dimensionless diameter $d_p^* = Ar^{\frac{1}{3}}$ and a dimensionless velocity $u^* = Re_{sv} \cdot Ar^{-\frac{1}{3}}$. For investigations of fluidized regimes at the cold-flow model and the pilot plant of the Dual Fluid Gasifier the Grace-diagram was used. For this purpose the author will not go into detail for other published maps. The use of regime maps allows the determination of the fluidization regime at occurring conditions [78, 89, 91].

Figure 2.10 presents the regime map of Grace modified by Schmid [78]. Fluidization regimes starting with the onset of bubbling fluidization, turbulent fluidization up to a fast fluidization regimes are plotted. Furthermore the classification by Geldart and relevant velocities are shown. For more detailed information the author refers to [20, 78].

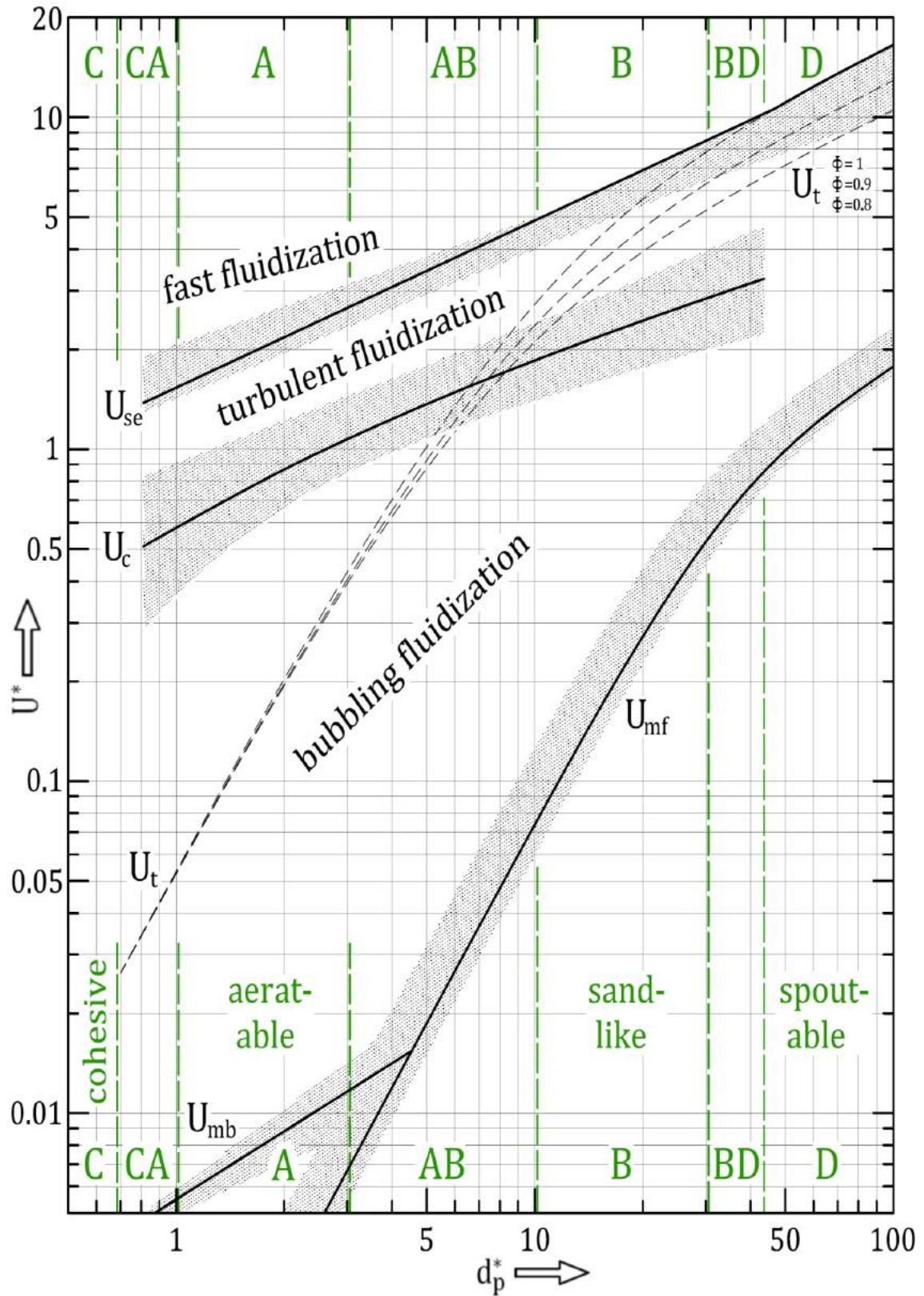


Figure 2.10: Flow regime map for fluidized beds showing typical ranges for regimes, velocities and Geldart's particle classification for density ratios of $400 < (\rho_p - \rho_g) / \rho_g < 9000$ [78]

3 Classical Dual Fluidized Bed Steam Gasification System

In this chapter the assembly and functionality of the classical DFB steam gasification pilot plant is shown. This pilot plant represents the former pilot plant before the installation of a novel pilot plant which is investigated within the present work. Additionally, main results conducted at the TU Wien are listed.

3.1 Assembly and Functionality of the Classical Dual Fluidized Bed Steam Gasification Pilot Plant

In order to avoid misunderstandings the latest generation of the Dual Fluidized Bed steam gasification pilot plant illustrated in Figure 3.1 is referred to as classical Dual Fluidized Bed steam gasification pilot plant or the abbreviation classical DFB pilot plant. A chronological overview of the development in the design of classical DFB pilot plants can be found elsewhere [44]. The Dual Fluidized Bed steam gasification pilot plant consists of two reactors to ensure a separation of the combustion zone and the gasification zone. As a result of the separation two gas streams can be yielded and thus a nitrogen free product gas with a high content of hydrogen in the range of 35 - 40 vol.-%_{db} and a medium calorific heating value of 12 - 14 MJ/Nm³ can be produced [29].

Circulating bed material provides the required sensible heat for the overall endothermic gasification reaction in the gasification reactor. The basic principle of an allothermal Dual Fluidized Bed steam gasification system has already been described in Chapter 2.1.2. An overview of main operating conditions and the basic geometry is illustrated in Table 3.1. As operable temperature range in the combustion reactor a range of 750 - 920°C is given. A combustion temperature of 750°C is extremely low and not state of the art. However, some test runs at the classical DFB pilot plant at this temperature were found in literature. The arrangement of the classical DFB reactor system including downstream

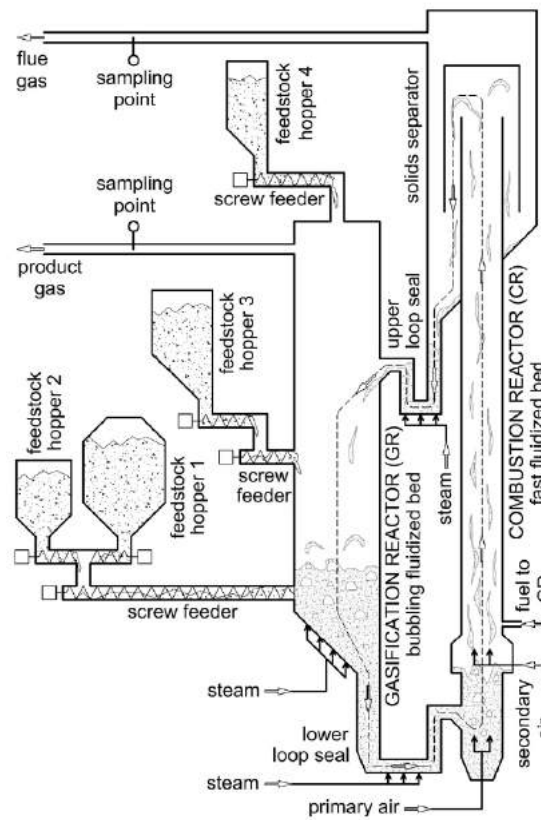


Figure 3.1: Schematic description of the classical Dual Fluidized Bed steam gasifier at the TUW [92], dismantled in February 2013

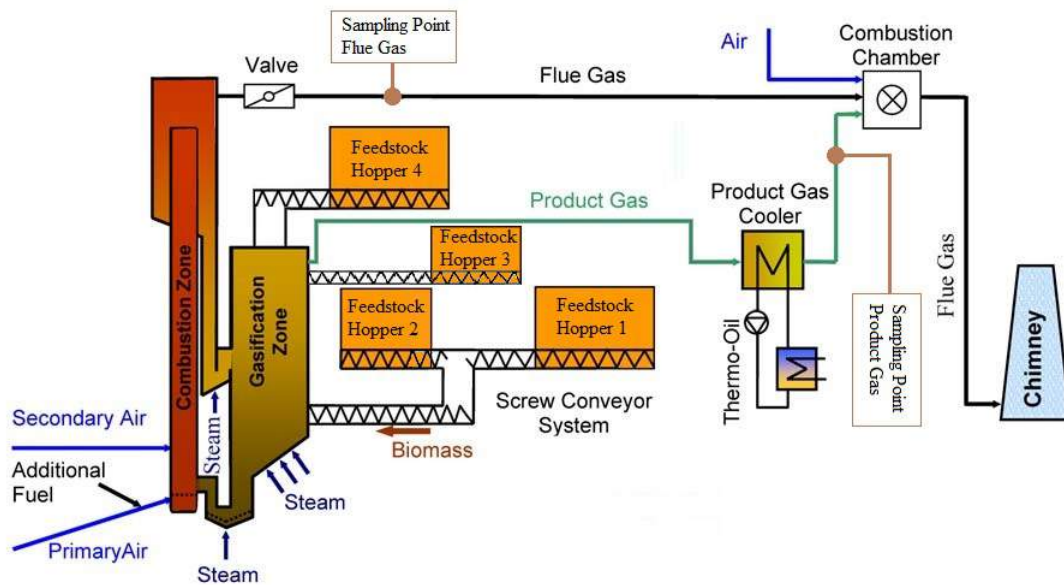


Figure 3.2: Flowchart of the classical Dual Fluidized Bed steam gasification pilot plant at the TU Wien, modified from [23]

units is depicted in Figure 3.2. A detailed overview of both reactors' cross sections, a description of main sampling points and the inlet nozzles are shown in Figure 3.3. TAP is the measurement point for the temperature of the primary air, TAS the temperature of the secondary air, TSSD the temperature of the steam to the bottom siphon, TSSU the temperature of the steam to the upper siphon, TASG the temperature of the steam to the gasification reactor. G1-G6 indicate pressure indicators along the gasification reactor and C1-C7 pressure indicators along the combustion reactor. SD1 presents the pressure indicator for the bottom siphon and SU1 & SU2 the pressure indicators for the upper siphon.

The gasification reactor (marked as gasification zone in Figure 3.2) consists of a bubbling bed in the bottom and a freeboard above, where gas-gas reaction may take place. Four feedstock hoppers were installed to ensure different feeding positions and co-gasification as shown in Figure 3.2. The combustion reactor was designed as fast fluidized bed. A more detailed description of the classical DFB steam gasification pilot plant can be found elsewhere [29, 43, 96].

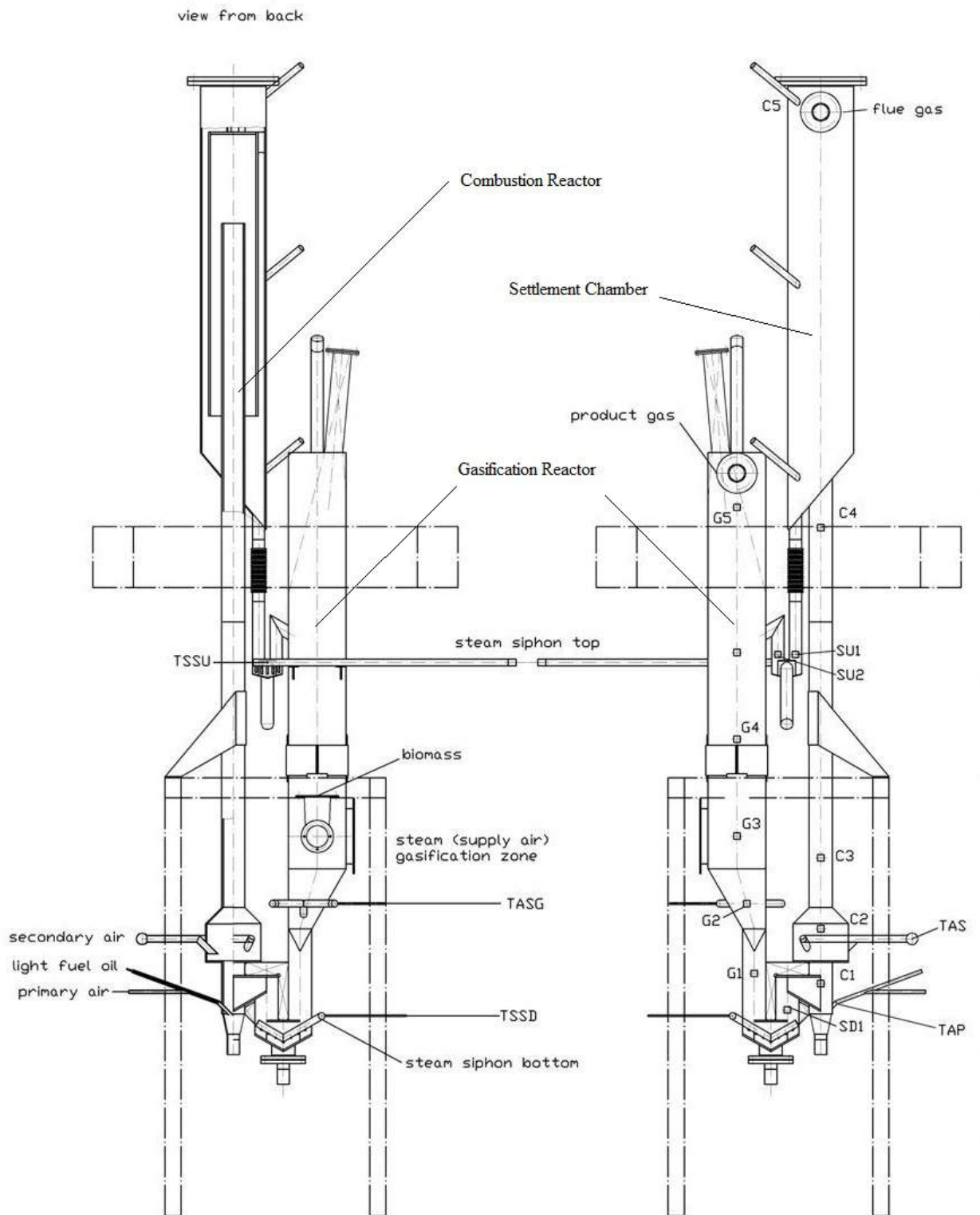


Figure 3.3: Technical drawing of the classical DFB test plant on a scale of 1:10 [23]

Table 3.1: Overview of main operating conditions and the basic geometry of the classical DFB system, modified from [29, 98]

	Unit	Gasification reactor	Combustion reactor
Operating parameter			
Operable temperature range	°C	650 - 870	750 - 920
Fuel power	kW	≈ 100	
Pressure	-	close to atmospheric conditions	
Fluidization regime	-	bubbling fluidized bed	fast fluidized bed
Fluidization agent	-	steam	air
Steam-to-fuel ratio	kg _{steam} /kg _{fuel,waf}	0.5 - 2.0	-
Bed material particle size	μm	200 - 800	
Basic geometry			
Overall reactor height	m	2.35	3.9
Average height of freeboard	m	1.7	-
Average height of bubbling bed	m	0.65	-
Geometry	-	conical bottom section with square-shaped upper freeboard section	cylindrical
Reactor inner dimensions	mm	270 x 270 ¹	∅ 98 ²

1 Inner dimensions of the freeboard

2 Cylindrical fast fluidized bed section of combustion reactor

3.2 Experimental Results of the Classical DFB Pilot Plant

In this section an overview of main operating parameters and results gathered at the classical DFB pilot plant at the TU Wien is given. These results allow the comparison of similar investigations regarding performance and impact of the new design. Table 3.2 illustrates data published by Kern et. al. [33], Koppatz et. al. [47], Schmid et. al. [92] and Wilk et. al. [97, 98, 101]. All investigations were conducted using wood pellets as feedstock at similar fuel input in a range of 90 - 100 kW. Test runs were carried out using either fresh olivine or used olivine as bed material with a mean particle size in the range of 370 - 510 μm. Table 3.3 gives a detailed analysis of chemical parameters of fresh and used/coated olivine.

Table 3.2: Overview of results conducted at the classical DFB pilot plant using wood pellets as feedstock. Sum of nitrogen and other gas components result in 100 vol.-%_{db}

Bed material	-	fresh olivine [29]	fresh olivine [101]	fresh olivine [92]	used olivine [101]
Mean bed material particle size	μm	370	510	520	510
Bed material inventory	kg	100	100	100	100
Gasification temperature	$^{\circ}\text{C}$	850	850	802	850
Combustion temperature	$^{\circ}\text{C}$	910	912	862	878
Feedstock input	kW	90	97	97	97
Steam to fuel ratio	$\text{kg}_{\text{steam}}/\text{kg}_{\text{fuel,waf}}$	0.60	0.78	0.80	0.86
In-bed feeding					
H ₂	vol.-% _{db}	39.3	44.8	35.3	43.5
CO	vol.-% _{db}	30.5	27.3	29.1	22.3
CO ₂	vol.-% _{db}	16.2	17.7	17.3	22.8
CH ₄	vol.-% _{db}	9.3	8.4	11.1	8.1
C ₂ H ₄	vol.-% _{db}	1.9	1.4	n.p.	1.9
C ₂ H ₆	vol.-% _{db}	0.2	0.1	n.p.	0.2
C ₃ H ₈	vol.-% _{db}	n.p.	0.1	n.p.	0.3
GC-MS tar	$\text{g}/\text{Nm}^3_{\text{db}}$	7.1	3.5	11.7	2.6
Grav. tar	$\text{g}/\text{Nm}^3_{\text{db}}$	1.5	2.4	6.0	2.0
On-bed feeding					
H ₂	vol.-% _{db}	32.8	42.0	n.p.	43.3
CO	vol.-% _{db}	34.7	32.0	n.p.	23.9
CO ₂	vol.-% _{db}	14.6	15.1	n.p.	21.5
CH ₄	vol.-% _{db}	10.3	8.6	n.p.	8.1
C ₂ H ₄	vol.-% _{db}	2.7	1.8	n.p.	2.0
C ₂ H ₆	vol.-% _{db}	0.2	0.1	n.p.	0.2
C ₃ H ₈	vol.-% _{db}	n.p.	0.2	n.p.	0.3
GC-MS tar	$\text{g}/\text{Nm}^3_{\text{db}}$	16.8	7.5	n.p.	3.4
Grav. tar	$\text{g}/\text{Nm}^3_{\text{db}}$	9.7	3.4	n.p.	1.4

n.p. not published

Table 3.3: Bed material analysis of fresh and used olivine [34]

	Unit	Fresh olivine	Used/coated olivine
MgO	wt.-%	46.8	40.0
SiO ₂	wt.-%	39.8	34.9
CaO	wt.-%	0.9	10.0
Fe ₂ O ₃	wt.-%	10.3	8.1
K ₂ O	wt.-%	0.32	3.8
Na ₂ O	wt.-%	0.43	0.73
Al ₂ O ₃	wt.-%	0.40	0.60
Cr ₂ O ₃	wt.-%	0.28	0.55
MnO	wt.-%	0.15	0.29
P ₂ O ₅	wt.-%	0.03	0.25
Cl	wt.-%	0.10	0.21
NiO	wt.-%	0.31	0.20
SO ₃	wt.-%	0.06	0.06
Others	wt.-%	0.12	0.31

The following definitions clarify terms used to determine the results of the investigations.

- The **steam to fuel ratio** is defined as the total mass flow of steam and the mass flow of water in the feedstock (water content of feedstock) divided by the water and ash free mass flow of the feedstock according to Eq. 3.1.

$$\frac{S}{F} = \frac{\dot{m}_{fluidization} + \dot{m}_{water,feedstock}}{\dot{m}_{feedstock_{waf}}} \left[\frac{\text{kg}_{\text{steam}}}{\text{kg}_{\text{fuel,waf}}} \right] \quad (3.1)$$

- The **steam to carbon ratio** is described as the total mass flow of steam and the mass flow of water in the feedstock (water content of feedstock) divided by the mass flow of carbon in the feedstock according to Eq. 3.2 [100].

$$\frac{S}{C} = \frac{\dot{m}_{fluidization} + \dot{m}_{water,feedstock}}{\dot{m}_{carbon,feedstock}} \left[\frac{\text{kg}_{\text{steam}}}{\text{kg}_{\text{carbon,feedstock}}} \right] \quad (3.2)$$

- The **residence time** τ describes the time period a particle remains in a specific area. Mostly this refers to the residence time of a particle in the bubbling bed of the gasification reactor, in the freeboard/counter-current column of the gasification reactor or along the height of the combustion reactor. The residence time of a particle is calculated using the simulation software IPSEpro. More detailed information

about the calculation can be found elsewhere [70].

- The **overall cold gas efficiency** η_g describes the chemical energy of product gas divided by the chemical energy of the feedstock to the gasification reactor and the chemical energy of the additional fuel to the combustion reactor. The equation of the overall cold gas efficiency is illustrated in Eq.3.3 [60].

$$\eta_g = \frac{\dot{m}_{PG} \cdot lhv_{PG}}{\dot{m}_{fuel} \cdot lhv_{fuel} + \dot{m}_{addfuel} \cdot lhv_{addfuel}} \quad \left[\frac{\text{kW}_{PG}}{\text{kW}_{fuel}} \right] \quad (3.3)$$

- The **cold gas efficiency** η_{cg} is defined as the chemical energy of the feedstock entering the gasification reactor divided by the chemical energy of the product gas. The equation of the cold gas efficiency is shown in Eq.3.4.

$$\eta_{cg} = \frac{\dot{m}_{PG} \cdot lhv_{PG}}{\dot{m}_{fuel} \cdot lhv_{fuel}} \quad \left[\frac{\text{kW}_{PG}}{\text{kW}_{fuel}} \right] \quad (3.4)$$

- The **fuel related water conversion** $X_{H_2O, fuel}$ describes the ratio of the consumed water in the GR divided by total mass of water and ash free feedstock entering the GR. The equation of the fuel related water conversion is shown in Eq.3.5 [60].

$$X_{H_2O, fuel} = \frac{\dot{m}_{fluid} \cdot w_{H_2O, fluid} + \dot{m}_{fuel} \cdot w_{H_2O, fuel} - \dot{m}_{PG} \cdot w_{H_2O, PG}}{(1 - w_{H_2O, fuel} - w_{ash, fuel}) \cdot \dot{m}_{fuel}} \quad \left[\frac{\text{kg}_{H_2O}}{\text{kg}_{fuel, waf}} \right] \quad (3.5)$$

- The **steam related water conversion** X_{H_2O} describes the ratio of the consumed water in the GR divided by total mass of water entering the GR. The equation of the steam related water conversion is shown in Eq.3.6 [60].

$$X_{H_2O} = \frac{\dot{m}_{fluid} \cdot w_{H_2O, fluid} + \dot{m}_{fuel} \cdot w_{H_2O, fuel} - \dot{m}_{PG} \cdot w_{H_2O, PG}}{\dot{m}_{fluid} \cdot w_{H_2O, fluid} + \dot{m}_{fuel} \cdot w_{H_2O, fuel}} \quad \left[\frac{\text{kg}_{H_2O}}{\text{kg}_{H_2O}} \right] \quad (3.6)$$

For steam gasification $w_{H_2O, fluid} = 1$ and can be omitted in this case.

- The **carbon conversion in the GR** X_c is defined as the amount of carbon leaving the gasification reactor with the product gas divided by the amount of carbon entering the gasification reactor. The equation of the carbon conversion is shown in

Eq. 3.7 [33].

$$X_c = \frac{\dot{m}_{c,PG}}{w_c \cdot \dot{m}_{fuel}} \quad [-] \quad (3.7)$$

3.3 Overview of Key Findings of the Classical DFB Pilot Plant

Main results and findings obtained by numerous test runs at the TUW are summarized below:

- a wide range of different fuels was tested proving the high fuel flexibility of the classical DFB pilot plant. Soft wood pellets, waste wood, saw dust, hard wood, palm fruits, palm leaves, sugarcane bagasse, sugarcane residues, reed, wheat bran, several polymers and coal were gasified successfully,
- different kinds of bed materials (metallic and non-metallic) were used as heat carrier. During the operation of the gasification processes the bed material particles form an inner and outer layer at the surface. Calcium-rich layers enhance the catalytic activity of the particle. Bed material coating showed a positive effect on tar reduction in the product gas stream [35, 39]. A more detailed description can be found in [36]. Several types of bed material were successfully tested and published in [46, 48, 67, 103] including bed materials with high catalytic effects such as limestone and bed materials with no catalytic effects such as silica sand. Bed material that already were used in gasification processed and formed catalytic layers are defined as used bed material, in comparison to fresh olivine that was not used in any process before,
- co-gasification of lignite with wood pellets, lignite with polyethylene, and polymer waste with wood pellets was conducted with highly satisfactory results regarding the performance of the process. Experiments showed that co-gasification can lead to beneficial advantages of different fuel properties, even small amounts of lignite in the fuel mix can reduce the tar content significantly for the gasification process [31]. More detailed information can be found in [30, 31, 98],
- the conversion and distribution of fuel nitrogen, sulphur, and chlorine was investigated. Sulphur and nitrogen mainly convert to H₂S and NH₃ and remain in the product gas stream. On the contrary, a vast majority of chlorine from the fuel is bounded to the ash [97, 99],

- particle size of the bed material and the amount of steam plays a major role for the gasification processes. Small particles require less steam to guarantee similar fluidization properties. This results in a decreased steam to fuel ratio. A greater turbulence of small particles can be realized and leads to an increased of water and carbon conversion and promotes the gas-solid contact [32]. Smaller bed material particles lead to significant lower contents of GC-MS tar and slightly lower contents of gravimetric tar, since a higher turbulence and a higher specific particle surface can be obtained [43]. Very small particles (<1 mm) lead to entrainment into the freeboard of the GR and therefore show a lack of gas-solid contact [101],
- gasification properties can be influenced by the fuel feeding position. As shown in Figure 3.1 and 3.2 the GR of the classical DFB pilot plant was equipped with three feedstock conveyors. Investigations showed better performances for in-bed feeding for fuel showing a high amount of volatiles to enhance the gas-solid contact in the bubbling bed. Thus, the gas composition reached smaller deviations to the WGS-equilibrium and better tar reforming performance compared to on-bed feeding with similar fuels [33, 42, 101] and
- inorganic matter, such as ash and bed material plays a major role in the performance of the gasification operation. Alkali, alkali earth metals, and potassium showed to be mainly responsible for bed material agglomeration in the reactor systems as well as fouling and slagging in the downstream units [37].

Based on these findings and experiences acquired by test runs conducted at the classical DFB pilot plant the novel DFB pilot plant was designed. A detailed description can be found in Chapter 4.

4 Methodology - Novel Dual Fluidized Bed Steam Gasification Pilot Plant

In Chapter 4 the methodology used to design the novel DFB gasification pilot plant is shown. To clarify the nomenclature the novel pilot plant is named as novel Dual Fluidized Bed steam gasification pilot plant abbreviated as novel DFB pilot plant.

4.1 Cold Flow Model of the Novel DFB Pilot Plant

In order to investigate the fluid dynamics of the novel DFB pilot plant a cold flow model (CFM) was constructed and assembled at the TU Wien, as shown in Figure 4.1. The aim of the cold flow model was to gain a better understanding of the fluid dynamics occurring inside the novel DFB test plant, especially in the novel counter-current gasification reactor system. A detailed description of the cold flow model can be found in literature [16, 56, 78].

Figure 4.2 shows a pipe and instrumentation diagram of the cold flow model. Numerous pressure indicators along different plant sections allow the recording of pressure data to evaluate the state of fluidization at different air mass flow streams. Bronze particles as bed material were used in the cold flow model and olivine was used in the novel DFB pilot plant, since the Reynolds numbers, Archimedes numbers and density ratios $\frac{(\rho_p - \rho_g)}{\rho_g}$ are similar for bronze and air and olivine and steam [16, 78].

The gasification reactor was made from acrylic glass and designed with a square cross section and a constriction ratio (A_c/A) of 25.8% where A is the full area in the GR column and A_c is the reduced area in the constriction [16]. The combustion reactor was designed in a circular cross section.

Several investigations have been conducted with varying parameters regarding input streams and particle sizes to examine optimal operating conditions for the fluidized bed system. Schmid [78] published the experimental results shown in Figure 4.3. The illustration highlights optimal operating conditions using two different particle sizes with a d_p of

64 μm and 79 μm (bronze sphere). Blue triangles show the pressure and pressure gradient along the height of the gasification reactor with a d_p of 64 μm and blue dots with a d_p of 79 μm at a total fluidization flow of the GR of 10.4 Nm^3/h and 12.4 Nm^3/h , respectively. Red dots and triangles show the pressure course along the height of the combustion reactor at a total air volume flow of 20.4 Nm^3/h and 24.4 Nm^3/h .

Fuchs [16], Martinovic [56] and Schmid [78] showed good performance of the cold flow model for both particle sizes in terms of the fluid dynamics of the new design. The combustion reactor showed the desired fast fluidized bed regime along the height with smooth differences for changing particle sizes. The pressure gradients in the counter-current column showed evenly distributed bed material in the reaction zones. The top two zones showed a minimum of hold-up, since only fine particles got entrained in the upper part. The bigger the pressure gradients are the higher is the hold up of particles in the constriction.

In the lower part of the gasification reactor a bubbling bed occurs as shown in Figure 4.3 on the very left. The step-like profile again symbolizes the constrictions installed. The results show optimal operation conditions for the used fluidized bed system using bronze particles in various sizes.

Based on findings obtained from the cold flow model investigations, the novel DFB pilot plant was constructed. Especially findings about the relation between the volume flow of the fluidization agent into the gasification reactor and the time when flooding in the counter-current column occurs was of special interest. These results were considered for the technical design of the counter-current column.

More detailed information about the fundamentals of the cold flow model, its design and results are published by Schmid, Fuchs and Martinovic in several publications [16, 56, 85, 89, 90, 91].



Figure 4.1: The cold flow model system is shown. Pressure indicators (blue tubes) and air inlet tubes (white tubes) are illustrated

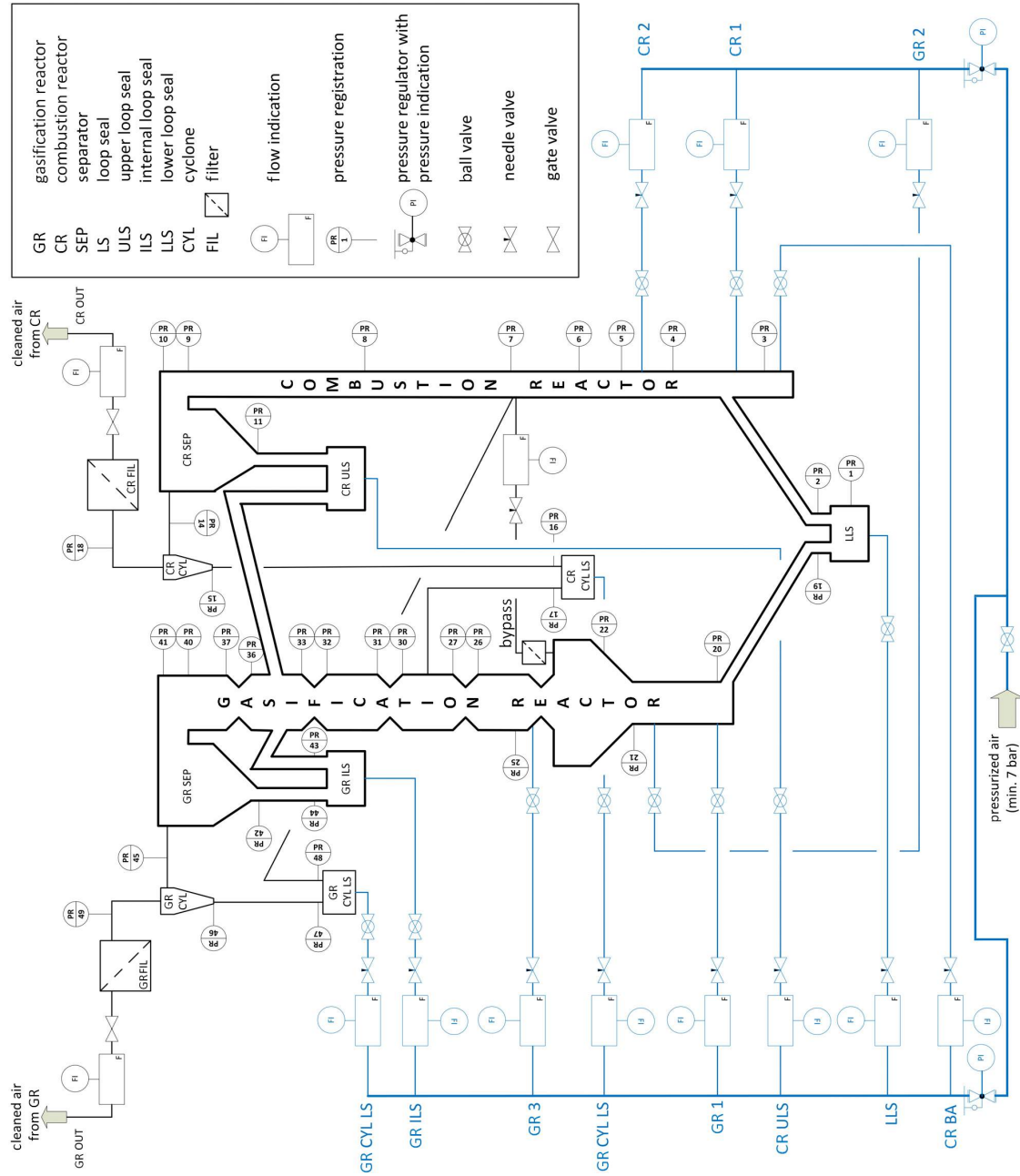


Figure 4.2: Pipe and instrumentation design of the cold flow model. Investigations were carried out to examine the fluid dynamic of both reactors, GR and CR [78]

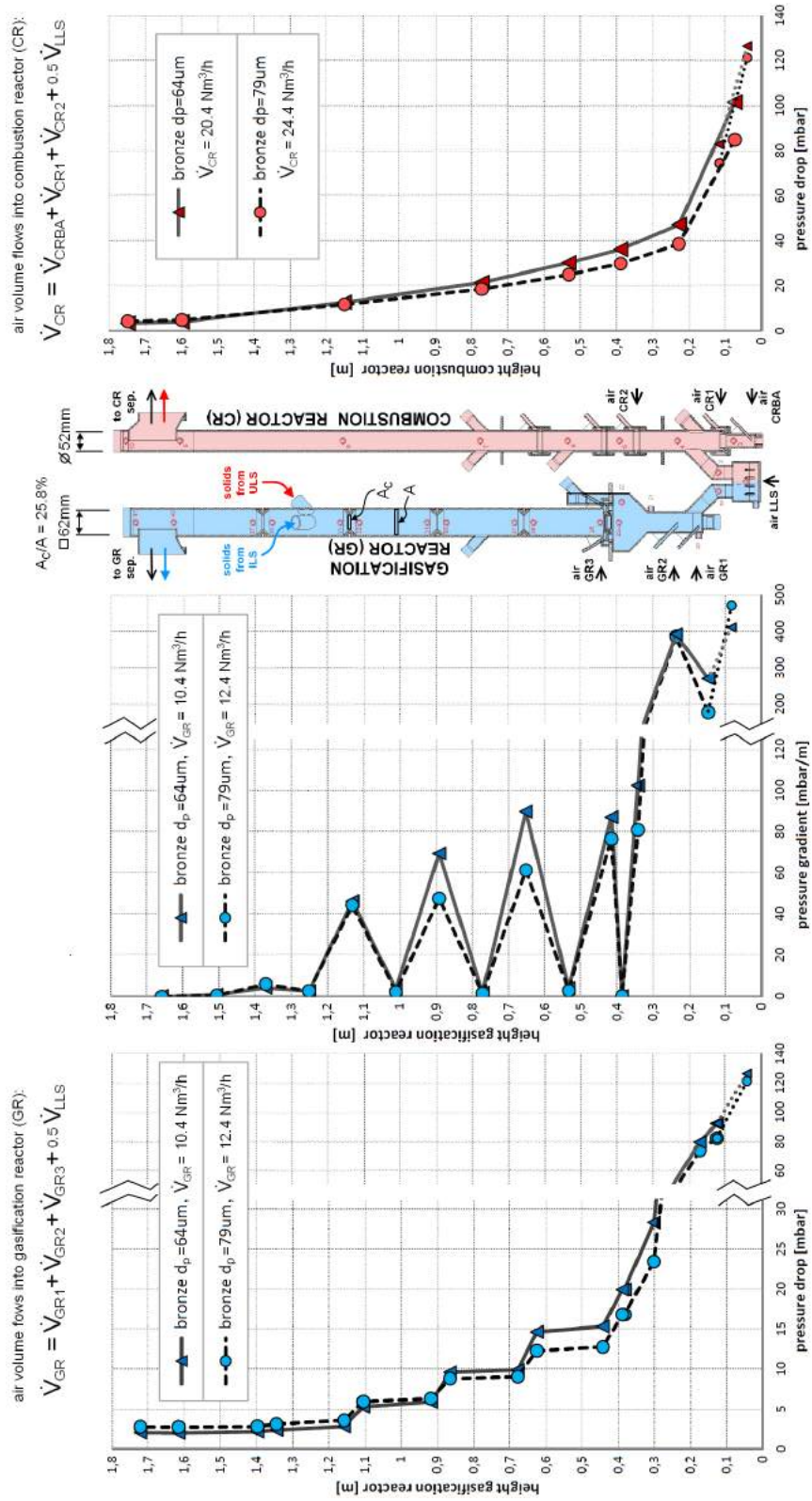


Figure 4.3: Experimental results at the CFM showing optimal operating points using bronze particles in various sizes [78]

4.2 IPSEpro - Simulation Software for Modelling and Calculation of Processes

For the estimation of the mass and energy balances of the novel DFB pilot plant the simulation software IPSEpro was used. IPSEpro is a software tool based on stationary, equation-oriented flow sheet modelling. A detailed overview about functionality and structure of the simulation tool can be found in Proell [70]. The simulation software was used to benefit from several advantages as listed below [43]:

- estimation of mass and energy balances for the calculation and design of the novel 100 kW DFB pilot plant,
- determination of process states, conditions, and properties occurring,
- calculation of process key figures,
- better interpretation of experimental results, and
- validated models for the investigation of scaled-up plants.

Figure 4.4 shows exemplary results for a mass and energy balance calculated with IPSEpro to design the novel DFB test plant based on the classical DFB reactor gasifier unit. Figure 4.4 also highlights main design data of the process itself. The figure includes a fuel bypass from the GR to the CR. This bypass was planned but not installed until now and was replaced by the additional fuel input of natural gas.

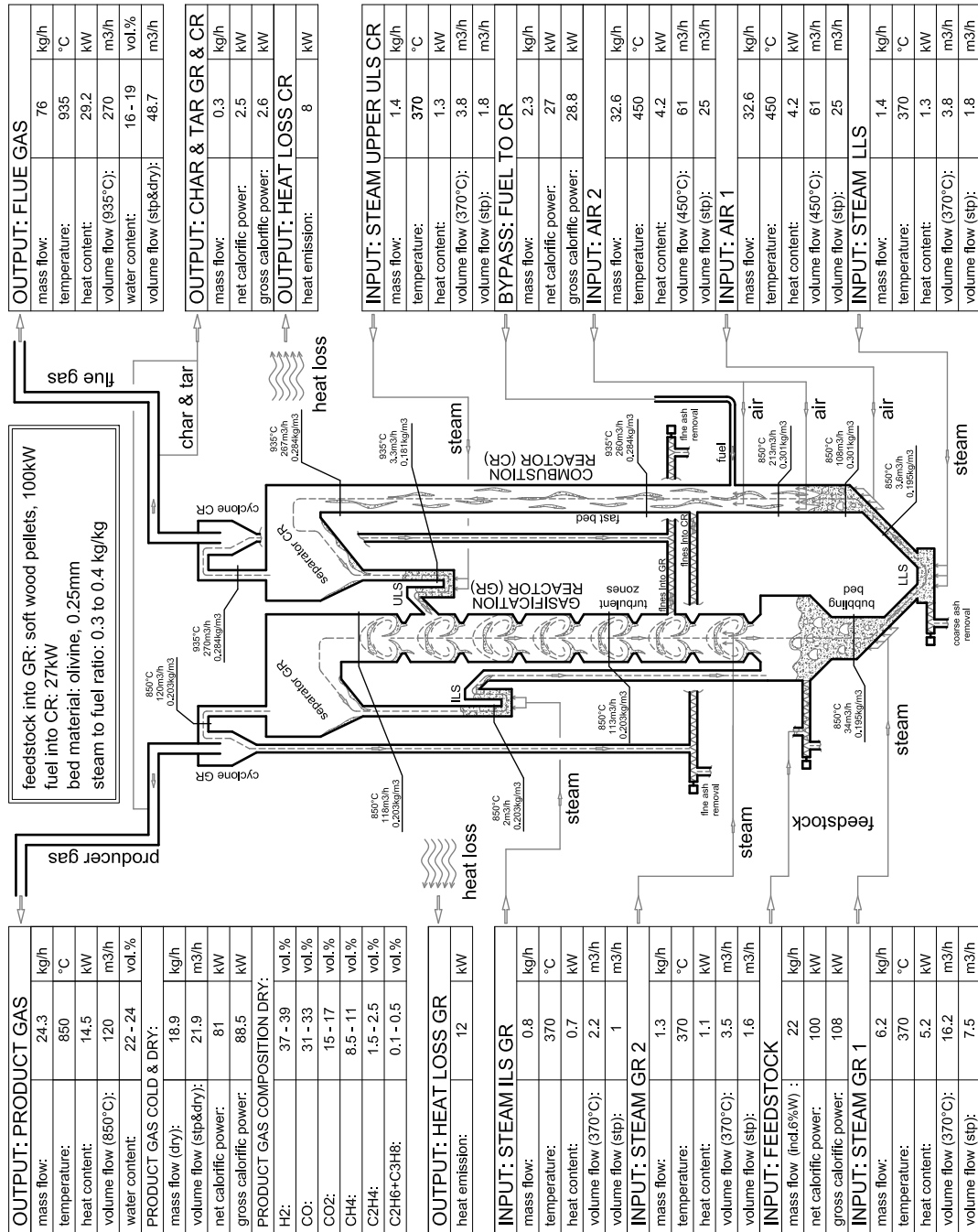


Figure 4.4: Overview of design values of the mass and energy balance calculated by the use of the simulation software IPSEpro [1]

4.3 Novel Dual Fluidized Bed Steam Gasification Pilot Plant

Based on results of the classical DFB pilot facility, experiences with commercial plants in Güssing and Oberwart, fundamental findings of cold flow model test runs as well as mass and energy balances obtained from simulation software IPSEpro, a 100 kW dual fluidized bed steam gasification pilot plant has been constructed and assembled at the TUW and started up in 2015. The aim of this new concept was an increased in-situ conversion of hydrocarbons to produce a high quality product gas and to increase the fuel flexibility. The main idea behind the new system was to replace the freeboard of the classical DFB pilot plant with a counter-current column to improve the gas/solids contact time. Basic geometric parameters together with design parameters are listed in Table 4.1. Obviously, a wide range of gasification temperatures in all sections are adjustable. Higher gasification temperatures in the upper gasification reactor (counter-current column) can be achieved although lower gasification temperatures in the lower gasification reactor (bubbling bed) were set. Turbulent zones in the upper gasification reactor together with higher gasification temperatures may influence tar reforming and tar cracking processes and therefore the quality of the product gas. The fluidization ratio U/U_{mf} prove occurring fluidization regimes in each section. As calculated, U/U_{mf} greater 1 ensure a bubbling bed in the lower gasification reactor, whereas values in the ratio between 40 - 55 ensure turbulent zones in the upper gasification reactor. Additionally, very high fluidization ratios ensure a fast fluidized bed along the height of the combustion reactor. For a better understanding, Figure 4.7 and 4.9 display a schematic overview of the reactor system. As presented in Figure 4.5 the novel DFB pilot plant is divided into four main parts:

- solid fuel supply,
- gas production,
- gas cooling, cleaning and utilization, and
- control system for measurement and control technology.

Table 4.1: Main design values for geometric and operating parameters of the reactor system of the novel DFB pilot plant, modified from [84]

Parameter	Unit	Lower gasification reactor	Upper gasification reactor	Combustion reactor
Range of temperature ¹	°C	700 - 850	800 - 950	830 - 980
Fuel power	kW	40 - 110		30 - 57 ²
Pressure	-	close to atmospheric conditions		
Fluidization regime	-	bubbling bed	turbulent zones	fast fluidized bed
Fluidization agent	-	steam	steam	air
Amount of bed material	kg	75 - 110		
Superficial gas velocity, U (in fluidized bed)	m/s	0.47 - 0.93	1.7 - 2.1	6.3 - 7.6
Minimal fluidization velocity U_{mf}	m/s	0.037	0.037	0.028
Fluidization ratio, U/U_{mf}	-	13 - 25	40 - 55	220 - 270
Terminal velocity, U_t	-	2.06	2.06	1.61
Fluidization ratio, U/U_t	-	0.23 - 0.45	0.8 - 1.1	3.8 - 4.8
Mean bed material diameter of olivine for calculation of fluid dynamics	μm	250	250	250
Fluidization media for calculation of fluid dynamics	-	Product gas	Product gas	Flue gas
Cross section for calculation	mm	68 x 490	128 x 128	\varnothing 125
Height of reactor part	m	1.03	3.33	4.73
Geometry	-	Conical bottom section	Square-shaped upper constriction section	Cylindrical
Inner dimensions of reactor parts	mm	560 x 490 68 x 490	128 x 128	\varnothing 125

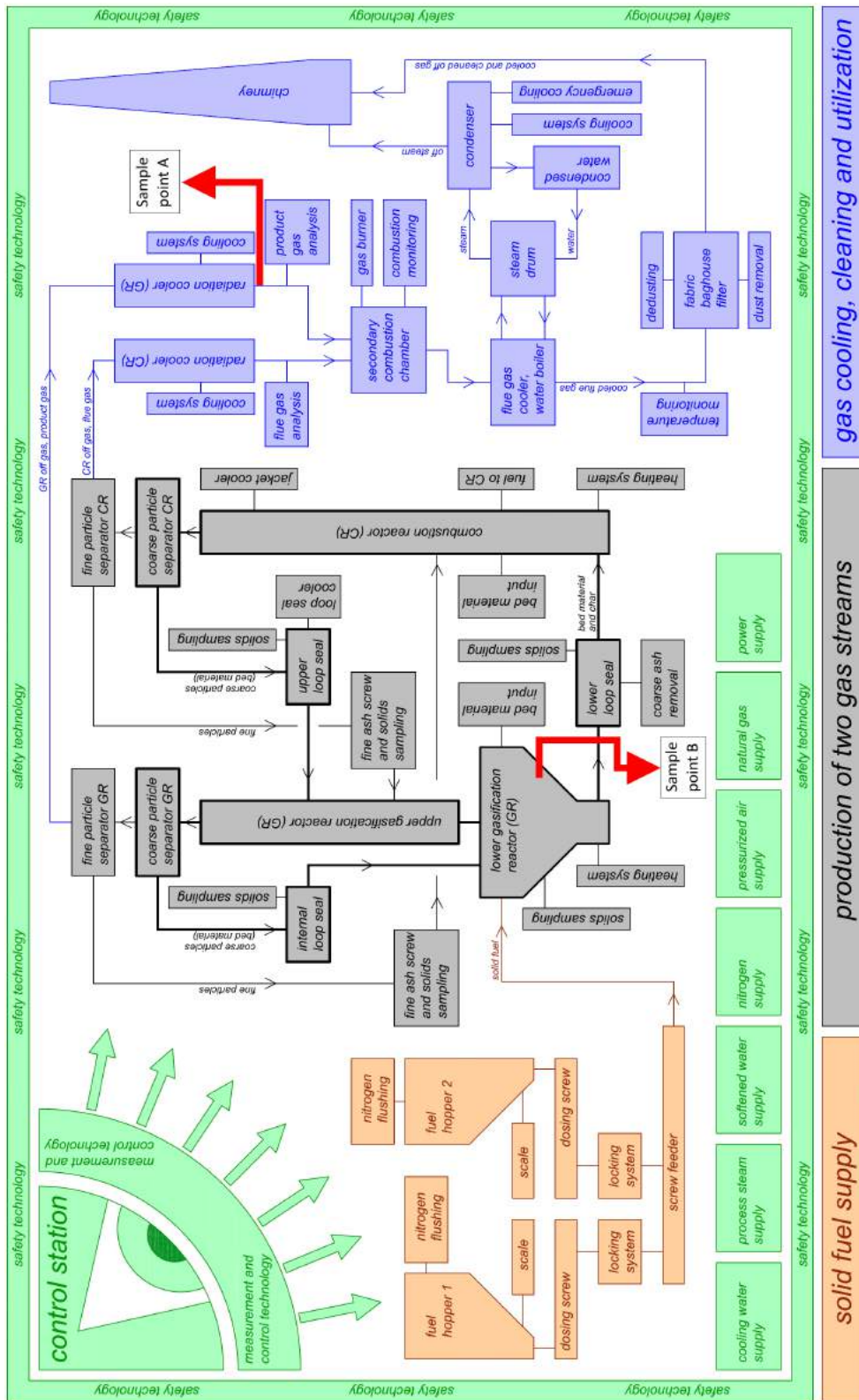


Figure 4.5: Basic flow sheet of the overall novel DFB test plant, adapted from [78]

Figure 4.5 presents the basic flow sheet of the novel test plant. The part marked in green presents the control room. Since nearly all input streams can be adjusted in the control room fast changes of input streams and a safe environment during operation are ensured. The following input streams can be adjusted manually:

- input of steam,
- input of air (primary, secondary, and tertiary),
- input of air for combustion of additional fuel,
- input of nitrogen, and
- input of natural gas to the post combustion chamber.

A process control system (PCS) was realized using the software APROL provided by the company Bernecker and Rainer. This software allows the integration of programmable logic controllers (PLC) for the visualization of the process. Main parameters, as listed below, can be adjusted during operation and output parameters are displayed simultaneously:

- input of feedstock (both hoppers),
- input of additional fuel to CR,
- controlling of all conveyors and valves, and
- activation of emergency shut-down.

The main output parameters include, among others, the following:

- mass flow of feedstock,
- temperature and pressure along the whole process chain,
- mass flow of product and flue gas stream,
- product and flue gas composition,
- composition of exhausted gas after the post combustion chamber, and
- overview of the cooling cycles.

Main advantages of APROL and a detailed description of the measuring and control system of the novel DFB test plant can be found elsewhere [77]. A picture of the control room is

shown in Figure 4.6.



Figure 4.6: Process control system with flow meters for air (left), steam (middle), and computers to operate the PCS (right)

The fuel supply as marked in orange in Figure 4.5 includes two fuel hoppers and a screw to convey the feedstock into the lower gasification reactor onto the bubbling bed. To operate in-bed feeding a further feeding position has been considered, but not yet realized. Thus, a further feeding position was considered to enable the feeding of feedstock into the constriction part of the gasifier (constriction four). Currently only the lower fuel input feeding screw (on-bed feeding) is installed.

Figure 4.7 shows the positions of the lower and upper feeding screw where the lower conveyor screw is equipped with two hoppers. This arrangement allows to convey two different feedstocks simultaneously into the gasification reactor (GR) to realize co-gasification. Thus, feedstocks with low softening temperatures such as plastics can be conveyed successfully into the gasifier due to a cooling jacket at the end of the feeding screw at the inlet to the GR.

The reactor system represents the heart of the novel DFB test facility marked in grey in Figure 4.5. It includes two reactors with its particle separator units. The reactor system is shown in Figure 4.7 and 4.9. Figure 4.8 shows the basic principle of the Dual Fluidized Bed steam gasification system.

The novel concept was designed as an allothermal dual fluidized bed system using steam in the gasification reactor as gasification and fluidization agent and air in the combustion

reactor (CR) . Both reactors, the CR and the GR are connected via two loop seals, the upper loop seal (ULS) and lower loop seal (LLS).

To provide heat for the allothermal process, circulating catalytic bed material (BM) together with not completely gasified biomass (residual char) is transported from the bottom of the GR into the CR via the LLS. The bed material is heated up in the CR where combustion of the char and additional fuel occurs. It is transported along the CR via ULS into the top of the GR where the hot bed material provides energy for overall endothermic gasification reactions.

The GR is equipped with an internal loop seal (ILS) to recirculate separated bed material particles and not oxidized char from the coarse particle separator into the lower part of the gasification reactor.

Additional loops after both cyclones of each gas stream allowing the recirculation of fine and high catalytic particles (since the specific surface is greater) into the GR and the CR via screw conveyors. A recirculation of fines should enhance the effect of catalytic bed material. During the first investigations of the novel plant, both recirculation screws were deactivated.

The novel DFB reactor system is equipped with two particle separation units on each gas stream. Bigger particles are separated gently in the settlement chamber at low velocities in the first phase. This should minimize the effect of attrition and abrasion of bed material particles. In the second phase a cyclone is used to reduce the share of fines in the gas stream to a minimum. This concept of separation enables the use of small and soft particles (e.g. limestone, dolomite). Otherwise soft particles undergo attrition and abrasion and are entrained by the gas stream.

The GR (marked in blue in Figure 4.7) is designed as a bubbling bed in the bottom combined with a turbulent to fast fluidization regime along the height of the reactor. The upper part of the GR consists of six reaction zones. These six chambers can be described as cascades of stirred vessels [68]. The reaction zones enable different fluidization regimes. In each constriction a turbulent zone occurs, since the diameter is decreased at constant mass flows. Above the constrictions the increasing diameter of the column results in a bubbling bed to fast fluidized bed. These turbulent zones along the upper GR allow a good intermixing of hot bed material, residual char particles, tar, product gas and gasification agent [85]. The cross section of each constriction can be adjusted manually. The free cross section of the constriction can be adjusted from 0% up to a A_c/A - ratio of 49%. A more detailed description of the constriction units can be found in [11]. To do so, the

fluid dynamics can be changed during investigation.

Several investigations at the cold flow model were conducted at the TUW to examine the behavior of particles and gases in these constrictions. Schmid et al. [78, 85, 90] published results of changing fluidization behaviors of solids between the reduced cross sections and the free cross section. Along the height of the GR the solids' densities show oscillating behaviors based on changing cross sections. These obstacles result in changing fluidization regimes along the height from small bubbling beds in each chamber up to fast fluidization regimes in each constriction. High gas velocities in each constriction and good intermixing of solids and gases should result in high gas-solid contact times and lead to higher hydrocarbon conversions. For more detailed information about the behavior of solids and gases in the reactor system, in particular in the reaction zones along the GR, the author wants to refer to Schmid et al. [78, 82, 83, 87].

The gasification reactor and all loop seals are fluidized with steam to avoid dilution of the product gas with nitrogen. The combustion reactor marked in red in Figure 4.7 is designed for a fast fluidized regime along the height, using air as fluidization agent. The primary to tertiary air inlet at the bottom of the CR allow a better control of the global solids circulation rate. Air for the combustion of additional fuel allows to regulate the combustion temperature and to compensate heat losses.

This new design implies several advantages compared to the classical DFB design [68, 78, 82, 83, 87]:

- lower fluidization volume flows but higher velocities due to a reduced diameter of the upper part of the GR in comparison to the freeboard of the classical DFB,
- higher fluidization velocities resulting in an increased hold-up of bed material in the GR,
- increasing contact time for solids and gases,
- enhanced gas-solid interaction,
- the counter-current effect of solids and gases in the GR leads to a maximization of chemical and physical driving forces for occurring chemical reactions,
- lower steam to fuel ratios are resulting in a higher overall efficiency,
- utilization of smaller bed material particle sizes,
- adjustable constrictions to realize favourable fluidization regimes in the reaction

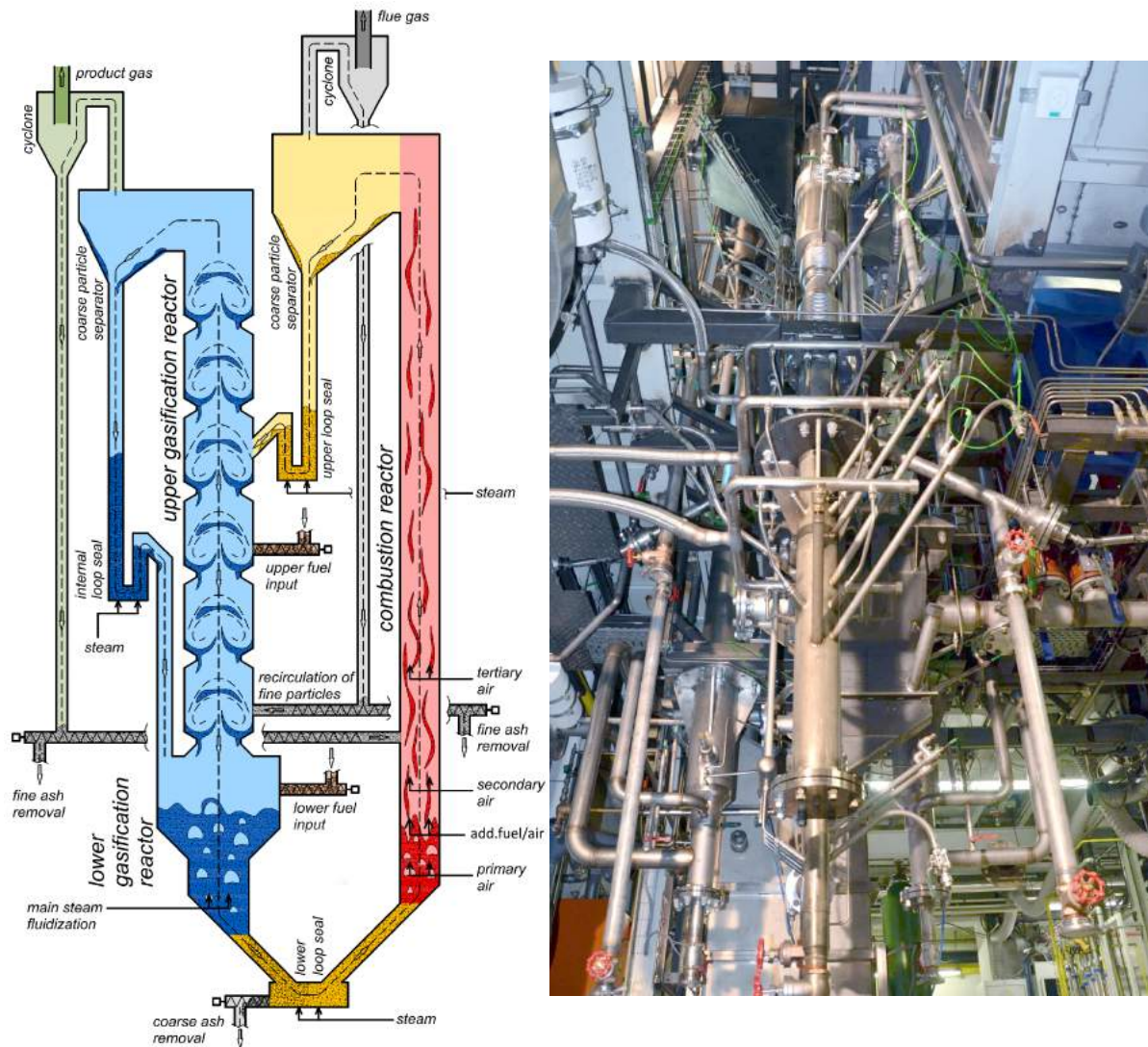


Figure 4.7: Schematic illustration of the reactor design of the novel DFB pilot plant at the TU Wien (left), modified from [78] and an illustration of the uninsulated combustion reactor (right)

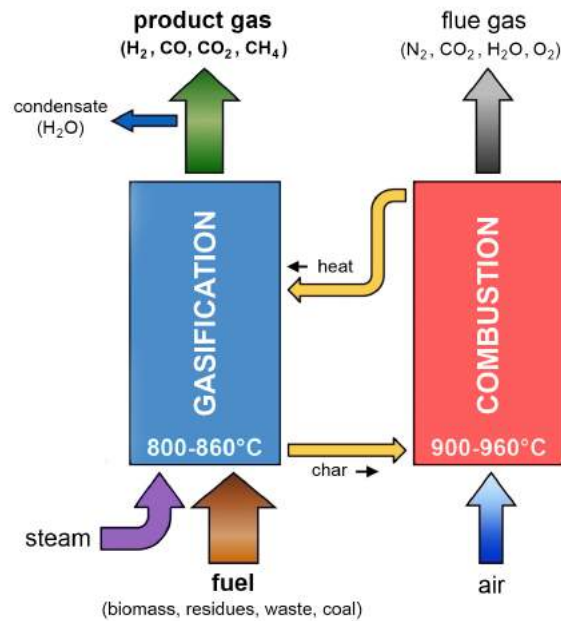


Figure 4.8: Basic principle of the Dual Fluidized Bed steam gasification system, modified from [78]

zones,

- lower attrition and abrasion effects of bed material due to a more gentle separation in using a combination of settlement chamber and cyclone separator,
- higher feedstock flexibility with higher gas quality,
- the global circulation rate is mainly controlled by the primary fluidization air supply in the CR and is no longer related to the air input for combustion in the CR,
- ash, coarse particles, and solids can be removed at the LLS during test run,
- extensive measurement, control, and safety equipment, and
- inspection glasses located at both hoppers, bubbling bed, settlement chambers, combustion chamber, and boiler.

Further features were not considered throughout this thesis but my influence the performance of the novel DFB pilot plant positively:

- recirculation of entrained fines (highly catalytic particles) by the separation unit into the gasification reactor,
- different fuel feeding positions allow the usage of feedstock with specific fuel param-

eters (with respect to the share of volatiles), and

- sampling points for fine and coarse ash in each loop seal.

The downstream units, such as gas cooling, cleaning, and utilization, are highlighted in blue in Figure 4.5. The product gas (PG) stream and flue gas (FG) stream are separately cooled down to approximately 400°C by radiation coolers to avoid tar condensation. The radiation coolers consist of a double-walled cylinder which is cooled with water in the outer layer. If necessary, air can be introduced into the cavity between hot gas and cooled water [77]. Followed by the post combustion chamber the cooled PG and FG are 1) mixed and burned in a safe manner, 2) cooled down to 200°C in a water boiler and 3) filtered in a bag filter to assure a dust free exhausted gas before it is released into the chimney. Detailed information about the design and functionality of the installed radiation coolers and further downstream units can be found in [11]. Diem [11] also published a description of the novel DFB test plant in detail. In the context of the construction of the novel DFB test plant three patents were registered [71, 86, 88].

4.4 Measuring Equipment of the Novel DFB Pilot Plant

The novel DFB pilot plant is equipped with extensive measurement equipment for better interpretation and evaluation of the data obtained during test runs. The software APROL records data continuously throughout all test runs and ensures a high safety standard. Table 4.2 lists the measuring equipment installed at the novel DFB pilot plant. Figure 4.9 presents the gas production unit. Red and gray dots symbolize measuring points for both, temperature and pressure (left). Circled sample points symbolize main temperatures used as operating temperatures for all test runs. Additional details about the measurement and control equipment can be found in [77].

Table 4.2: Overview of measuring equipment of the classical DFB and novel DFB test plant, modified from [43, 77]

	Temp.	Pressure	Mass/Vol. flow	Gas analytic	Weight	Motor speed	Level
Novel DFB test plant							
Supply	31	4	11	0	2	1	0
Gas production	50	48	0	0	0	3	0
Downstream	24	18	2	22	0	1	4
Total ¹	105 (27)	70 (16)	13 (8)	22 (22)	2 (2)	5 (2)	4 (4)

¹ Values in brackets illustrate the number of measurements at the classical DFB pilot plant

- Temperature and pressure:

The number of temperature and pressure indicators is listed in Table 4.2, where the majority of measuring indicators is positioned along the gas production unit. Pressure and temperature sensors are sketched as red and gray dots in Figure 4.9. Each dot represents a combined measuring point for temperature and pressure measuring. The temperature sensors are realized as Ni/CrNi thermocouples (Type K; range -270 - 1273°C). Pressure sensors, mainly Kalinski (0 - 500 mbar), but also Endress Hauser (0 - 1 bar) and Rosemount (0 - 1 bar) are installed [43, 77]. To clarify the positioning of temperature and pressure indicators along the bubbling bed of the GR, Figure 4.10 and 4.11 show their positions in detail.

- Mass and volume flow:

The novel DFB test plant is equipped with mass and volume flow meters, mainly used for steam and air supply. Tacosetter Tronic and Krohne (H250) instruments are applied. Barthel measuring orifices are located after both radiation coolers of each gas stream to measure the volume flow in actual cubic meters of the cooled product and flue gas. Detailed descriptions and calculations of both orifices can be found in [77].

- Gas analysis:

Several measuring devices are used to determine the composition of the product gas, flue gas, and exhausted gas (after the post combustion chamber). The product gas components H₂, CO, CO₂, CH₄, and O₂ and flue gas components CO, CO₂, O₂, NO, NO₂, SO₂, and N₂O are continuously determined by a Rosemount NGA 2000 device. The exhausted gas components CO, CO₂ and O₂ are measured also determined by a Rosemount NGA 2000 device. The water content is measured during each tar sampling. Furthermore, a Perkin Elmer gas chromatograph (GC) determines CO, CO₂, CH₄, O₂, N₂ and the hydrocarbons C₂H₄, C₂H₆, and C₃H₈ continuously every 15 minutes.

The simplified measuring chain is shown in Figure 4.12.

Since the gas chromatograph and Rosemount devices are very sensitive to particles and moisture, the gas stream undergoes a specific cleaning line. The cleaning line is shown in Figure 4.13, where dust and char are removed by a particle filter and tar components by the following impinger bottles. A more specific explanation can be found elsewhere [33].

Two separate sampling points allow to examine tar and gas compositions either above the bubbling bed in the lower part of the gasification reactor as well as after both radiation coolers. Measurements at both sampling points can be conducted simultaneously. In

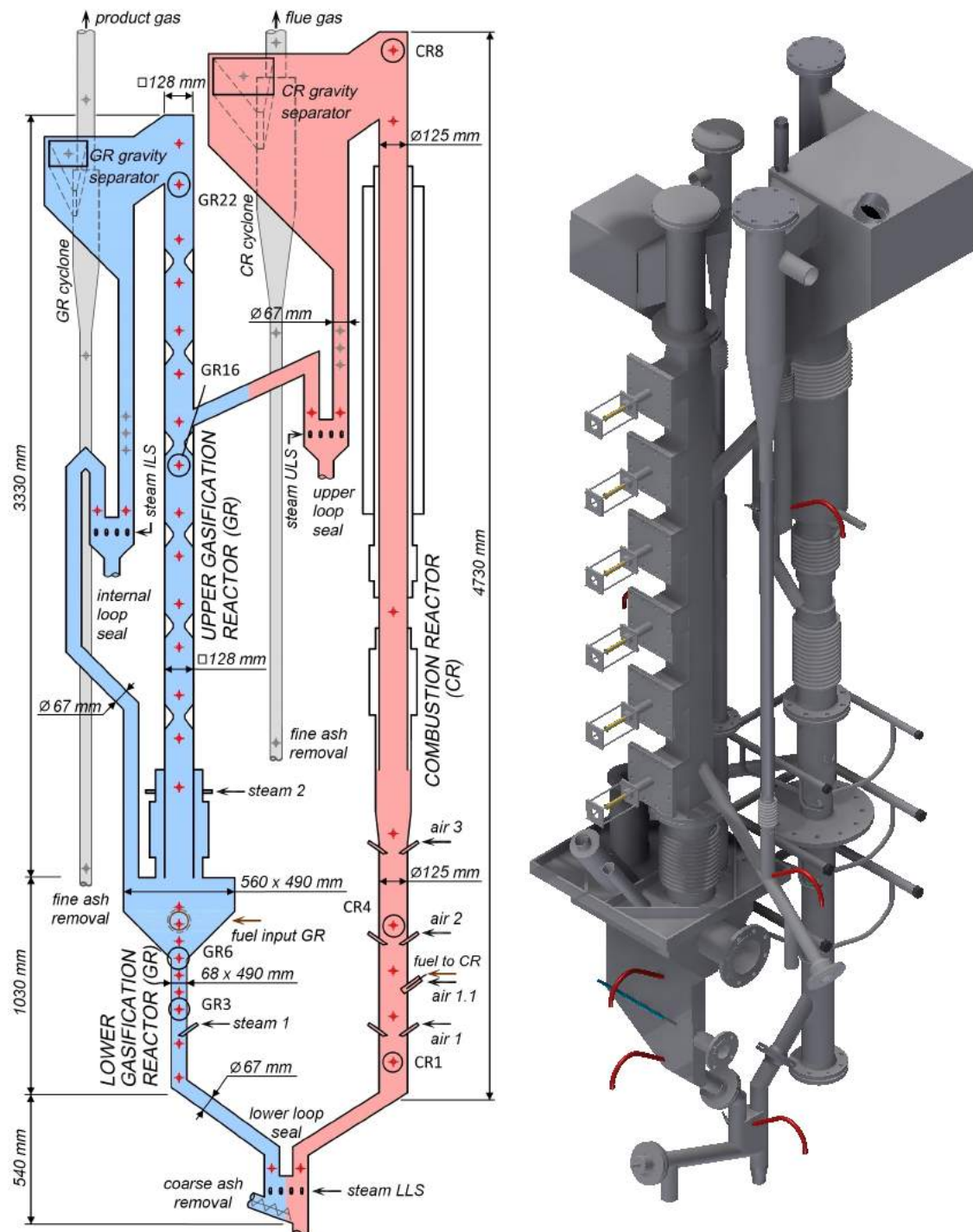


Figure 4.9: Location plan of measurements along the gasification and combustion reactor at the novel DFB pilot plant, based on [11, 78]

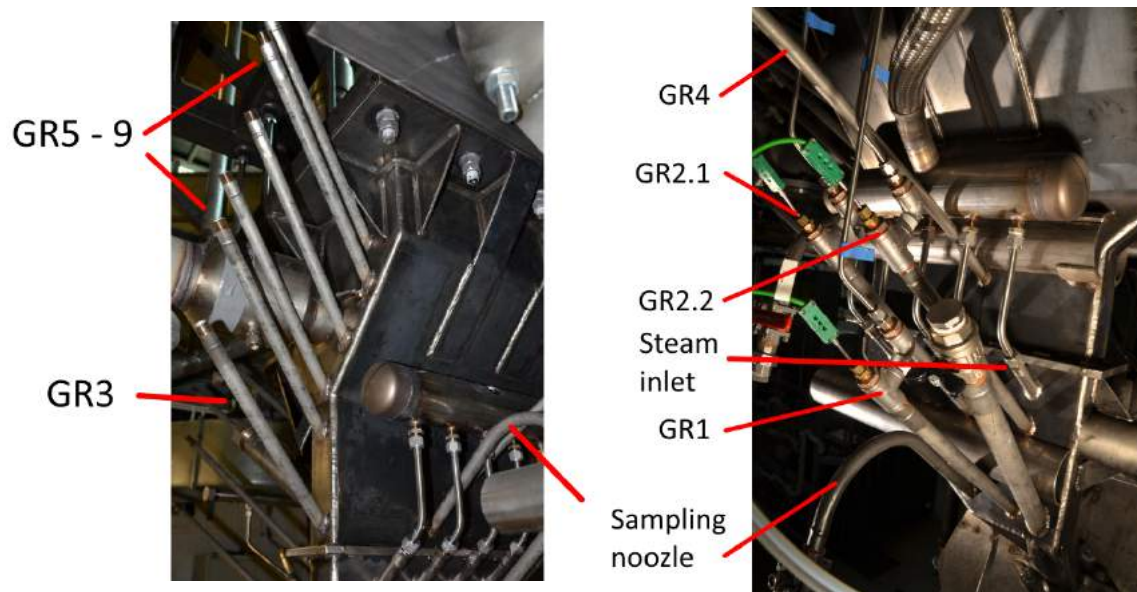


Figure 4.10: Position of measurements along the bubbling bed of the gasification reactor. GR1, GR2 and GR4 are located along the broadside, whereas GR3 and GR5 to GR9 are shifted by 90 degrees

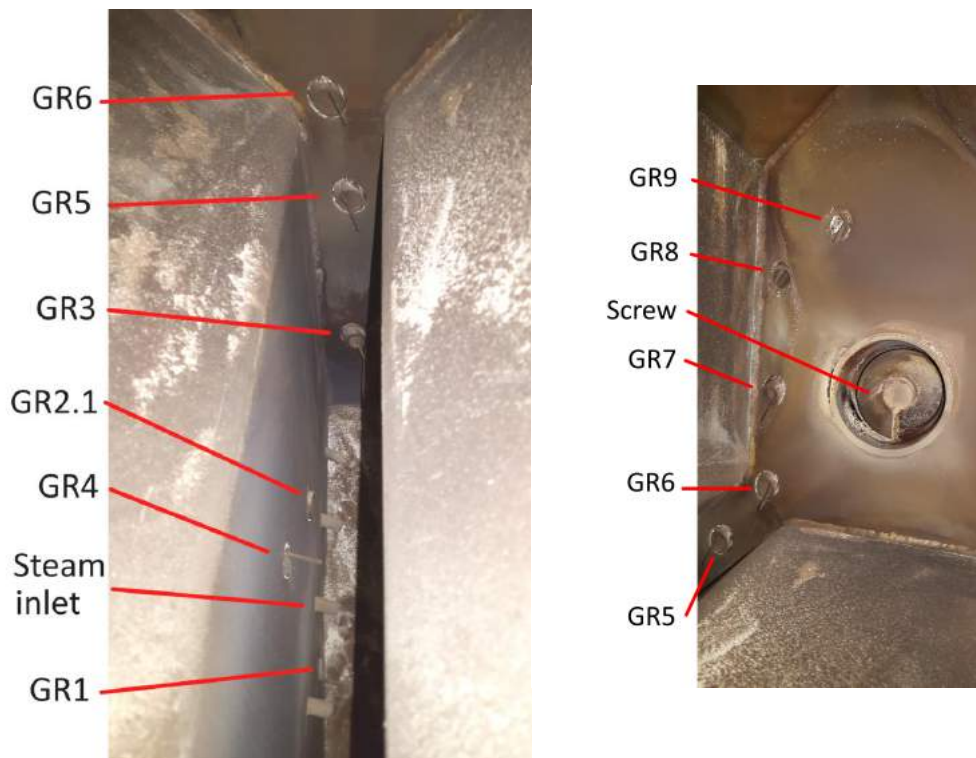


Figure 4.11: Arrangement of measurements in the bubbling bed of the GR. The feedstock screw is illustrated on the right picture. The top of the bubbling bed was between GR7 and GR8 for all investigations

Figure 4.5 both sample points are marked.

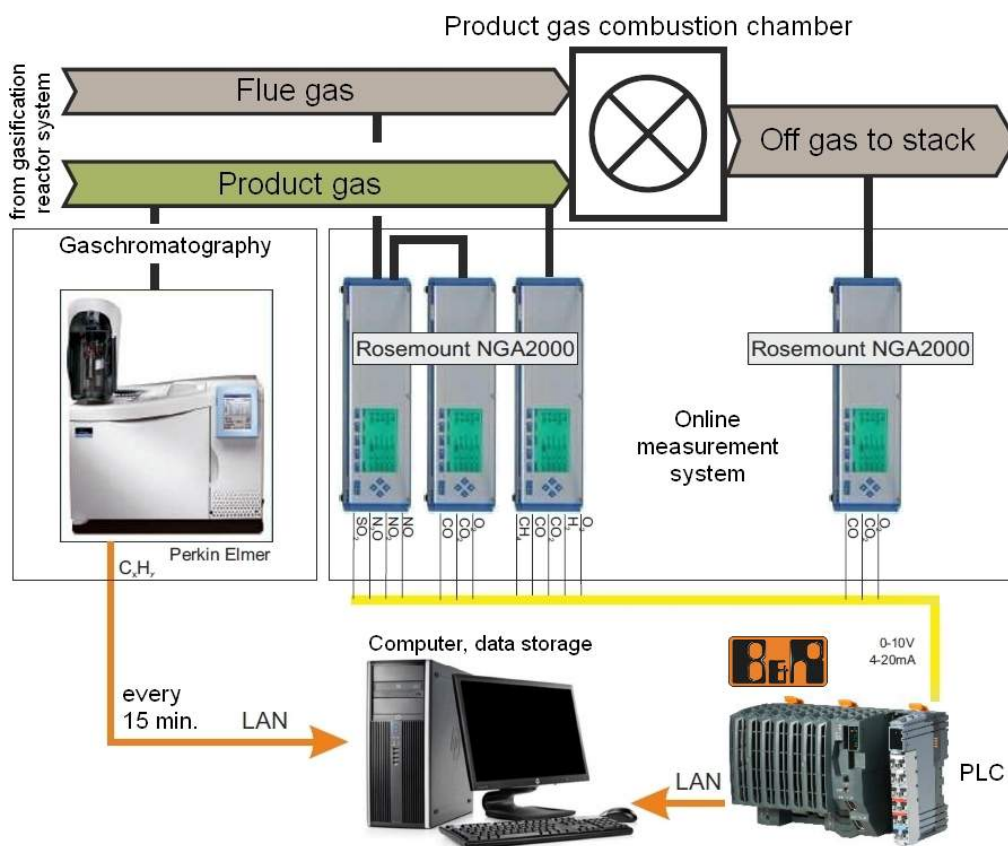


Figure 4.12: Overview of online and offline measuring devices used to determine gas components, [79]

- Tar, char, and dust measurement:

The analysis of tar, char, and dust compounds in the product gas stream is conducted with a sampling line as presented in Figure 4.14. A probe is used to sample a gas stream isokinetically. Since the sample stream includes solid particles (dust and char) a cyclone and quartz wool stuffed filter cartridge separates solid matter. To avoid tar condensation and thermal decomposition of compounds, the sampling line is heated in a given range. The sampling line includes a series of six impinger bottles, containing a tar absorbing solvent, mainly toluene. The impinger bottles are cooled in a cold bath down to -10°C to -8°C by a cryostat, where tar components condensate and are separated from the product gas stream. Liquid phases from impinger bottles are unified and separated from the water phase. To analyse GC-MS tar, a sample of the water free phase is taken for analysis. Furthermore, the solvent is removed by atmospheric evaporation, dried and weighted for gravimetric tar analysis. GC-MS tar analysis includes tar species as shown in Figure 2.4 inter alia. This measurement excludes toluene, benzene and xylene (BTX-compounds),

since toluene is used as solvent. Since gravimetric and GC-MS tar overlap in a certain range, a clear distinction between both may cause problems. A more detailed description can be found elsewhere [18, 43, 58, 62, 102]. The process of analysis, calculation and sampling for GC-MS tar is described in [26], named the guideline of the TUW. This guideline is based on the report [9], where isopropanol is used as solvent instead of toluene. Since toluene is not miscible with water, the water content of the product gas stream can be defined easily.

GC-MS tar analysis is performed by using a Perkin Elmer Autosystem XL gas chromatograph with Perkin Elmer Turbomass mass spectrometer.

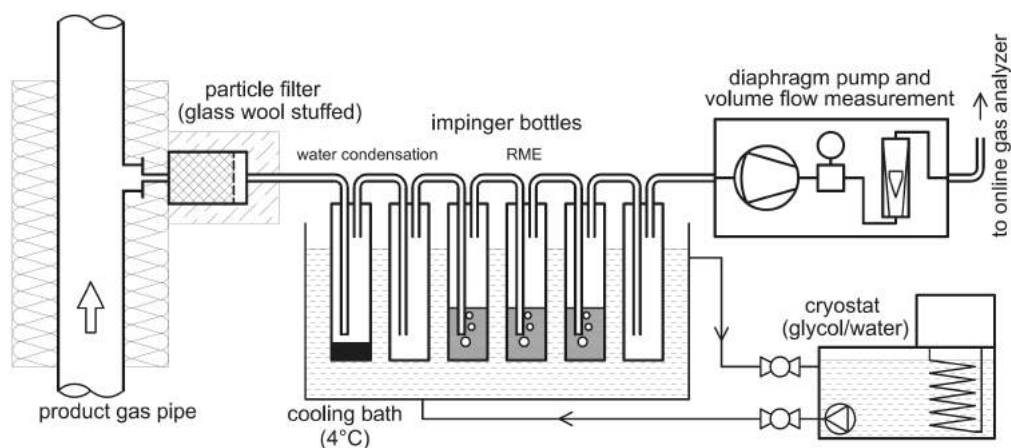


Figure 4.13: Schematic drawing of the cleaning line for gas analysis [33], modified from [92]

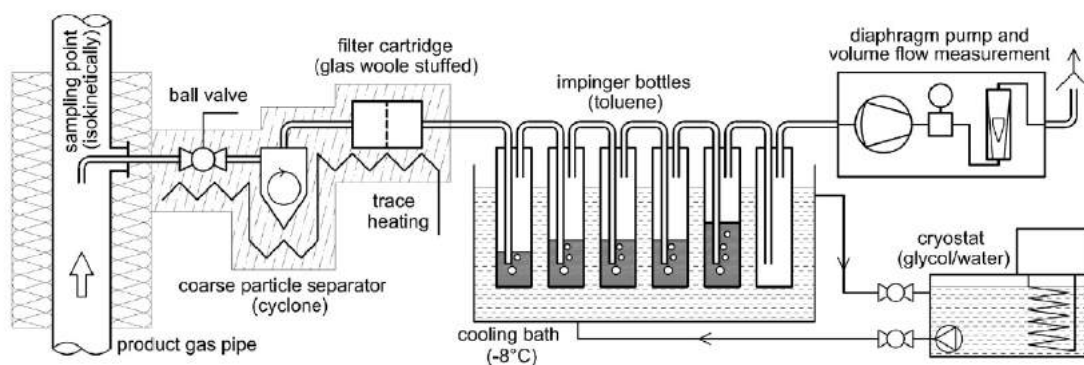


Figure 4.14: Schematic drawing of the tar sampling line [43, 92]

4.5 Solid Sampling

The novel DFB pilot plant is equipped with two different solid sampling/removal systems allowing 1) sampling of organic matter at each loop seal for further analyses and 2) removing solids at five positions during test runs. The first mentioned sampling system (cf. Figure 4.15) is positioned at each loop seal. This system allows to take samples during operation to identify state of the conversion of organic matter (residual char) and the presence of inorganic matter. The sample box is flushed with argon before sampling to ensure an inert atmosphere and thus to avoid side reactions (combustion with oxygen of carbonaceous matter). Additionally, sufficient vacuum due to a water-jet-pump allows a comfortable sampling process.

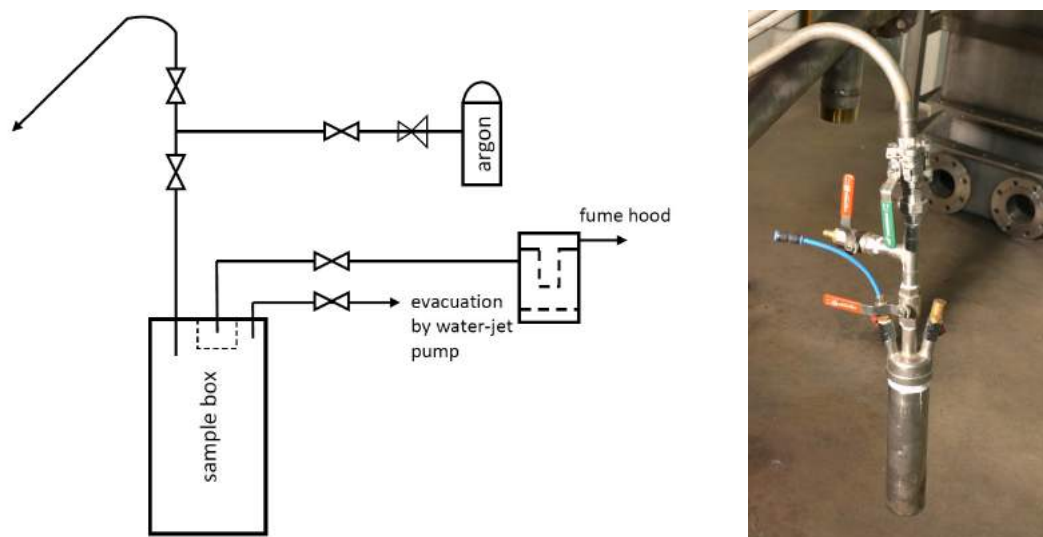


Figure 4.15: Schematic design of the sampling box for solids sampling (left) [43] and a picture during investigation at the LLS (right)

The second mentioned sampling system is constructed to remove solids, coarse, and fine ash out of system. The aim is to remove ash and inorganic matter via a conveyor at the LLS to prevent agglomeration that may inhibit the fluidized bed system. Two additional removal positions are linked with the fine ash screw conveyors after the cyclone separator of each gas pathway. Fine ash screw conveyors can be operated in opposite direction to remove fine ash and inorganic matter. This sample position enables the analysis of fine solids re-entering the gasification reactor. Two further sample positions are located after both radiation coolers. All removal boxes are made inert to avoid further reactions during sampling. No vacuum atmosphere is needed since the particles are either conveyed via screw or due to gravity. A schematic arrangement of the system is displayed in Figure 4.16. The novel DFB pilot plant was equipped with the mentioned sampling system. However,

no samples were taken throughout the first investigations.

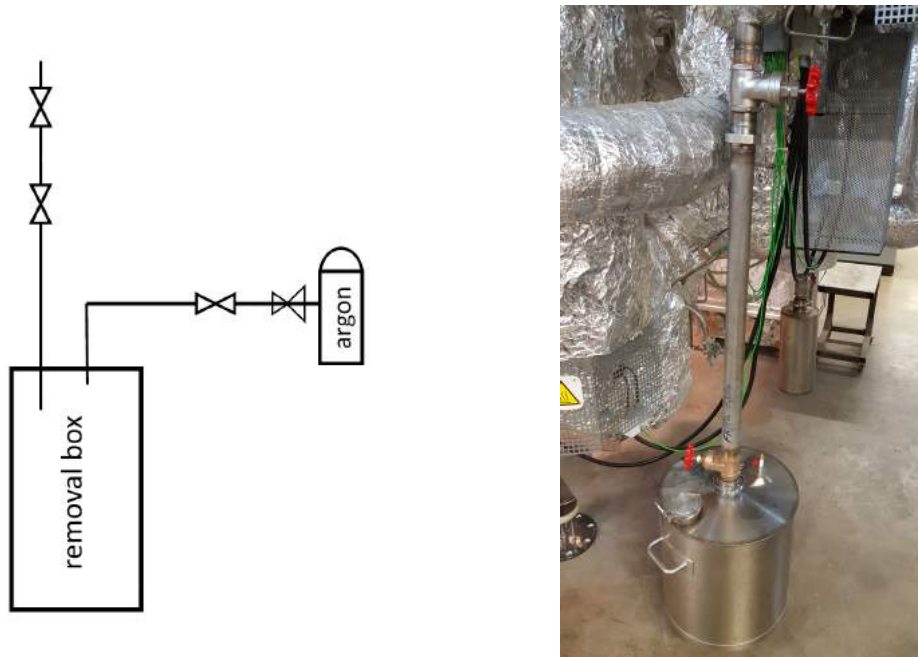


Figure 4.16: Schematic arrangement of the system to remove organic and inorganic matter (left) modified from [43] and a picture during investigation (right)

5 Experimental Results at the Novel DFB Pilot Plant

In this chapter the first results of the investigations conducted at the novel DFB pilot plant are presented. The first part deals with the test run concerning fluid dynamics in the new reactors. Furthermore, the commissioning phase of the novel DFB pilot plant using wood pellets as feedstock and fresh olivine as bed material is illustrated. All further gasification test runs were carried out using wood pellets, sugarcane bagasse pellets or exhausted olive pomace (EOP) pellets as feedstock. Fresh olivine and a mixture of fresh olivine and a defined share of limestone (abbreviated as "mixture") were used as bed material. Investigations conducted differ in fuel power (partial fuel power versus full fuel power), gasification temperature, type and properties of the bed material, steam to fuel ratio, and feedstock materials. To clarify all accomplished results, Table 5.1 gives an overview about the nomenclature of all test runs and Table 5.2 summarises main parameters of all conducted test runs.

Table 5.1: Overview of all conducted test runs and used abbreviations

Name	Date	Operation points
Experiment 1	2015_10_06	OP1 - 4
Experiment 2	2015_10_14	OP1 - 2
Experiment 3	2015_10_20	OP1 - 4
Experiment 4	2015_10_28	OP1
Experiment 5	2015_12_09	OP1

For a better illustration, Figure 5.1 depicts images of all feedstocks used for these test runs. Additionally, images of bed materials used are shown in Figure 5.2. Since a detailed analysis of the feedstock including fuel and ash properties is essential for the interpretation of processes occurring, Table 5.3 lists main feedstock properties of all feedstocks investigated. The elementary composition of olivine and limestone is presented in Table 5.4.

To better reflect the conditions prevailing during test runs, 31 temperature and pressure

Table 5.2: Overview of all accomplished test runs, related variations, and main operating parameters

Name	Feedstock	Bed material	GR3/6 [°C]	GR16 [°C]	Steam/fuel kg _{steam} /kg _{fuel,waf}	Fuel power [kW]
Temperature variation						
Experiment 1 OP1	wood pellets	fresh olivine	644/655	825	0.77	94
Experiment 1 OP2	wood pellets	fresh olivine	638/670	851	0.72	94
Experiment 1 OP3	wood pellets	fresh olivine	659/693	878	0.72	94
Experiment 1 OP4	wood pellets	fresh olivine	676/693	907	0.70	97
Load variation						
Experiment 2 OP1	wood pellets	fresh olivine	822/840	943	1.60	47
Experiment 2 OP2	wood pellets	fresh olivine	814/835	950	0.87	92
Bed material variation						
Experiment 2 OP2	wood pellets	fresh olivine	814/835	950	0.87	92
Experiment 3 OP4	wood pellets	mixture	829/848	965	0.87	97
Steam to fuel ratio variation						
Experiment 3 OP3	wood pellets	mixture	820/846	963	0.71	97
Experiment 3 OP4	wood pellets	mixture	829/848	965	0.87	97
Experiment 2 OP2	wood pellets	fresh olivine	814/835	950	0.87	92
Experiment 2 OP1	wood pellets	fresh olivine	822/840	943	1.60	47
Performance of counter-current column						
Experiment 3 OP4	wood pellets	mixture	829/848	965	0.87	97
Feedstock variation						
Experiment 3 OP4	wood pellets	mixture	829/848	965	0.87	97
Experiment 4 OP1	sugarcane bagasse	mixture	791/806	942	1.04	83
Experiment 5 OP1	EOP	mixture	737/758	861	1.06	84



Figure 5.1: Presentation of feedstocks used in this work. Milled wood and wood pellets (left), raw EOP and pelletized EOP with CaCO_3 (middle) and chopped sugarcane bagasse and sugarcane bagasse pellets (right). In order to reach better dosing characteristics and avoid blockages in the fuel dosing system, all feedstocks were pelletized



Figure 5.2: All bed materials used are shown. Fresh olivine (left), fresh limestone (middle) and a mixture of fresh olivine and fresh limestone (right)

Table 5.3: Fuel and ash analysis of feedstock used

Fuel parameter	Unit	Wood pellets [80]	Sugarcane bagasse [2]	EOP raw	EOP CaCO ₃
General parameter					
Water content	wt.-%	7.2	7.7		11.8
Volatiles	wt.-% _{db}	85.4	83.7		75.8
Residual char	wt.-% _{db}	14.6	16.3		24.2
LHV	kJ/kg	17400	16310	n.a.	15240
LHV (dry)	kJ/kg _{db}	18940	17860	18983	17620
Elemental composition					
Ash content ¹	wt.-% _{db}	0.2	2.3	4.7	11 ²
Carbon (C)	wt.-% _{db}	50.7	47.8		49.4
Hydrogen (H)	wt.-% _{db}	5.9	5.8		5.9
Oxygen (O) ³	wt.-% _{db}	43.0	43.6		38.8
Nitrogen (N)	wt.-% _{db}	0.21	0.40		1.04
Sulphur (S)	wt.-% _{db}	0.005	0.05		0.11
Chlorine (Cl)	wt.-% _{db}	0.005	0.06		0.14
Ash analysis					
SiO ₂	wt.-% _{db}	6.6	70.8		12.9
Al ₂ O ₃	wt.-% _{db}	1.6	5.6		2.5
CaO	wt.-% _{db}	55.2	4.5		11.9
Fe ₂ O ₃	wt.-% _{db}	0.9	2.1		1.2
K ₂ O	wt.-% _{db}	13.4	5.9		42.5
Na ₂ O	wt.-% _{db}	1.1	0.7		4.1
MgO	wt.-% _{db}	8.3	4.3		6.1
P ₂ O ₅	wt.-% _{db}	3.1	2.2		8.1
Others	wt.-% _{db}	9.8	5.3		10.7
Ash melting behaviour					
Softening temp.	°C	1335	1180	840	750 - 890
Spherical temp.	°C	n.m.	1210	n.m.	>1500
Hemi-spherical temp.	°C	n.m.	1260	n.m.	>1500
Flow temp.	°C	1438	1330	1440	>1500

1 Ash content at 550°C

2 Including ash, CaCO₃ and CaO

3 Oxygen content was calculated

n.m. not measured

n.a. not available

Table 5.4: Bed material analysis of olivine and limestone [84]

Fuel parameter	Unit	Fresh olivine	Limestone
CaCO ₃	wt.-%	<0.1	95 - 97
MgO	wt.-%	48 - 50	-
MgCO ₃	wt.-%	-	1.5 - 4.0
SiO ₂	wt.-%	39 - 42	0.4 - 0.6
Al ₂ O ₃	wt.-%	-	0.2 - 0.4
Al ₂ O ₃ +Cr ₂ O ₃ +Mg ₃ O ₄	wt.-%	0.7 - 0.9	-
Fe ₂ O ₃	wt.-%	8.0 - 10.5	0.1 - 0.3
CaO	wt.-%	<0.4	-
NiO	wt.-%	<0.1	-
Trace elements	wt.-%	<0.1	-
Hardness	Mohs	6 - 7	3
Particle density	kg/m ³	≈ 2850	≈ 2650
Particle density (after full calcination)	kg/m ³	-	≈ 1400

sensors were installed along the gasification and combustion reactor. Significant temperatures were selected as operating temperatures. To define overall temperatures in the bubbling bed of the gasification reactor, temperatures GR3 and GR6 were assigned. The temperature GR3 shows a representative overall temperature for the lower part of the bubbling bed, since the diameter of the bubbling bed decreases to a minimum in this part. Temperature GR6 is defined as the temperature just below the top of the bubbling bed. Since the diameter at the height of GR6 is wider compared to the bottom, gradients in temperature over the area may arise. Experiments showed a constant height of the bubbling bed throughout the entire investigations conducted at the height of sensor GR8.

The temperature profile along the height of the bubbling bed is illustrated in Figure 5.7. Obviously, an uniform temperature in the bubbling bed of the gasification reactor as expected is not observable. The reason for the outlier at the height of about 900 cm can be explained by the positioning of temperature and pressure sensors. All measurements are taken at the inside of the reactors wall, but not located one under another. Therefore temperature measurements are influenced by the gradients over the cross section. Temperatures GR1, GR2, and GR4 are located on the front side of the bubbling bed, whereas GR3 and GR5 to GR9 were shifted by 90 degree. For a better understanding, Figure 4.10 and 4.11 shows the arrangement of measurement points. Furthermore, the temperature gradients along the bubbling bed may indicate a reduced intermixing of bed material and fuel particles. In contrast to temperature sensors, pressure measurements indicate the actual pressure in the reactors without gradients over the cross section.

To describe the gasification process, mostly GR3, GR6, GR16, and GR22 are the char-

acteristic measurements. GR16 is located just below the input of hot bed material coming from the combustion reactor and represents the characteristic temperature along the counter-current column since no large gradients occur over the height. Sensor GR22 is located in the last constriction just below the connection to the separator unit of the gasification reactor and presents the temperatures at the very top of the gasification reactor.

To reflect the combustion process CR1, CR4, and CR8 are used. CR1 is located in the very bottom and CR8 at the top of the combustion reactor, still in contact with hot bed material. CR4 is located close to the additional fuel input and therefore presents the hottest part along the combustion reactor.

Two different sampling positions for tar measurements were installed. The benefit of two independent sampling points is the ability to measure tar and the product gas composition simultaneously after the gasification reactor and just above the bubbling bed of the gasification reactor. Therefore, significant assessments can be done for the performance of the counter-current column. Sampling point A is located after the radiation cooler of the product gas stream, sampling position B is just above the bubbling bed of the gasification reactor. In order to clearly assign both sampling positions, Figure 4.5 shows a schematic illustration.

The following definitions are used to define air and steam mass flows entering both reactors during test runs. All input streams are illustrated in Figure 4.9:

- steam input consists of 100% of the mass flow of steam 1, steam 2, and ILS and 75% of the mass flow of ULS and LLS, since a third of both most likely enters the combustion reactor, calculated with IPSEpro, and
- air input is defined as the sum of all air inputs entering the combustion reactor. This comprises the primary, secondary, tertiary air (air 1, air 2, air 3), and combustion air for the additional fuel (air 1.1).

To clearly assign the positions of the main operating temperatures, Figure 4.10 depicts the position of all measurements installed.

5.1 Evaluation of the Fluid Dynamics of the Novel DFB Pilot Plant

In Section 5.1 the results of the cold flow investigation conducted on the novel DFB pilot plant by Pasteiner [66] and Schmid [78] are used to compare occurring fluidization regimes during the gasification process. As comparative test run, experiment3 OP4 was considered, since best possible conditions were reached.

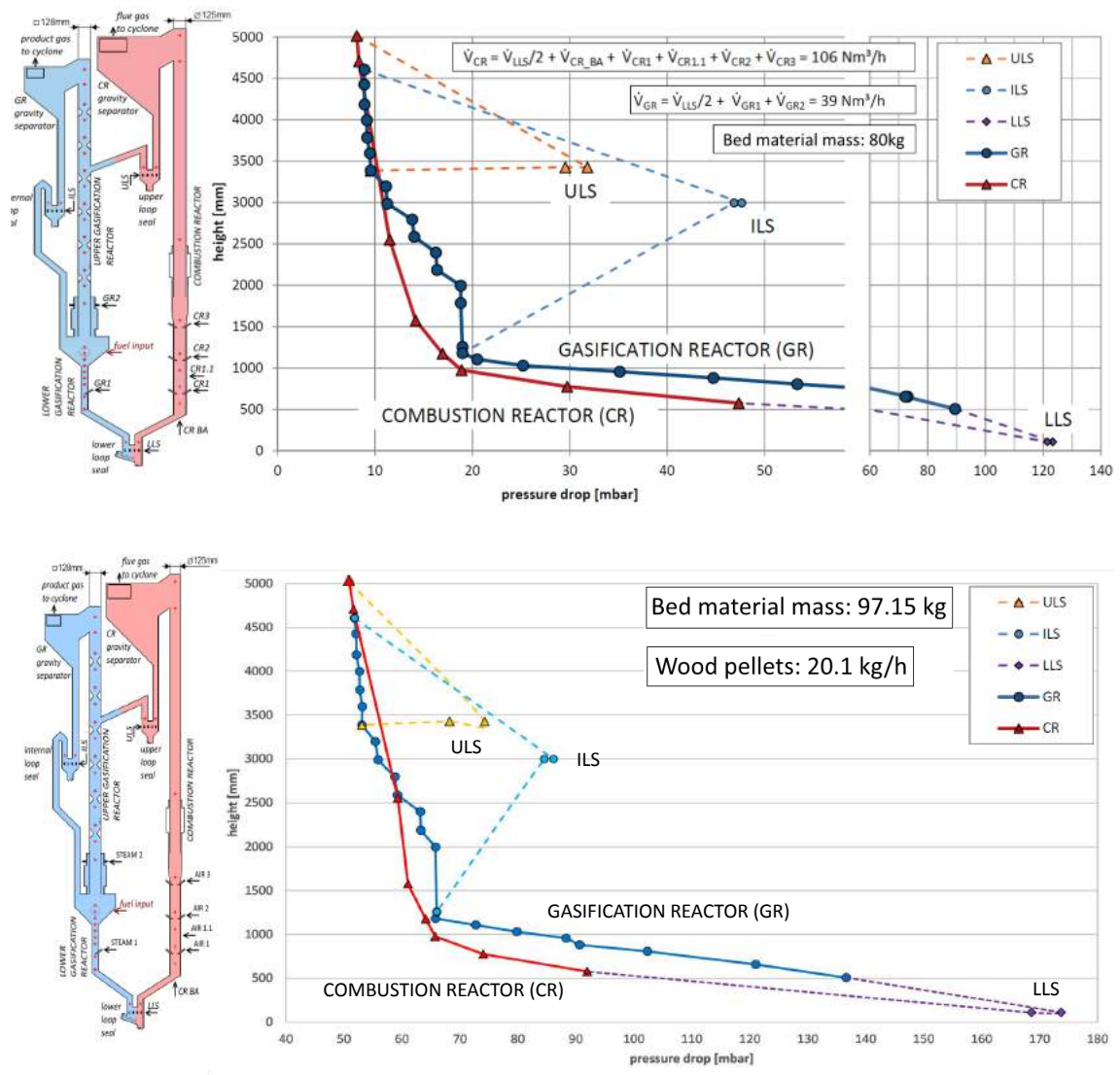


Figure 5.3: Pressure profile during the cold flow investigation in the novel DFB pilot plant [66, 78] (top) and during gasification process (below)

Pressure and pressure gradient profiles are indispensable for the examination of fluidiza-

tion regimes and bed material distribution. Therefore, pressure profiles along the height of the gasification and combustion reactor are illustrated and discussed. Figure 5.3 displays two pressure profiles, where the upper picture presents the pressure profile of the novel DFB pilot plant during the cold operation and the picture below shows the pressure profile during the gasification process. The pressure profile of the cold flow investigation was already discussed by Pasteriner [66] in detail. During the gasification process the input of steam was set to 14.1 kg/h and 63.6 Nm³/h for air, respectively. Three fluidization regimes can be recognized in the pressure profile during the gasification and cold flow mode. In the lower part of the gasification reactor, the blue line indicates a bubbling bed ending at the height of about 1000 mm. Above the bubbling bed a step-like pressure profile occurred, signaling the counter-current column with the constrictions installed. Each step presents one single constriction. The profile of the combustion reactor presents a fast fluidized bed along the entire height. For detailed information about fluidization regimes, Figure 2.7 shows the different fluidization profiles along the height.

Additionally, results of the pressure drop of all loop seals are presented. Since the static pressure difference of each loop seal is significantly higher than the pressure in the part of each reactor before and after, an intermixing of air and product gas can be avoided and therefore no nitrogen slip into the product gas stream occurs. To ensure a sufficient bed material circulation in both reactors, the pressure in the lower part of the gasification reactor should be higher than the pressure occurring in the lower part of the combustion reactor as shown in both pressure profiles.

The comparison of both pressure profiles in Figure 5.3 shows an excellent correspondence. Equal fluidization regimes occur for cold flow investigations and for gasification processes although the properties of the fluids differ.

Since the counter-current column is of special interest for reaching the aim of an enhanced contact time and intermixing of particles and fluids, Figure 5.4 depicts the upper part of the gasification reactor in detail, displayed as pressure gradient along the height. The pressure gradient presents the mass distribution over the constrictions. The higher the pressure gradient is, the more mass is held in the relevant constriction by the fluidization agent. C1 to C6 indicate all constrictions along the column as shown schematically on the left side.

The pressure profile in Figure 5.4 represents a nearly equally distributed counter-current column. Only constriction two (C2) shows a slightly higher pressure gradient and therefore a higher particle hold up. Thus, constriction five (C5) and six (C6) above the inlet of hot bed material from the combustion reactor differ. Since bed material particles from the

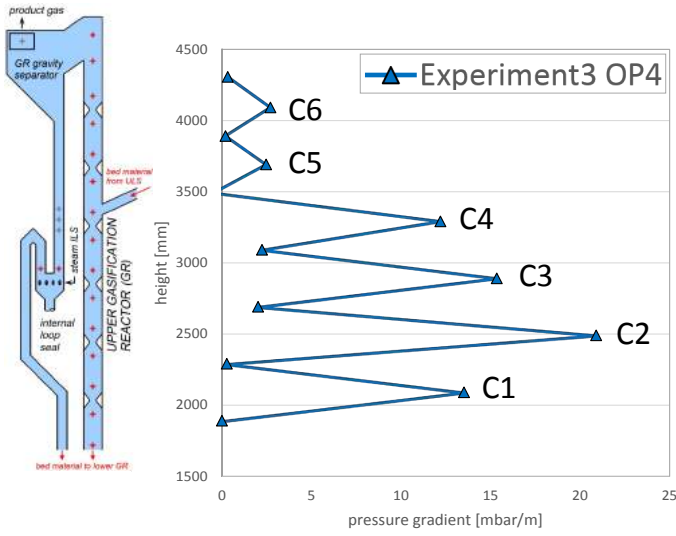


Figure 5.4: Pressure gradient profile of the counter-current column of the gasification reactor during gasification process

combustion reactor enter the counter-current column just above constriction four, the solids move downwards reverse to the gas flow of volatiles and steam. Therefore, only fine particles are carried into the region of constriction five and six, resulting in lower pressure gradients and temperatures. At the height of 3500 mm a pressure gradient below 0 is illustrated. Theoretically a pressure gradient below 0 cannot be realized, but measuring errors lead to this result. The pressure gradient was calculated according Eq. 5.1 [56].

$$p(H_\alpha)dH = \lim_{H_i \rightarrow H_\alpha} \left(\frac{p(H_\alpha) - p(H_i)}{H_\alpha - H_i} \right) \cong \frac{p(H_j) - p(H_i)}{H_j - H_i} \quad (5.1)$$

$$H_\alpha = H_i + \frac{H_i - H_j}{2}$$

The fluidization diagram proposed by Grace can be used to visualize the occurring fluidization regimes. Relevant operating points published by Pasteiner are compared to those of experiment 3 OP4. The dimensionless velocity u^* and dimensionless particle diameter d_p^* were calculated for an operating point in the lower GR, in the free section of the counter-current reactor and constriction of the counter-current reactor. Thus, both dimensionless numbers were calculated to visualize an operating point in the combustion reactor. The definition of both parameters was described in Subsection 2.3.3. Relevant fluid dynamics parameters are listed in Table 5.5.

Table 5.5: Parameter of the test runs operated as cold flow and gasification process, modified from [66]

Operation parameter	Unit	Cold flow operation		Experiment 3 OP4			
		Pasteiner [66]	Lower GR	GR	GR	GR	CR
Temperature	°C	20	835	847	965	965	968
Pressure in the reactors	bar	ambient pressure					
Gas density ρ_g	kg/m ³	1.18	0.21	0.21	0.19	0.19	0.28
Particle density ρ_p	kg/m ³	2900	2900	2900	2900	2900	2900
Kinematic viscosity ν	m ² /s	1.5×10^{-5}	1.7×10^{-4}	1.7×10^{-4}	2.0×10^{-4}	2.0×10^{-4}	1.7×10^{-4}
Sauter diameter d_{sv}	μm	118	285	285	285	285	285
Sphericity ϕ	-	≈ 0.85	≈ 0.85	≈ 0.85	≈ 0.85	≈ 0.85	≈ 0.85
Archimedes number Ar	-	176	110	107	83	83	81
Dimensionless particle diameter d_p^*	-	5.6	4.8	4.7	4.4	4.4	4.3
Dimensionless velocity U^*	-	- ¹	0.1	0.5	1.1	3.2	4.2
Bed material inventory	kg	80	97	97	97	97	97
Superficial gas velocity U	m/s	n.p.	0.31	1.41	3.35	10.1	10.8
Cross section for calculation	mm	68 x 490	68 x 490	68 x 490	128 x 128	43 x 126	∅125

¹ As illustrated in Figure 5.5

Measuring orifices were used to calculate volume flows of the product and flue gas. To simplify the illustration and calculation, all constrictions were expected to be fully open. Thus, different bed material particle diameters were neglected, since the majority of bed material (73%) has a sauter diameter of $d_p = d_{sv} = 285 \mu\text{m}$. Schmalz showed a deviation of the volume flow calculation to volume flow measuring of 7%, where the calculated value resulted in too high values [77], but in good agreement with simulation data. Figure 5.5 depicts the Grace diagram including all operating points inspected. Red and blue symbols show the results of the cold flow model investigations, whereas black symbols present the accomplished results of experiment 3 OP4 conducted at the novel DFB pilot plant. The results show a very good accordance of both test runs for occurring fluidization regimes. The novel DFB pilot plant results in an operation field for the bubbling bed in the GR. The minimum value of the bubbling bed was calculated with a minimum gas volume flow only comprising of the steam input of steam 1. The maximum value was calculated with the full product gas flow measured by the orifice after the gasification reactor. Since the real gas flow is not known, u^* lies inbetween the operation field displayed.

5.2 Commissioning Test Run at the Novel DFB Pilot Plant

After checking all sensors, actuators, cooling and heating cycles, a first commissioning test run was conducted. For this investigation wood pellets as feedstock and fresh olivine as bed material were used. Relevant temperatures during commissioning are displayed in Figure 5.6. No analysis of the product gas was conducted, since the primary aim was to prove main procedures during heating up, gasification, and cooling down mode.

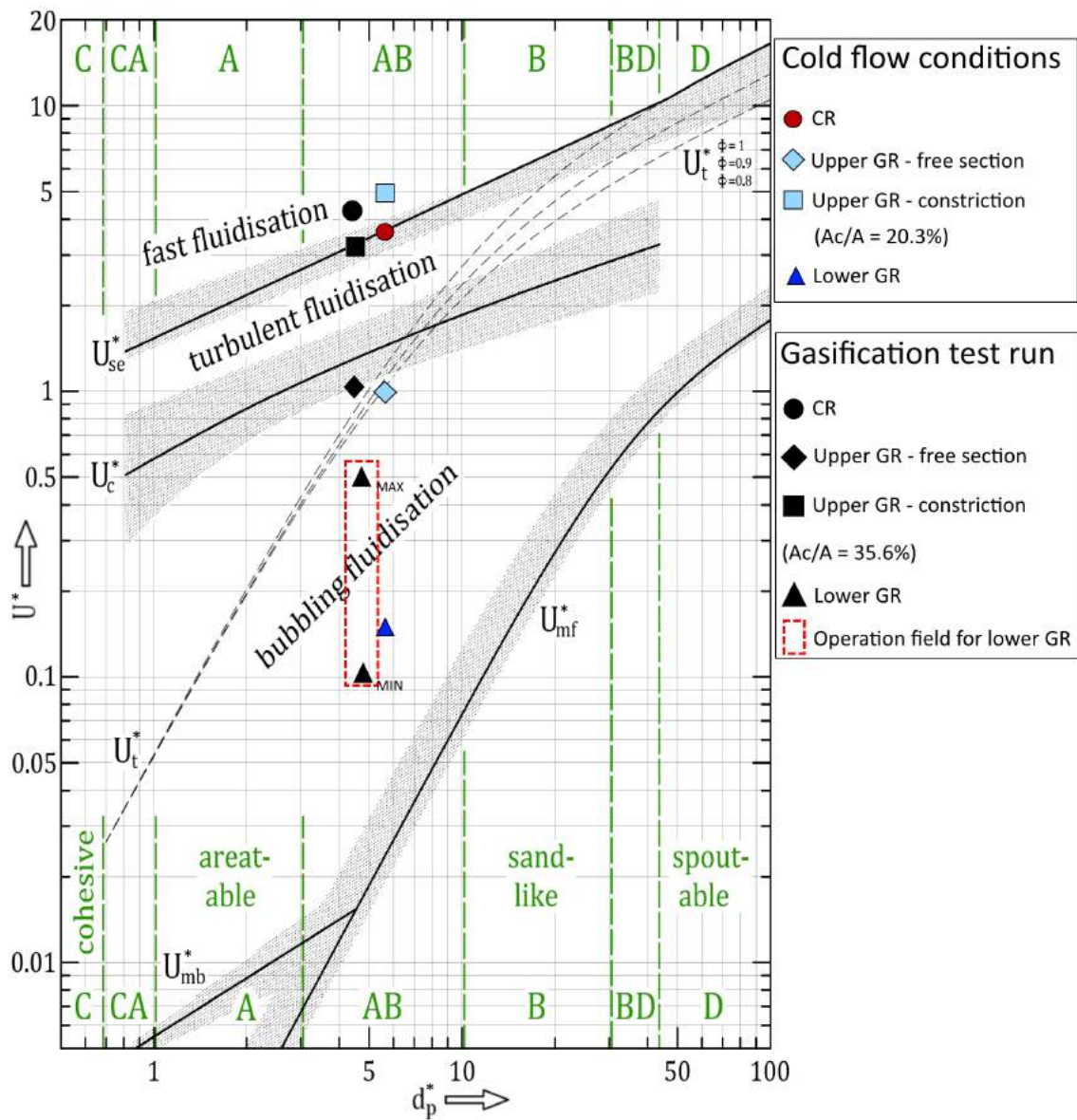


Figure 5.5: Operating points of the novel DFB pilot plant for the cold flow investigation and the gasification process modified from Pasteiner [66]. Both axes of the regime map are indicated in logarithmic units [78]

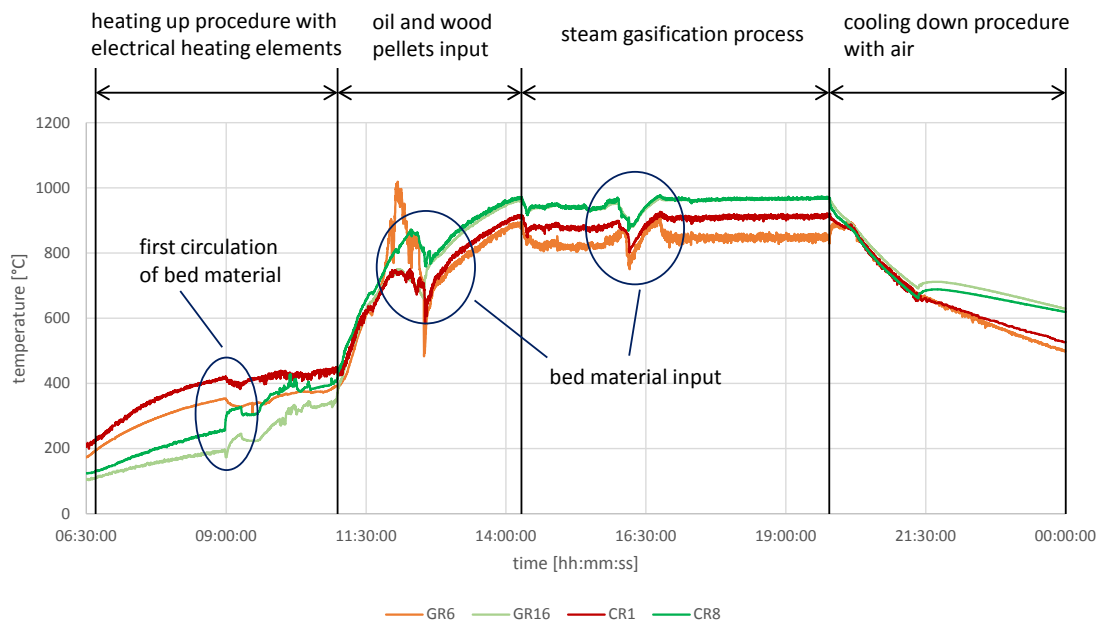


Figure 5.6: Progress of relevant gasification and combustion temperatures during commissioning test run

The overall process of a test run can be divided into four sections:

- heating up procedure using electrical heating elements,
- heating up procedure using electrical heating combined with combustion of wood pellets together with fuel oil,
- gasification process using steam as fluidization agent, and
- cooling down process.

The heating up procedure was conducted with electrical heating elements. All air inlets of the CR and GR were heated electrically up to a maximum temperature of 620°C. In the first phase temperatures in the bubbling bed of the GR should exceed 450°C, since the ignition temperature of wood pellets is above 400°C. Simultaneous, the temperature in the combustion reactor near the oil-inlet (CR4) should rise above 450°C to exceed the ignition temperature of fuel oil. This first step during the commissioning run lasted for about 5 hours. Figure 5.6 shows a sharp increase of all temperatures when firing of wood pellets and oil started. Experiences gained from the classical DFB pilot plant showed better heating up conditions feeding wood pellets first. At 9:00 the fluidization flow was increased resulting in a first circulation of bed material from the CR to the GR. Hot bed material from the CR was transported to the GR, where the counter-current

column was heated up first. The colder bed material from the lower gasification reactor was transported to the lower part of the combustion reactor, resulting in a decrease of temperature CR1.

Since the overall gasification reaction is endothermic, temperatures in the GR should be above the desired gasification temperatures of about 850°C before the gasification process itself started. Otherwise the temperatures in both reactors will decrease below the desired temperatures, when switching to steam fluidization.

At 14:15 the fluidization was switched to steam. After switching to steam, a steady state period during gasification process was desired and realized. Fresh bed material was added twice to the process, resulting in a decrease of all temperatures. As shown in Figure 5.6, adding cold bed material does not influence the process significantly and return to a steady state process very quickly.

The cooling down procedure starts with turning off the feeding screw and the oil input. At 20:00 the steam input was switched to air due to safety reasons to burn off remaining carbon, although steam is more efficient for the cooling process than air. The long period until the temperatures in both reactors reach values below 100°C confirms the high quality of the insulation.

5.3 Temperature Variation

Experiment 1 and 2 were combined to examine the influence of the gasification temperature on the performance of the novel DFB pilot plant. Main focus was placed on the deviation of the product gas composition (H_2 , CO, CO_2 , CH_4 , and higher hydrocarbons) and tar values (GC-MS and gravimetric). Experiment 1 was split into three operating points, OP1, OP2, and OP4 differing mainly in gasification temperature. All further operating parameters were held as constant as possible in order to achieve comparable conditions. Both experiments were carried out using wood pellets as feedstock and fresh olivine as bed material. Throughout all operating points, the fuel input was kept nearly constant at a value of 19.0 to 20.0 kg/h, respectively 92 to 97 kW. The steam to fuel ratio was in a range of 0.70 to 0.87 $kg_{steam}/kg_{fuel,waf}$. Tar and GC measurements were taken at sampling position A. The gasification temperature GR6 was varied in the range of 655 to 835°C.

For a better overview, Table 5.6 shows the main operating parameters of the accomplished test run. Since bed material properties have not been discussed yet in this section,

this table lists important information.

Table 5.6: Overview of operating parameters of the accomplished test run

Operation parameter	Unit	Experiment 1 OP1	Experiment 1 OP2	Experiment 1 OP4	Experiment 2 OP2
General bed material parameter					
Type of bed material	-	fresh olivine			
Fine bed material inventory	kg		0		12 (100 - 200 μ m)
Coarse bed material inventory	kg		83 (200 - 300 μ m)		70 (200 - 300 μ m)
Total bed material inventory	kg		83		82
Gasification reactor					
Feedstock	-	wood pellets			
Fluidization regime lower GR	-	bubbling bed			
Fluidization regime upper GR	-	turbulent zones			
Fuel feeding position in lower GR	-	on-bed feeding			
Temperature GR3	$^{\circ}$ C	644 \pm 4	638 \pm 3	676 \pm 2	814 \pm 3
Temperature GR6	$^{\circ}$ C	655 \pm 5	670 \pm 6	693 \pm 5	835 \pm 6
Temperature GR16	$^{\circ}$ C	825 \pm 4	851 \pm 4	907 \pm 2	950 \pm 2
Feedstock input	kg/h	19.5	19.4	20.0	19
Feedstock input	kW	94	94	97	92
Steam to fuel ratio	kg _{steam} /kg _{fuel,waf}	0.77	0.72	0.70	0.87
Steam to carbon ratio	kg _{steam} /kg _{carbon}	1.53	1.42	1.38	1.72
Total fluidization steam input	kg/h	12.9	11.9	11.8	14.3
Combustion reactor					
Fluidization regime	-	fast fluidized bed			
Temperature CR4	$^{\circ}$ C	893 \pm 11	913 \pm 12	984 \pm 8	978 \pm 8
Temperature CR8	$^{\circ}$ C	836.0 \pm 4	860 \pm 5	922 \pm 2	952 \pm 3
Fuel to combustion reactor	kW	53	53	53	46
Total air input	Nm ³ /h	58.8	58.8	63.9	58.8

Figure 5.7 shows the temperature profile (average values) of both reactors over the height for experiment 2 OP2. The counter-current column with its constrictions installed is shown in the upper part of the left profile, presenting the hottest part in the gasification reactor. Above the inlet of hot bed material from the CR to the GR a significant decrease of the temperature can be observed. This decrease may be explained by three phenomena. First, fine bed material and fuel particles are still present in this area and may promote endothermic gasification reactions. Furthermore, the upper part of the column is equipped with the settlement chamber. Since the diameter of the separator is far greater than the diameter of the column, heat losses may be dominant. Finally, the heat transport to the upper zone is small compared to the sections below, since only small particles are present there.

The bubbling bed of the gasification reactor does not show a consistent temperature over the height. As discussed in the introduction of Chapter 5, outliers occur due to different positions of the measurements. This profile substantiates the assumption that the intermixing of the bubbling bed does not result in a constant bed temperature, but in gradients over the cross section.

The combustion reactor shows a temperature profile as expected. The strong increase at the height between 700 - 1200 mm can be explained by the combustion of additional fuel and residual char. Above this maximum, a nearly constant temperatures along the

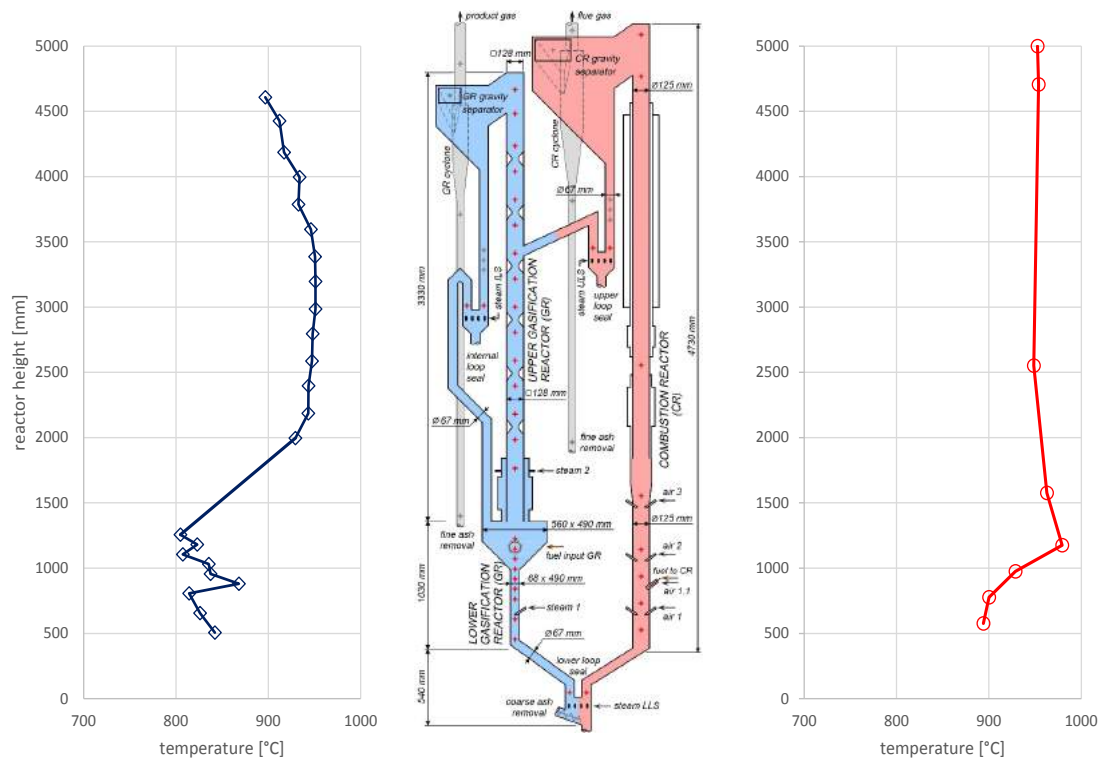


Figure 5.7: Average temperatures of experiment 2 OP2 along the height of both reactors are shown. The blue profile shows the GR, whereas the red profile shows the CR

height of the combustion reactor is shown, illustrating a fast fluidized bed.

The trends of the main product gas species are shown in Figure 5.8. The gasification temperature GR6 is used as characteristic temperature for the variation conducted. Rising gasification temperatures from 655 - 835°C lead to a strong increase of hydrogen from 23.8 to 38.7 vol.-%_{db} and a strong decrease of methane from 14.9 to 9.1 vol.-%_{db}. Carbon monoxide shows a slight decrease from 35.3 to 27.1 vol.-%_{db}, whereas carbon dioxide was slightly evaluated from 17.1 to 18.5 vol.-%_{db}. Ethylene inclines significantly down from 4.3 to 1.6 vol.-%_{db}.

Figure 5.9 presents trends of tar species along rising gasification temperature. It can be seen that the content of tar species are affected by the gasification temperature to lower values. A strong decrease of GC-MS and gravimetric tar are displayed down from 24.6 to 11.2 g/Nm³_{db} for GC-MS tar and 15.0 to 6.7 g/Nm³_{db} for gravimetric tar. The trend of ethylene is shown in Figure 5.9 to underline the statement of Kern. He published a correlation for the content of ethylene to the content of GC-MS tar to lower GC-MS tar at decreasing ethylene contents [29].

These findings agree with results of Kirnbauer et al. [38]. He reported the influence of the gasification temperature on tar reforming processes. Higher gasification temperatures lead to lower values of GC-MS and gravimetric tar. However, a recombination of tar compounds may occur at very high gasification temperatures and therefore negatively influence the tar reforming processes. A minimum of tar compounds in the product gas was measured at gasification temperatures of about 800°C.

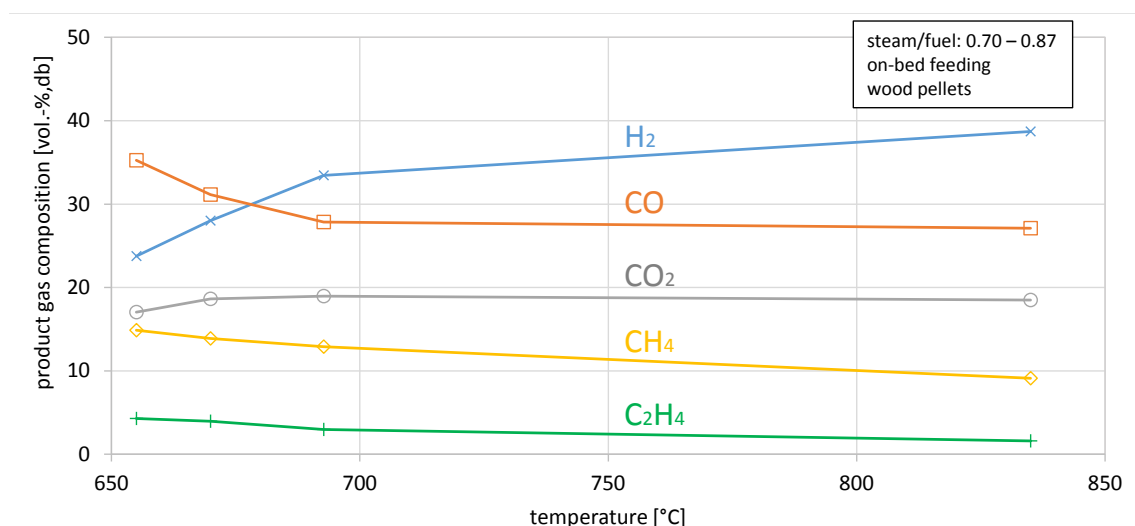


Figure 5.8: The impact of temperature variation on the contents of H₂, CO, CO₂, CH₄, and C₂H₄

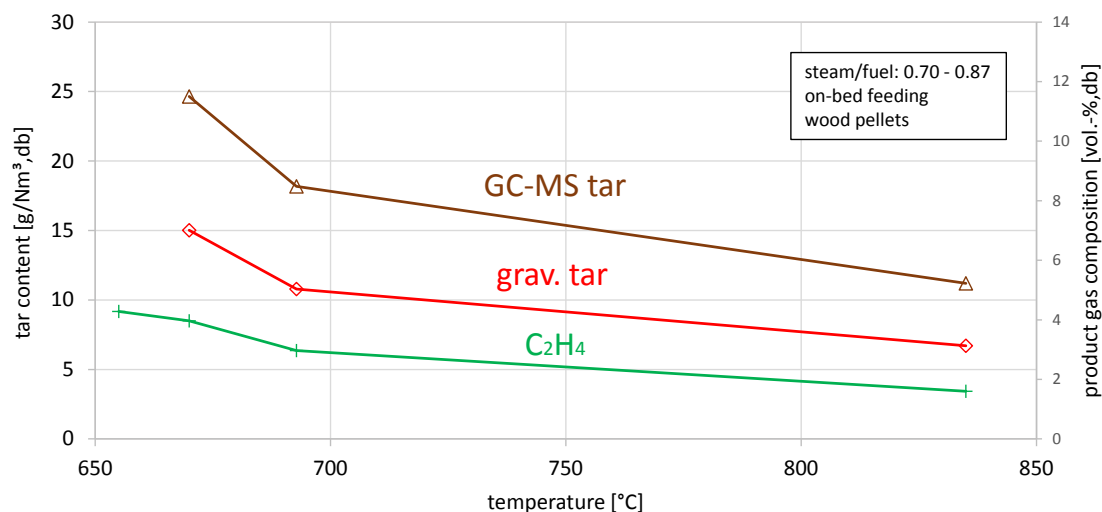
Figure 5.9: Progress of C₂H₄, GC-MS, and gravimetric tar

Table 5.7 lists values of main product gas components and tar species for the gasification temperature variation. The water content as well as dust and char contents of the product gas are shown.

Table 5.7: Comparison of product gas composition at varying gasification temperatures (GR6). All other gases, mainly nitrogen result in less than 2 vol.-%_{db} in total

	Unit	Experiment 1 OP1	Experiment 1 OP2	Experiment 1 OP4	Experiment 2 OP2
Temperature GR3	°C	644±4	638±3	676±2	814±3
Temperature GR6	°C	655±5	670±6	693±5	835±6
Temperature GR16	°C	825±4	851±4	907±2	950±2
H ₂	vol.-% _{db}	23.8±0.6	28.0±0.6	33.4±0.4	38.7±0.3
CO	vol.-% _{db}	35.3±0.7	31.1±0.6	27.9±0.2	27.1±0.3
CO ₂	vol.-% _{db}	17.1±0.2	18.6±0.2	19.0	18.5±0.5
CH ₄	vol.-% _{db}	14.9	13.9±0.2	12.9±0.3	9.1±0.2
C ₂ H ₄	vol.-% _{db}	4.3	4.0	3.0	1.6
C ₂ H ₆	vol.-% _{db}	0.6	0.5	0.2	0.1
C ₃ H ₈	vol.-% _{db}	0.03	0.02	0.0	0.0
Water content	vol.-%	n.m.	48	42	43
GC-MS tar	g/Nm ³ _{db}	n.m.	24.6	18.2	11.2
Grav. tar	g/Nm ³ _{db}	n.m.	15.0	10.8	6.7
Dust content	g/Nm ³ _{db}	n.m.	0.1	0.3	0.3
Char content	g/Nm ³ _{db}	n.m.	1.1	1.0	2.4

n.m. not measured

Kirnbauer et al. published product gas compositions at varying gasification temperatures between 740 - 880°C, using used olivine as bed material and wood pellets as feedstock. Kirnbauer measured hydrogen to have the greatest share, followed by carbon monoxide and carbon dioxide in nearly same amounts and methane to be the lowest at a gasification temperature of 820°C. The tendency to higher contents of CO and lower contents of CO₂

with increasing gasification temperature was published [38].

Hofbauer and Rauch [25] published similar results as Kirnbauer for temperatures in the range of 780 - 900°C. These results show that not only the gasification temperature influences the product gas composition, but also the steam to fuel ratio, the type of bed material (catalysts), and fuel properties. All results match closely with the published results at the novel DFB pilot plant.

5.4 Fuel Power Variation

The intention of experiment 2 was mainly to evaluate the performance of the novel DFB pilot plant in terms of quick changes in the fuel power. Product gas species and tar contents are displayed but not discussed in detail, since operating parameters were not in similar ranges. Regarding the steam to fuel ratio, significant deviations were inspected in the range of 0.87 - 1.60. The investigation was carried out using wood pellets as feedstock and fresh olivine as bed material. Two different operating points, OP1 and OP2, were analysed. Only sampling point A was taken into account.

Along operating point 1, the feedstock was fed onto the bubbling bed with an amount of 9.8 kg/h, respectively 47 kW, whereas OP2 was executed by feeding 19.0 kg/h or 92 kW. All other relevant parameters were held as constant as possible. The gasification temperature in the bubbling bed varied between 814 to 822°C for GR3 and between 835 to 840°C for GR6. GR16 was mainly in the range of 943 to 950°C. The total fluidization steam input was 13.2 kg/h, in average throughout the entire test run, which corresponds to a steam to fuel ratio of 1.60 for OP1 and 0.87 for OP2. In both cases the bed material consisted of different particle diameters as shown in Table 5.8. A small fraction of the total inventory (15%) consisted of fresh olivine with a mean particle diameter of 100 - 200 μm , the remaining part was fresh olivine with a mean diameter of 200 - 300 μm .

Figure 5.10 shows main gasification and combustion temperatures during the investigation. Times of tar and GC measurements are illustrated. Obviously, temperature GR22 increases for higher fuel power. Data of pressure gradients show higher values for constriction five and six. Therefore, it can be assumed that a high fraction of hot bed material and fines are accumulated in this zones and may led to higher temperatures in the area above the inlet of ULS. To maintain a proper overview of the test run, Table 5.8 presents all relevant operation parameters.

Table 5.9 gives a detailed overview of the product gas composition of both operating

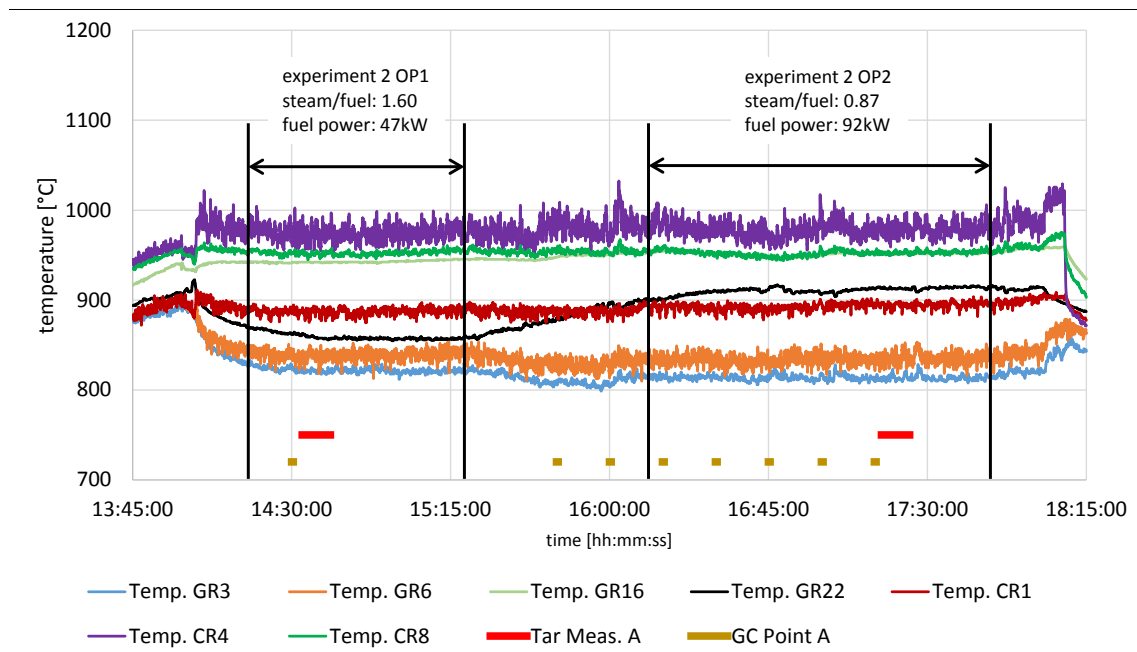


Figure 5.10: Progress of relevant temperatures of both reactors during gasification process. Operating points and sampling times are depicted

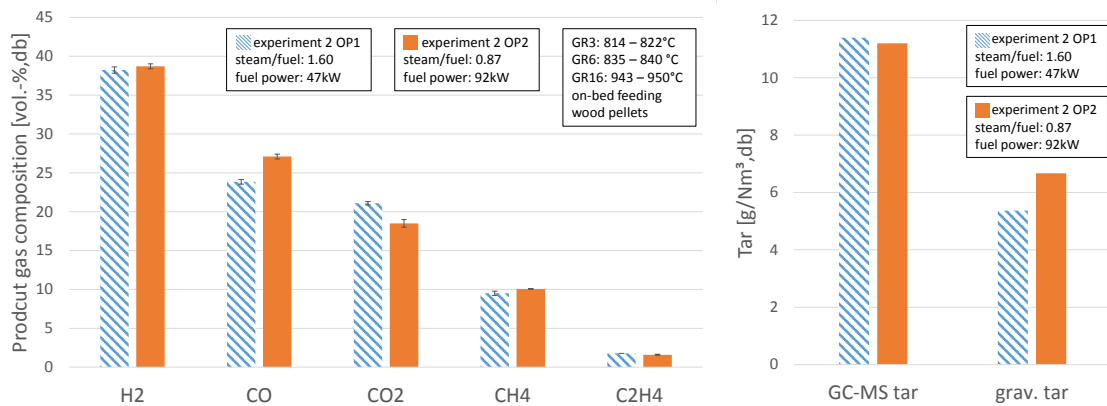


Figure 5.11: Values for main product gas components (left) and for GC-MS and gravimetric tar (right) at varying fuel power and steam to fuel ratio

Table 5.8: Summary of main operating parameter for fuel power variation

Operation parameter	Unit	Experiment 2 OP1	Experiment 2 OP2
General bed material parameter			
Type of bed material	-	fresh olivine	
Fine bed material inventory	kg	12 (100 - 200 μ m)	
Coarse bed material inventory	kg	70 (200 - 300 μ m)	
Total bed material inventory	kg	82	
Gasification reactor			
Feedstock	-	wood pellets	
Fluidization regime lower GR	-	bubbling bed	
Fluidization regime upper GR	-	turbulent zones	
Fuel feeding position in lower GR	-	on-bed feeding	
Temperature GR3	$^{\circ}$ C	822 \pm 3	814 \pm 3
Temperature GR6	$^{\circ}$ C	840 \pm 5	835 \pm 6
Temperature GR16	$^{\circ}$ C	943 \pm 1	950 \pm 2
Feedstock input	kg/h	9.8	19.0
Feedstock input	kW	47	92
Steam to fuel ratio	kg _{steam} /kg _{fuel,waf}	1.60	0.87
Steam to carbon ratio	kg _{steam} /kg _{carbon}	3.17	1.72
Total fluidization steam input	kg/h	14.1	14.3
Combustion reactor			
Fluidization regime	-	fast fluidized bed	
Temperature CR4	$^{\circ}$ C	974 \pm 8	978 \pm 8
Temperature CR8	$^{\circ}$ C	952 \pm 2	952 \pm 3
Fuel to combustion reactor	kW	56	46
Total air input	Nm ³ /h	50.0	58.8

 Table 5.9: Comparison of product gas composition at varying fuel load parameters. Other gases, mainly nitrogen show a maximum of 3.0 vol.-%_{db}

	Unit	Experiment 2 OP1	Experiment 2 OP2
Fuel power	kW	47	92
H ₂	vol.-% _{db}	38.2 \pm 0.3	38.7 \pm 0.3
CO	vol.-% _{db}	23.8 \pm 0.2	27.1 \pm 0.3
CO ₂	vol.-% _{db}	21.1 \pm 0.2	18.5 \pm 0.5
CH ₄	vol.-% _{db}	9.5 \pm 0.3	9.1 \pm 0.2
C ₂ H ₄	vol.-% _{db}	1.8	1.6
C ₂ H ₆	vol.-% _{db}	0.1	0.1
C ₃ H ₈	vol.-% _{db}	0.0	0.0
Water content	vol.-%	57	43
GC-MS tar	g/Nm ³ _{db}	11.4	11.2
Grav. tar	g/Nm ³ _{db}	5.4	6.7
Dust content	g/Nm ³ _{db}	0.4	0.3
Char content	g/Nm ³ _{db}	0.8	2.4

points measured at sampling position A. The product gas species and tar contents for both operating points are shown in Figure 5.11.

Varying fuel power in the range of 47 to 92 kW and varying steam to fuel ratios in the range of 0.87 - 1.60 only show a low impact on main product gas components and tar species of the novel DFB pilot plant. In OP1 more auxiliary fuel is required in the combustion reactor to maintain the reaction temperatures although more energy is required in OP2 for the overall gasification process (see Table 5.8). It can be assumed that a higher fuel power leads to a disproportionate increase of residual char fed to the combustion reactor and therefore less fuel oil is required to regulate the temperatures. A significant higher content of char in the product gas was measured for OP2. This can be explained by a higher input of feedstock and therefore a higher content of char that may exit the gasification reactor unconverted.

The investigations show that fast changes in fuel power at steam to fuel ratios in the range of 0.86 - 1.60 does not influence the main product gas properties, as well as, fluidization properties of the gasification process and can easily be conducted during operation if needed.

5.5 Bed Material Variation

In this section the influence of bed material properties on the gasification process is analysed using fresh olivine and a mixture of fresh olivine and limestone. Wood pellets were gasified via on-bed feeding. For this consideration, experiment 2 OP2 and experiment 3 OP4 were performed. To obtain significant results, all relevant operating parameters were kept as constant as possible. The average amount of feedstock was set to 19.0 kg/h (92 kW) for OP2 and 20.1 kg/h (97 kW) for OP4, in average. The average temperatures in the bubbling bed of the gasifier were between 814°C and 829°C at GR3 and 835°C to 848°C at GR6. The upper part of the GR reached temperatures of 950°C to 965°C at GR16. Temperatures in the combustion reactor were in the range of 978°C to 983°C at CR4 and 952°C to 966°C at CR8. The steam to fuel ratio was set to 0.87 for both operating points. For each test run, tar and product gas were sampled after the gasification reactor at sampling position A. For a better overview, Table 5.10 shows main operating parameters.

Figure 5.12 shows results of the main product gas components for OP2 and OP4 (left) and values for GC-MS and gravimetric tar (right). The corresponding values are listed in

Table 5.10: Operating parameter of accomplished investigations with different bed materials

Operation parameter	Unit	Experiment 2 OP2	Experiment 3 OP4
General bed material parameter			
Type of bed material	-	fresh olivine	fresh olivine & limestone
Fine olivine inventory	kg	12 (100 - 200 μ m)	17 (100 - 200 μ m)
Coarse olivine inventory	kg	70 (200 - 300 μ m)	
Limestone inventory	kg	0	10 (250 - 600 μ m)
Total bed material inventory	kg	82	97
Gasification reactor			
Feedstock	-	wood pellets	
Fluidization regime lower GR	-	bubbling bed	
Fluidization regime upper GR	-	turbulent zones	
Fuel feeding position in lower GR	-	on-bed feeding	
Temperature GR3	$^{\circ}$ C	814 \pm 3	829 \pm 4
Temperature GR6	$^{\circ}$ C	835 \pm 6	848 \pm 5
Temperature GR16	$^{\circ}$ C	950 \pm 2	965 \pm 2
Feedstock input	kg/h	19.0	20.1
Feedstock input	kW	92	97
Steam to fuel ratio	$\text{kg}_{\text{steam}}/\text{kg}_{\text{fuel,waf}}$	0.87	
Steam to carbon ratio	$\text{kg}_{\text{steam}}/\text{kg}_{\text{carbon}}$	1.72	
Total fluidization steam input	kg/h	14.3	15.1
Combustion reactor			
Fluidization regime	-	fast fluidized bed	
Temperature CR4	$^{\circ}$ C	978 \pm 8	983 \pm 7
Temperature CR8	$^{\circ}$ C	952 \pm 3	966 \pm 3
Fuel to combustion reactor	kW	46	50
Total air input	Nm ³ /h	58.8	63.6

Table 5.11.

Limestone as a share of the bed material leads to a higher H_2 content of 43.6 vol.-%_{db}, whereas H_2 reaches a value of 38.7 vol.-%_{db} for olivine. The amount of CO and CH_4 decreases from 27.1 to 21.7 vol.-%_{db} (CO) and 10.1 to 9.1 vol.-%_{db} (CH_4), respectively. CO_2 increases from 18.5 to 20.6 vol.-%_{db}. C_2H_4 shows to be half as much for OP4 compared to OP2. A similar tendency is detectable for GC-MS and gravimetric tar which even show a decrease of 60% for GC-MS and 77.6% for gravimetric tar.

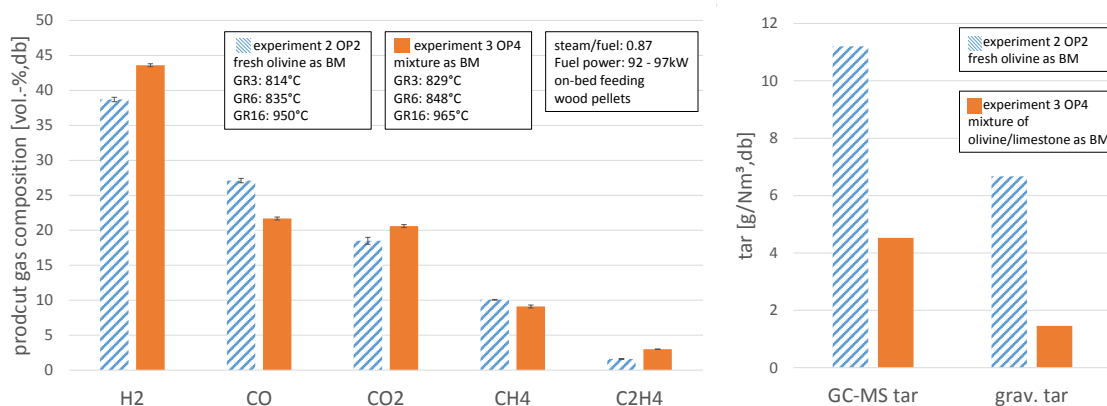


Figure 5.12: Values for main product gas components (left) and for GC-MS and gravimetric tar (right) for fresh olivine and a mixture of fresh olivine and fresh limestone as bed material

Table 5.11: Comparison of product gas composition for different bed materials. All samples were measured at sampling position A. Other gases, mainly nitrogen reach maximum values of 1.6 vol.-%_{db}

	Unit	Experiment 2 OP2	Experiment 3 OP4
Type of bed material	-	fresh olivine	fresh olivine & limestone
H ₂	vol.-% _{db}	38.7±0.3	43.6±0.2
CO	vol.-% _{db}	27.1±0.3	21.7±0.3
CO ₂	vol.-% _{db}	18.5±0.5	20.6±0.4
CH ₄	vol.-% _{db}	10.1	9.1±0.2
C ₂ H ₄	vol.-% _{db}	1.6	0.8
C ₂ H ₆	vol.-% _{db}	0.1	0.04
C ₃ H ₈	vol.-% _{db}	0.0	0.0
Water content	vol.-%	43	38
GC-MS tar	g/Nm ³ _{db}	11.2	4.5
Grav. tar	g/Nm ³ _{db}	6.7	1.5
Dust content	g/Nm ³ _{db}	0.3	0.4
Char content	g/Nm ³ _{db}	2.4	1.2

The bed material variation at the novel DFB pilot plant shows a clear trend to lower tar

values using a mixture of fresh olivine and limestone as bed material. Furthermore, hydrogen increases significantly using the mixture as bed material, whereas carbon monoxide decreases simultaneously. These findings agree with Koppatz et al. [49] and other authors.

Koppatz et al. published an increased product gas quality, since higher hydrogen contents and lower tar values can be gained using limestone as bed material. Limestone favors gasification reactions, mainly influencing the water gas shift and tar reforming reactions, acting as catalytic active bed material. The char content in the product gas was lowered significantly using a mixture as bed material. A higher water and carbon conversion can be assumed, since the water content decreases from 43 to 38 vol.-% and the content of unconverted char in the product gas was lower. Further information about carbon conversion and water conversion in the gasification reactor can be found in Section 5.8.1.

5.6 Steam to Fuel Ratio Variation

The emphasis of Section 5.6 is to examine the impact of the steam to fuel ratio to the product gas composition. Experiment 3 OP3 and OP4 as well as experiment 2 OP1 and OP2 were performed. Since no tar measurements for OP3 were conducted, the tar formation could not be compared.

Experiment 3 was performed using a mixture of fresh olivine and limestone with a ratio of about 8:1 at a total of 97 kg. Since varying operating parameters effect the product gas composition, all main parameters were kept as constant as possible. The gasification temperatures were in a range of 820 to 829°C for GR3 and 846 to 848°C for GR6. In the upper part of the column temperatures between 963 and 965°C were measured for GR16. The combustion temperature was 983 to 987°C for CR4 and 965 to 966°C for CR8. The test run was conducted using wood pellets as feedstock at a load of 20 kg/h and 97 kW respectively. For the analysis the steam to fuel ratio was set to 0.71 for OP3 and 0.87 for OP4. Figure 5.13 shows trends of the gasification and combustion temperatures revealing a stable progress of temperatures.

A steam to fuel ratio increase by only 0.16 for experiment 3 shows small deviations into the direction of higher H₂ contents. Values for CO, CO₂, CH₄, and all higher hydrocarbons C₂H₄, C₂H₆, and C₃H₈ show a slight decrease for higher steam to fuel ratios. The greatest difference beside H₂ is observed for CH₄ with 10.2 vol.-%_{db} for OP3 and 9.1 vol.-%_{db} for OP4. According to [29], lower tar contents for OP4 can be assumed, since a decreasing content of ethylene can be examined.

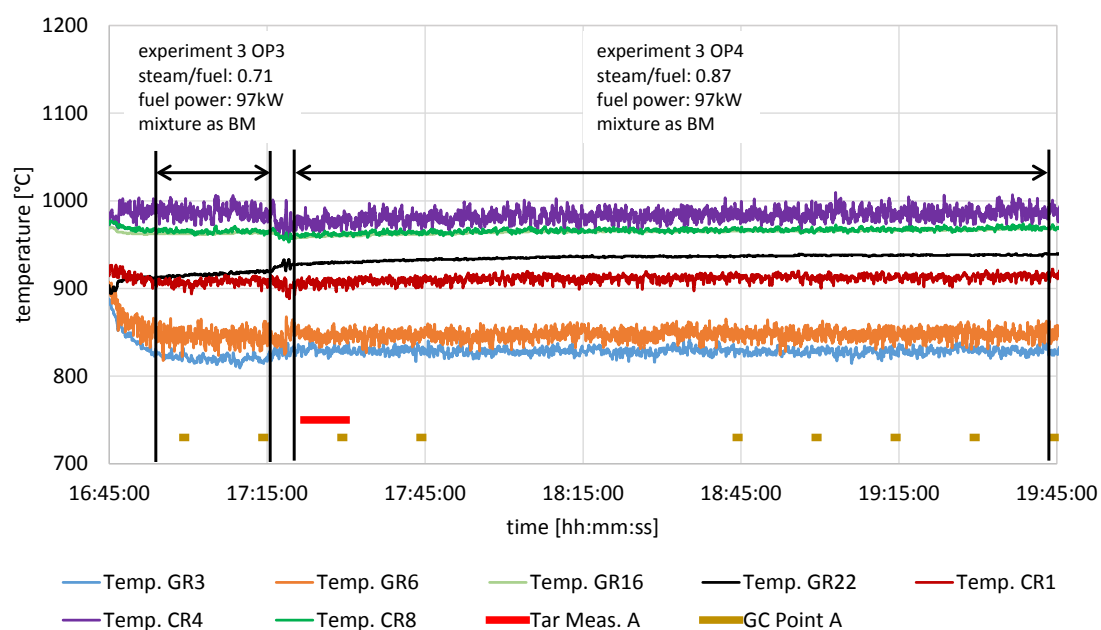


Figure 5.13: Progress of main gasification and combustion temperatures during experiment 3 OP3 and OP4

Table 5.12: Operating parameters of the accomplished investigations on steam to fuel ratios

Operation parameter	Unit	Experiment 3		Experiment 2	
		OP3	OP4	OP2	OP1
General bed material parameter					
Type of bed material	-	fresh olivine & limestone		fresh olivine	
Fine olivine inventory	kg	17 (100 - 200 μ m)		12 (100 - 200 μ m)	
Coarse olivine inventory	kg	70 (200 - 300 μ m)		70 (200 - 300 μ m)	
Limestone inventory	kg	10 (250 - 600 μ m)		0	
Total bed material inventory	kg	97		82	
Gasification reactor					
Feedstock	-	wood pellets			
Fluidization regime lower GR	-	bubbling bed			
Fluidization regime upper GR	-	turbulent zones			
Fuel feeding position in lower GR	-	on-bed feeding			
Temperature GR3	$^{\circ}$ C	820 \pm 4	829 \pm 4	814 \pm 3	822 \pm 3
Temperature GR6	$^{\circ}$ C	846 \pm 7	848 \pm 5	835 \pm 6	840 \pm 5
Temperature GR16	$^{\circ}$ C	963 \pm 1	965 \pm 2	950 \pm 2	943 \pm 1
Feedstock input	kg/h	20.1		19.0	9.8
Feedstock input	kW	97		92	47
Steam to fuel ratio	kg _{steam} /kg _{fuel,waf}	0.71	0.87	0.87	1.60
Steam to carbon ratio	kg _{steam} /kg _{carbon}	1.40	1.72	1.72	3.17
Total fluidization steam input	kg/h	12.0	15.1	14.3	14.1
Combustion reactor					
Fluidization regime	-	fast fluidized bed			
Temperature CR4	$^{\circ}$ C	987 \pm 7	983 \pm 7	978 \pm 8	974 \pm 8
Temperature CR8	$^{\circ}$ C	965 \pm 2	966 \pm 3	952 \pm 3	952 \pm 2
Fuel to combustion reactor	kW	57	50	46	56
Total air input	Nm ³ /h	63.2	63.6	58.8	50.0

Experiment 2 OP1 and OP2 were conducted at a steam to fuel ratio of 1.60 (OP1) and 0.87 (OP2) respectively. Main properties of experiment 2 was already described in Section 5.4. An overview of main operation parameters of the accomplished test run can be found in Table 5.12. Table 5.13 and Figure 5.14 present product gas composition of both test runs.

Experiment 2 was conducted using fresh olivine as bed material and wood pellets as feedstock for the gasification process. A fuel power of 92 kW for OP2 and 47 kW for OP1, respectively was adjusted. A detailed analysis of product gas components has already been described in Section 5.4.

Results show no significant changes in tar values, although great variations in steam to fuel ratios were set. A GC-MS tar content of 11.4 g/Nm³_{db} was measured for a steam to fuel ratio of 1.60, whereas 11.2 g/Nm³_{db} for a steam to fuel ratio of 0.87. The same trends for gravimetric tar were measured with 5.4 and 6.7g/Nm³_{db} respectively. No significant changes in the hydrogen content were measurable, resulting in a value of 38 vol.-%_{db} for both operating points. The same applies to the methane content showing values of 9.1 - 9.5 vol.-%_{db} in average. More significant deviations can be observed for carbon monoxide and carbon dioxide. CO reaches 27.1 vol.-%_{db} in OP2, and 23.8 vol.-%_{db} in OP1, whereas CO₂ reaches 18.5 vol.-%_{db} in OP2 and 21.1 vol.-%_{db} in OP1. A conducted steam to fuel ratio variation of 0.87 to 1.60 does not result in a significant decrease of tar components.

Hofbauer and Rauch [25] published decreasing tar contents for steam to fuel ratios between 0.15 - 0.4. Beginning from 0.4 the tendency to a lower tar content decreases significantly. It can be assumed that the tar formation can be influenced by a certain amount of steam, but may be saturated at higher quantities.

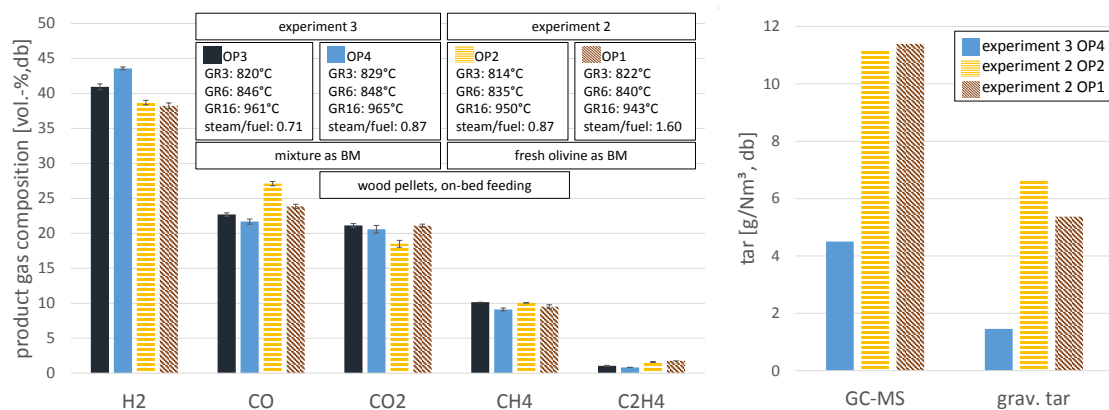


Figure 5.14: Main product gas components (left) and GC-MS and gravimetric tar (right) at varying steam to fuel ratios given as $\text{kg}_{\text{steam}}/\text{kg}_{\text{fuel,waf}}$

Table 5.13: Product gas components at varying steam to fuel ratios. Other gases, mainly nitrogen are < 1.3 vol.-%_{db}

	Unit	Experiment 3		Experiment 2	
		OP3	OP4	OP2	OP1
Steam to fuel ratio	kg_{steam}/kg_{fuel,waf}	0.71	0.87	0.87	1.60
Type of bed material	-	fresh olivine & limestone		fresh olivine	
H ₂	vol.-% _{db}	40.9±0.3	43.6±0.2	38.7±0.3	38.2±0.3
CO	vol.-% _{db}	22.7±0.2	21.7±0.3	27.1±0.3	23.8±0.2
CO ₂	vol.-% _{db}	21.1±0.3	20.6±0.4	18.5±0.5	21.1±0.2
CH ₄	vol.-% _{db}	10.2	9.1±0.2	9.1±0.2	9.5±0.3
C ₂ H ₄	vol.-% _{db}	1.0	0.8	1.6	1.8
C ₂ H ₆	vol.-% _{db}	0.08	0.05	0.10	0.10
C ₃ H ₈	vol.-% _{db}	0.0	0.0	0.0	0.0
Water content	vol.-%	n.a.	38	43	57
GC-MS tar	g/Nm ³ _{db}	n.a	4.5	11.2	11.4
Grav. tar	g/Nm ³ _{db}	n.a	1.5	6.7	5.4

5.7 Tar Reduction and Change of the Product Gas Composition along the Counter-Current Column of the Novel DFB Pilot Plant

To examine the performance of tar reduction and the change of the product gas composition along the counter-current column of the novel DFB pilot plant, test runs were performed using different sampling points for product gas and tar as shown in Figure 4.5. Both sampling points should provide comparable measurements to evaluate tar reforming along the counter-current column. The first measurement was taken at sampling point B slightly above the bubbling bed of the gasification reactor to gain data of the product gas and tar at the inlet of the counter-current column. The second measurement was sampled after the column at the outlet of the product gas radiation cooler, sampling point A. The comparison of both results should give first significant findings about the efficiency of the counter-current column in terms of tar reduction. Experiment 3 OP4A and OP4B were used, since optimal conditions were found. Table 5.14 shows a summary of relevant operating parameters of the accomplished test run.

Figure 5.15 presents the impinger bottles after the tar measurement. The measurement at sampling point B is shown on the left, whereas the measurement at sampling point A is shown on the right. This comparison should give an initial assessment about the tar reduction along the counter-current column of the gasification reactor. The darker the solution the more tar compounds are present.

Figure 5.16 displays results of the accomplished test runs. Values of product gas com-

Table 5.14: Operating parameter of accomplished investigations to evaluate the performance of tar reduction on the product gas composition of the novel design

Operation parameter	Unit	Experiment 3 OP4
General bed material parameter		
Type of bed material	-	fresh olivine & limestone
Fine olivine inventory	kg	17 (100 - 200 μ m)
Coarse olivine inventory	kg	70 (200 - 300 μ m)
Limestone inventory	kg	10 (250 - 600 μ m)
Total bed material inventory	kg	97
Gasification reactor		
Feedstock	-	wood pellets
Fluidization regime lower GR	-	bubbling bed
Fluidization regime upper GR	-	turbulent zones
Fuel feeding position in lower GR	-	on-bed feeding
Temperature GR3	$^{\circ}$ C	829 \pm 4
Temperature GR6	$^{\circ}$ C	848 \pm 5
Temperature GR16	$^{\circ}$ C	965 \pm 2
Feedstock input	kg/h	20.1
Feedstock input	kW	97
Steam to fuel ratio	kg _{steam} /kg _{fuel,waf}	0.87
Steam to carbon ratio	kg _{steam} /kg _{carbon}	1.72
Total fluidization steam input	kg/h	15.1
Combustion reactor		
Fluidization regime	-	fast fluidized bed
Temperature CR4	$^{\circ}$ C	983 \pm 7
Temperature CR8	$^{\circ}$ C	966 \pm 3
Fuel to combustion reactor	kW	50
Total air input	Nm ³ /h	63.6



Figure 5.15: Impinger bottles after tar measurement at sampling point B (left) and sampling point A (right)

ponents of both sampling points are shown (left) and tar contents for GC-MS and gravimetric tar (right). As listed in Table 5.15 a significant difference of the product gas composition can be observed. Since CO_2 increases from 14.8 to 20.6 vol.-%_{db} along the column, CO and CH_4 decreases from 35.1 to 21.7 vol.-%_{db} and from 11.6 to 9.1 vol.-%_{db}, respectively. A difference of up to 38 % is observed for H_2 , increasing from 31.4 to 43.6 vol.-%_{db}.

All higher hydrocarbons reach significantly lower values. The same applied for GC-MS and gravimetric tar, where GC-MS tar decreases from 16.6 to 4.5 g/Nm³_{db}. Gravimetric tar shows an even more significant reduction of over 88% from 12.1 to 1.5 g/Nm³_{db}.

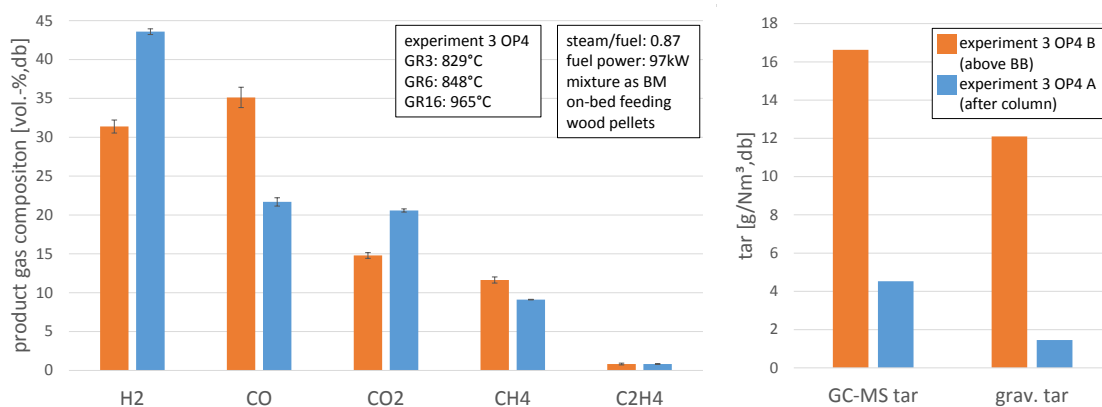
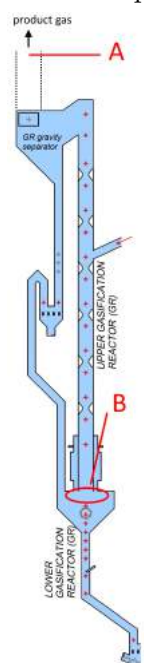


Figure 5.16: Main product gas components (left) and values for tar (right) at different sampling points for on-bed feeding of wood pellets

Taking a closer look at the product gas composition above the bubbling bed, some new insights can be gained. Regarding the heterogeneous reactions, the Boudouard reaction (Eq.2.4) may be a dominating reaction in the bubbling bed since carbon monoxide is the dominating component in the product gas. At prevailing gasification temperatures in the range of 829 - 848°C the equilibrium constant is strongly on the side of the products. Regarding homogeneous reactions, the water gas shift reaction (Eq. 2.6) is likely to be responsible for the significant increase of hydrogen and carbon dioxide in the counter-current column. Thus, it can be assumed that the conversion reaction of methane along carbon dioxide reforming (Eq. 2.8) may be a dominating reaction as well, producing carbon monoxide and hydrogen. This may enhance the water gas shift reaction, since an excess of carbon monoxide is present. The conversion of methane during steam gasification (Eq. 2.7) can nearly be neglected, since Kuba et al. [51] published findings about low conversion rates of methane (< 1 %) at temperatures up to 860°C, whereas no significant differences are published for fresh and used olivine. Similar findings can be assumed for gasification temperatures up to 965°C.

Table 5.15: Values of tar and product gas composition at sampling point A and B to evaluate the performance of the counter-current column. Other gases, mainly nitrogen are <1.3 vol.-%_{db}. The dashed lines before sampling point A should present the heat exchanger



	Unit	Experiment 3 OP4	
Temperature GR3	°C	829±4	
Temperature GR6	°C	848±5	
Temperature GR16	°C	965±2	
Sampling point	-	B	A
H ₂	vol.-% _{db}	31.4±0.6	43.6±0.2
CO	vol.-% _{db}	35.1±0.7	21.7±0.3
CO ₂	vol.-% _{db}	14.8±0.2	20.6±0.4
CH ₄	vol.-% _{db}	11.6±0.2	9.1±0.2
C ₂ H ₄	vol.-% _{db}	3.5	0.8
C ₂ H ₆	vol.-% _{db}	0.50	0.05
C ₃ H ₈	vol.-% _{db}	0.025	0.001
Water content	vol.-%	31	38
GC-MS tar	g/Nm ³ _{db}	16.6	4.5
Grav. tar	g/Nm ³ _{db}	12.1	1.5
Dust content	g/Nm ³ _{db}	120.0	0.4
Char content	g/Nm ³ _{db}	7.2	1.2

Apparently, a significant reduction of GC-MS and gravimetric tar along the counter-current column can be observed. An increased contact time of the gaseous phase and solids in the counter-current column of the GR may favor the tar reforming process.

The specific effect of residence time, contact time and temperature on GC-MS tar species is shown in Figure 5.17. GC-MS tar components measured above the bubbling bed are compared with the remaining GC-MS tar components after the gasification reactor column. The brown bars in Figure 5.17 represent measured values for sample point B, whereas values from sampling point A are marked as blue dashed bars. It has to be taken into consideration that BTX (benzol, toluene and xylene) were not measured, since toluene was used as solvent.

Obviously, a significant decrease of the overall tar components can be observed. Light and heavy PAHs such as anthracene, chrysene, pyrene, fluoranthene, and naphthalene are stable and remained in nearly same to even higher quantities after the column.

Light aromatic compounds with functional groups such as phenol and mesitylene mostly results in a total reduction, most likely into benzene. Light PAHs compounds including oxygen, such as indanone, or functional groups show great reduction, most likely into

benzene or multi-ring (2-3 ring) hydrocarbons.

Regarding detectable tar components after the column, chrysene, pyrene, anthracene, and naphthalene show the lowest relative reduction, where naphthalene remains as the dominating tar component in the product gas with $3100 \text{ mg/Nm}_{db}^3$ at sample point B and $2440 \text{ mg/Nm}_{db}^3$ at sampling point A, respectively.

Kirnbauer et al. [39] published similar findings with naphthalene as the dominating tar species in the classical DFB pilot plant using fresh and used olivine as bed material and wood pellets as feedstock. The study of Kirnbauer et al. [38] proved the phenomena of accumulation of naphthalenes and PAHs with increasing temperature, whereas phenols, aromatic compounds, and furans show less decomposition at lower gasification temperature. These findings agree with the results shown in Figure 5.17, where PAHs slightly increased at higher gasification temperatures up to 950°C . The use of catalytic active bed material inhibits the recombination of these compounds [38].

Figure 5.18 illustrates a detailed list of present tar compounds after the counter-current column in the gasification reactor of the novel DFB pilot plant compared to results conducted at the classical DFB pilot plant [33, 53]. The operating parameters of both investigations are very similar which allows a proper comparison of the results. Both investigations were conducted using fresh olivine as bed material and wood pellets as feedstock. The feedstock was conveyed into the gasification reactor via on-bed feeding at 19 - 20 kg/h, in average.

The main operation parameters are listed in Table 5.16. Obviously, no freeboard temperature was measured by Kern, but can be assumed to be slightly lower than the temperature in the bubbling bed. Therefore, a difference of the gasification temperature in the upper part of the GR has to be mentioned and may influence the results obtained.

The new concept of the novel DFB pilot plant shows lower contents for every single GC-MS and gravimetric tar value compared to the classical system. Indole, 4-methylphenol, benzofuran and phenol can not be detected at all. A significant decrease of specific tar compounds is detected for phenylacetylene, styrene, 1H-indene, 1 and 2-methylnaphthalene, biphenyl and fluorene with a reduction greater than 50%. However, the reduction of naphthalene, acenaphthene, benzo(b)fluoranthene and benzo(k)fluoranthene is below 10 %. Nearly all multi-ring hydrocarbons undergo minor reductions than multi-ring hydrocarbons with reactive functional groups and partially oxidized groups. These findings underlines the statement that the counter-current column of the gasification reactor mainly affect heterocyclic aromatics and light aromatics. Heavy PAHs are very stable and are

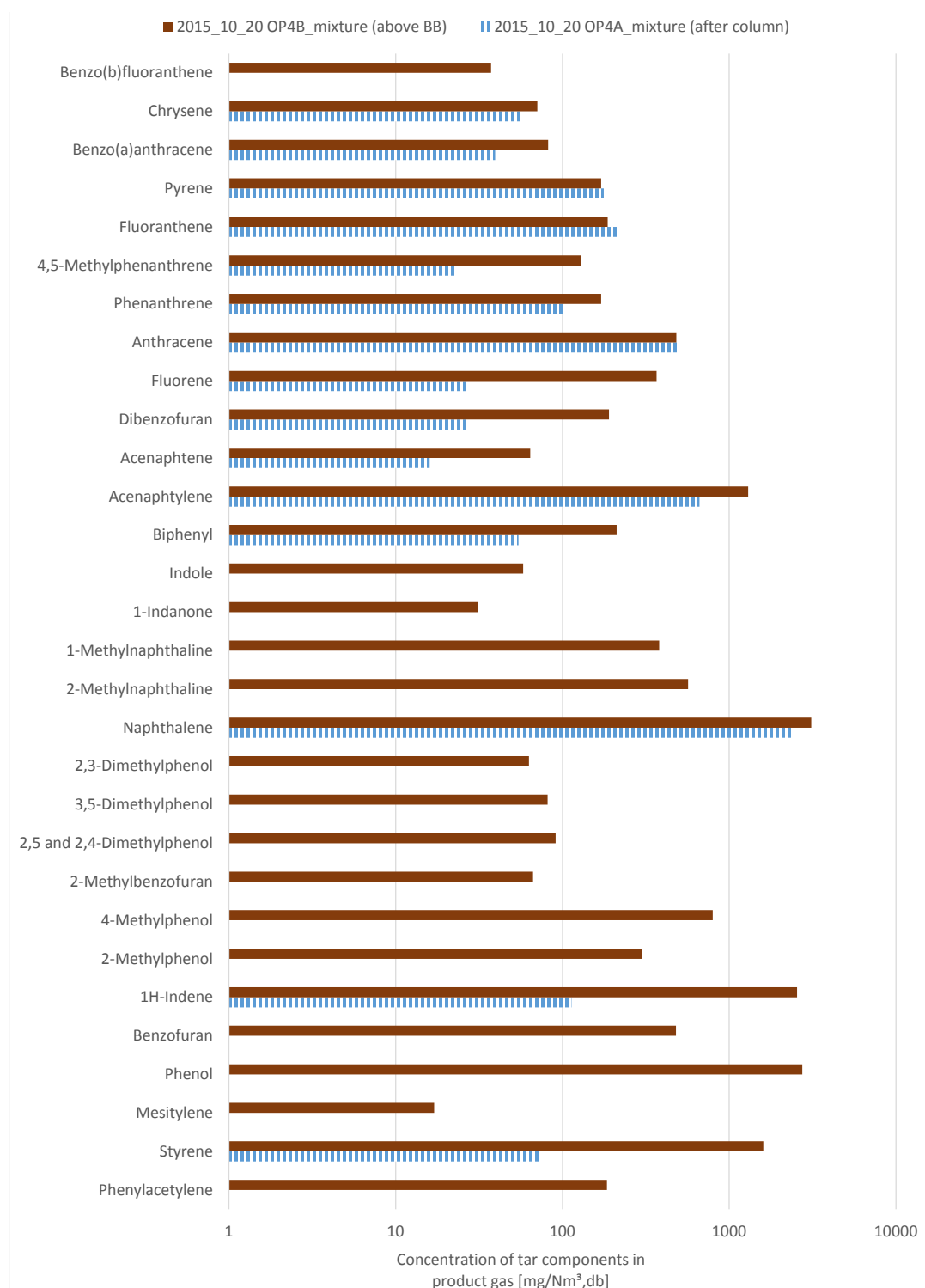


Figure 5.17: Overview of all measured GC-MS tar components occurring above the bubbling bed (OP4B) and after the counter-current column (OP4A) in logarithmic scale

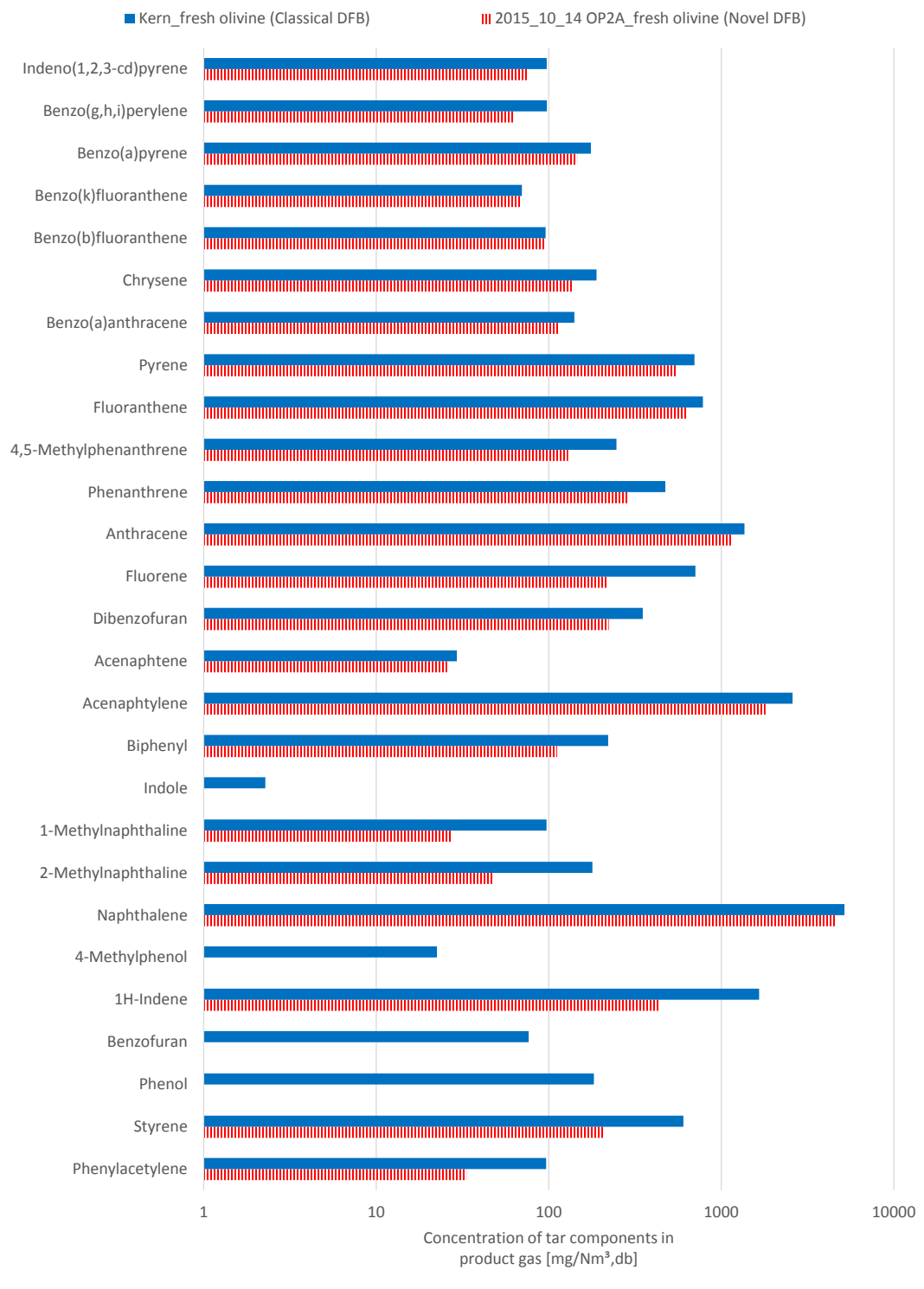


Figure 5.18: Illustration of arising tar components in the product gas after the gasifier of the new design compared to the classical DFB pilot plant. Tar components using fresh olivine as bed material and wood pellets are shown for on-bed feeding in logarithmic scale. Data of Kern are published in [33, 53]

Table 5.16: Operating parameter of investigation Experiment 2 OP2A and the investigations performed by Kern et al. [33] to demonstrate the tar reduction capability of the novel design

Operation parameter	Unit	Kern et al. [33]	Experiment 2 OP2A
General bed material parameter			
Type of bed material	-		fresh olivine
Fine olivine inventory	kg	0	12 (100 - 200 μ m)
Coarse olivine inventory	kg	100 (370 μ m)	70 (200 - 300 μ m)
Total bed material inventory	kg	100	82
Gasification reactor			
Feedstock	-		wood pellets
Fuel feeding position in lower GR	-		on-bed feeding
Temperature GR3	$^{\circ}$ C	-	814 \pm 3
Temperature GR6	$^{\circ}$ C	850	835 \pm 6
Temperature GR16	$^{\circ}$ C	-	950 \pm 2
Steam to fuel ratio	kg _{steam} /kg _{fuel,waf}	0.60	0.81
Steam to carbon ratio	kg _{steam} /kg _{carbon}	1.3	1.6
Tar compounds in GR			
GC-MS tar	g/Nm _{db} ³	16.8	11.2
Grav. tar	g/Nm _{db} ³	9.7	6.7

only slightly influenced by the increased contact time in the reaction zones.

However, a total tar reduction of nearly 33 % has been shown for GC-MS and gravimetric tar from 16.8 to 11.2 g/Nm_{db}³ and 9.7 to 6.7 g/Nm_{db}³, respectively. All tar compounds and their concentrations are listed in Appendix A.

Kraussler et al. [50] investigated tar reduction phenomena based on WGS-reactions employing a commercial Fe/Cr based catalyst. Kraussler published possible conversion steps of tar components. Phenylacetylene, styrene and 1H-indene are most likely to convert into BTX compounds. Furthermore a conversion of acenaphtylene to acenaphtene is very likely.

5.8 Feedstock Variation

In this section, the results of gasification tests conducted at the novel DFB pilot plant using various feedstock materials is presented. Following the standard feedstock wood pellets, investigations using sugarcane bagasse (SCB) and exhausted olive pomace (EOP) pellets as feedstock were performed. The operating parameters and an overview of the main results are shown in each subsection. A comparison of all feedstocks used throughout this work is conducted in Section 5.10. Since SCB and EOP required fuel preparation to ensure

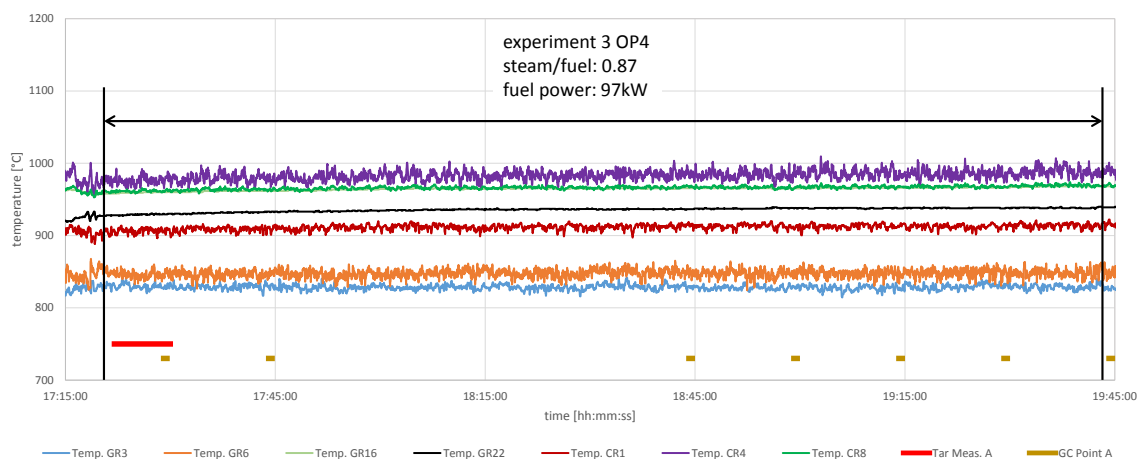


Figure 5.19: Progress of main gasification and combustion temperatures along steady state operating point OP4 using wood pellets as feedstock

sufficient dosing properties, the preparation of both feedstocks is explained in detail.

5.8.1 Wood Pellets

In this subsection experiment 3 OP4 is presented in detail as reference test run for wood pellets as feedstock. As bed material a mixture of fresh olivine and limestone was used. Figure 5.17 lists main operating parameters and main product gas compositions of the accomplished test run. During the investigation tar and product gas were sampled at sampling point A. A summary of the operating parameters and main product gas components of the accomplished test run can be found in Table 5.17. Main temperatures during the test run and the sampling times of tar and GC measurements are indicated by rectangles in Figure 5.19. The product gas composition of main components is displayed (left) and GC-MS and gravimetric tar are illustrated (right) in Figure 5.20.

Gasification of wood pellets at the novel DFB pilot plant showed similar results to prior steam gasification test runs at the classical DFB pilot plant. Hydrogen showed values of 43.6 vol.-%_{db} in average, whereas carbon monoxide yielded 21.7 vol.-%_{db}. Carbon dioxide and ethylene resulted in 20.6 vol.-%_{db} and 0.8 vol.-%_{db}, respectively. Methane resulted in 9.1 vol.-%_{db}. All higher hydrocarbons, excluding ethylene show values lower than 0.05 vol.-%_{db}. The water content of the product gas has been measured with 38 vol.-%. Low tar species were measured, where GC-MS tar reached 4.5 g/Nm³_{db} and the gravimetric tar 1.5 g/Nm³_{db}.

Wood pellets as feedstock for the steam gasification at the novel DFB pilot plant could

Table 5.17: Operating parameters and main product gas components for the gasification of wood pellets. Other gases such as nitrogen were <1.3 vol.-%_{db}

Operation parameter	Unit	Experiment 3 OP4	
General bed material parameter			
Type of bed material	-	fresh olivine & limestone	
Fine olivine inventory	kg	17 (100 - 200 μ m)	
Coarse olivine inventory	kg	70 (200 - 300 μ m)	
Limestone inventory	kg	10 (250 - 600 μ m)	
Total bed material inventory	kg	97	
General bed material parameter			
Feedstock	-	wood pellets	
Fluidization regime lower GR	-	bubbling bed	
Fluidization regime upper GR	-	turbulent zones	
Fluidization regime in CR	-	fast fluidized bed	
Fuel feeding position in lower GR	-	on-bed feeding	
		Gasification reactor	Combustion reactor
Temperature GR3	$^{\circ}$ C	829 \pm 4	-
Temperature GR6	$^{\circ}$ C	848 \pm 5	-
Temperature GR16	$^{\circ}$ C	965 \pm 2	-
Temperature CR4	$^{\circ}$ C	-	983 \pm 7
Temperature CR8	$^{\circ}$ C	-	966 \pm 3
Fuel input	kg/h	20.1	-
Fuel input	kW	97	50
Steam to fuel ratio	kg _{steam} /kg _{fuel,waf}	0.87	-
Steam to carbon ratio	kg _{steam} /kg _{carbon}	1.72	-
Total fluidization steam input	kg/h	15.1	-
Total air input	Nm ³ /h	-	63.6
H ₂	vol.-% _{db}	43.6 \pm 0.2	
CO	vol.-% _{db}	21.7 \pm 0.3	
CO ₂	vol.-% _{db}	20.6 \pm 0.4	
CH ₄	vol.-% _{db}	9.1 \pm 0.2	
C ₂ H ₄	vol.-% _{db}	0.8	
C ₂ H ₆	vol.-% _{db}	0.05	
C ₃ H ₈	vol.-% _{db}	0.001	
Water content	vol.-%	38	
GC-MS tar	g/Nm ³ _{db}	4.5	
Grav. tar	g/Nm ³ _{db}	1.5	
Dust content	g/Nm ³ _{db}	0.4	
Char content	g/Nm ³ _{db}	1.2	
Water conversion steam X _{H₂O} [84]	kg _{H₂O} /kg _{H₂O}	0.28*	
Water conversion fuel X _{H₂O,fuel} [84]	kg _{H₂O} /kg _{fuel,waf}	0.25*	
Cold gas efficiency η_{cg} [84]	%	88.9*	
Overall cold gas efficiency η_g [84]	%	58.7*	

* calculated with IPSEpro mass & energy balance

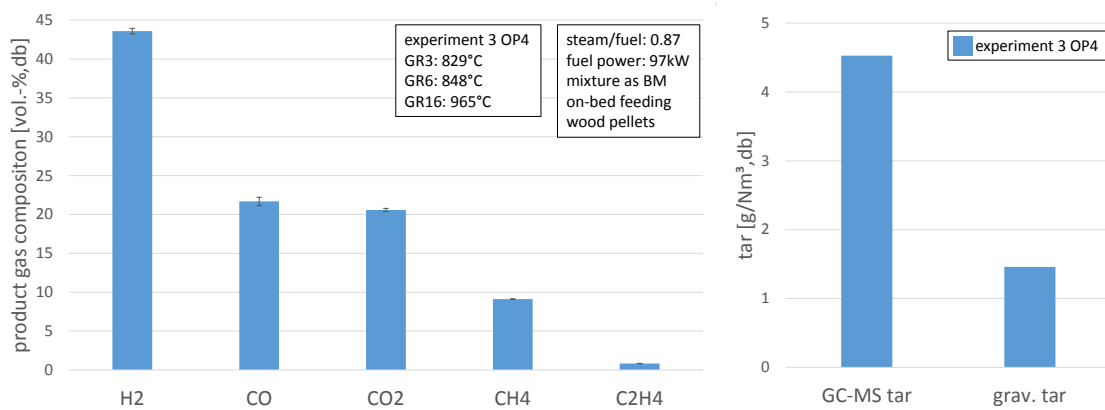


Figure 5.20: Values of main product gas components (left) and tar measurements, including GC-MS and gravimetric tar (right) for wood pellets at on-bed feeding

be completed successfully. The use of pelletized feedstock enable a proper conveying into the gasification reactor. Main product gas components resulted in similar values as reached at prior steam gasification test runs at the classical DFB pilot plant. High steam related water conversion rates were reached of up to $0.28 \text{ kg}_{H_2O}/\text{kg}_{H_2O}$. Most of the carbon entering the gasification reactor was gasified with a cold gas efficiency of 88.9%. An overall gas efficiency of 58.7% was reached at the novel 100kW DFB pilot plant.

5.8.2 Sugarcane Bagasse

Test run results with SCB as feedstock base on the work of Aguiari [2]. In a first step raw sugarcane bagasse had to be prepared for the gasification process, since conveying of raw sugarcane bagasse with the screw feeding system of the novel DFB pilot plant needed to be ensured. Therefore, raw sugarcane bagasse was grinded first using a hammermill to a particle size comparable to sawdust. Afterwards, the milled sugarcane bagasse was pelletized using a pelletizer as shown in Figure 5.21. Different matrices allow the production of various diameters. The process of pelletizing showed the best results when pelletizing pellets with 10 mm in diameter. Therefore, this diameter was chosen for all pellets throughout the entire investigation.

After the fuel preparation, sugarcane bagasse pellets were gasified in the novel DFB pilot plant using a mixture of fresh olivine and limestone as bed material. A detailed analysis of the feedstock and bed material can be found in Table 5.3 and 5.4, respectively. The gasification temperature was held as constant as possible at 802°C at GR3 and 816°C at GR6. The counter-current column was operated at 946°C at GR16. The combustion reactor temperature was set to 973°C for CR4 and 948°C for CR8. The fuel load onto the



Figure 5.21: Pelletizer manufactured by company Cissonius for feedstock preparation. PP200, 7.5kW, 380V

bubbling bed was set to 20.0 kg/h corresponding to 83 kW. The steam to fuel ratio was set to 0.98 corresponding to a total steam input of 17.3 kg/h.

During the investigation tar and product gas were sampled at sampling point A. A summary of the operating parameters and main product gas components of the accomplished test run can be found in Table 5.18. Characteristic temperatures and sampling times of tar and GC measurements are indicated by rectangles in Figure 5.22. The product gas composition including hydrogen, carbon monoxide, carbon dioxide, methane, and ethylene are displayed in Figure 5.23 (left). Additionally, GC-MS and gravimetric tar are illustrated (right).

As a results, hydrogen yields 38.4 vol.-%_{db} in average, whereas a carbon monoxide yield of 18.9 vol.-%_{db} has been reached. Carbon dioxide and ethylene show higher values than expected at 24.9 vol.-%_{db} and 2.11 vol.-%_{db}, respectively. Methane results in 11.3 vol.-%_{db}. All higher hydrocarbons, excluding ethylene show values lower than 0.13 vol.-%_{db}. The water content of the product gas has been measured with 50 vol.-%. Tar values are close to 9.9 g/Nm³_{db} for GC-MS tar and 2.6 g/Nm³_{db} for gravimetric tar.

The investigation showed that SCB as feedstock does not cause any relevant problems and therefore can be used for the DFB gasification process. The product gas composition is similar to the product gas composition of wood pellets. Although the feedstock feeding was processed as on-bed feeding, tar values were in an acceptable range below 10 g/Nm³_{db}. The test runs resulted in a cold gas efficiency of 95.9%, therefore only a small share of char enters the combustion reactor as residual char. This may explain the great share of additional fuel in the combustion reactor that is necessary to maintain the gasification temperature. The novel process showed a steam related water conversion of 0.21 kg_{H₂O}/kg_{H₂O} and an overall cold gas efficiency of 58.9%, calculated using IPSEpro.

Table 5.18: Operating parameters and main product gas components for the gasification investigation with sugarcane bagasse. Other gases such as nitrogen were <1.3 vol.-%_{db}

Operation parameter	Unit	Experiment 4 OP2	
General bed material parameter			
Type of bed material	-	fresh olivine & limestone	
Fine olivine inventory	kg	13 (100 - 200 μ m)	
Coarse olivine inventory	kg	58 (200 - 300 μ m)	
Limestone inventory	kg	16 (250 - 600 μ m)	
Total bed material inventory	kg	87	
General bed material parameter			
Feedstock	-	sugarcane bagasse pellets	
Fluidization regime lower GR	-	bubbling bed	
Fluidization regime upper GR	-	turbulent zones	
Fluidization regime in CR	-	fast fluidized bed	
Fuel feeding position in lower GR	-	on-bed feeding	
		Gasification reactor	Combustion reactor
Temperature GR3	$^{\circ}$ C	802 \pm 10	-
Temperature GR6	$^{\circ}$ C	816 \pm 10	-
Temperature GR16	$^{\circ}$ C	946 \pm 4	-
Temperature CR4	$^{\circ}$ C	-	973 \pm 8
Temperature CR8	$^{\circ}$ C	-	948 \pm 4
Fuel input	kg/h	20.0	-
Fuel input	kW	83	58
Steam to fuel ratio	kg _{steam} /kg _{fuel,waf}	0.98	-
Steam to carbon ratio	kg _{steam} /kg _{carbon}	2.14	-
Total fluidization steam input	kg/h	17.3	-
Total air input	Nm ³ /h	-	61.1
H ₂	vol.-% _{db}	38.4 \pm 0.3	
CO	vol.-% _{db}	18.9 \pm 0.2	
CO ₂	vol.-% _{db}	24.9 \pm 0.3	
CH ₄	vol.-% _{db}	11.3 \pm 0.3	
C ₂ H ₄	vol.-% _{db}	2.11 \pm 0.1	
C ₂ H ₆	vol.-% _{db}	0.13	
C ₃ H ₈	vol.-% _{db}	0.0	
Water content	vol.-%	50	
GC-MS tar	g/Nm ³ _{db}	9.9	
Grav. tar	g/Nm ³ _{db}	2.6	
Dust content	g/Nm ³ _{db}	17.2	
Char content	g/Nm ³ _{db}	6.8	
Water conversion steam X _{H₂O} [81]	kg _{H₂O} /kg _{H₂O}	0.21*	
Water conversion fuel X _{H₂O,fuel} [81]	kg _{H₂O} /kg _{fuel,waf}	0.22*	
Cold gas efficiency η_{cg} [81]	%	95.9*	
Overall cold gas efficiency η_g [81]	%	58.9*	

* calculated with IPSEpro mass & energy balance

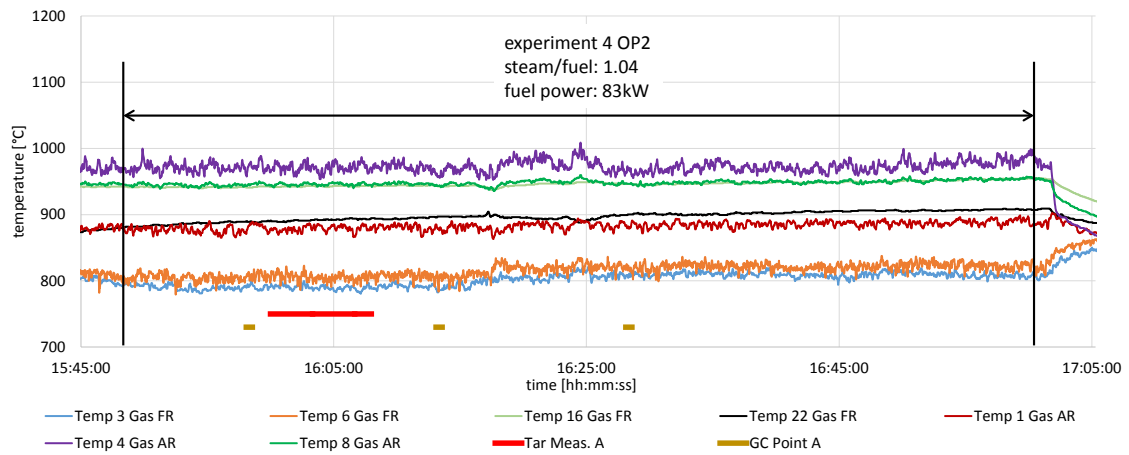


Figure 5.22: Progress of main gasification and combustion temperatures along steady state operating point using sugarcane bagasse pellets as feedstock

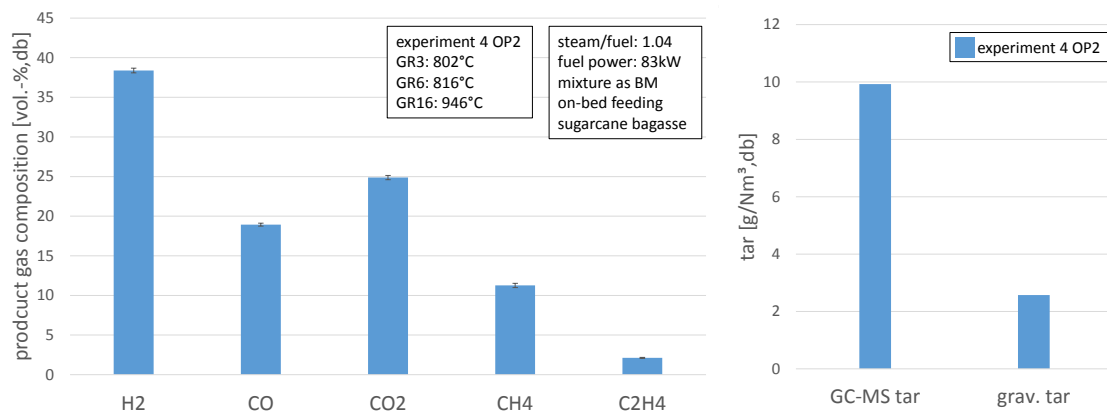


Figure 5.23: Values of main product gas components (left) and tar measurements, including GC-MS and gravimetric tar (right) for sugarcane bagasse pellets for on-bed feeding

5.8.3 Exhausted Olive Pomace

In this subsection, the applicability of exhausted olive pomace (EOP) as feedstock in the novel DFB pilot plant is investigated. EOP is a by-product of the olive oil production after the extraction of its oil, mainly originating from Mediterranean countries such as Spain, Italy and Greece. Due to the high availability, EOP has a great potential as renewable energy source.

A fuel analysis of EOP is shown in Table 5.3. Compared to softwood pellets, EOP showed a considerable difference in the ash melting behavior. EOP has a significantly lower softening temperature ($\approx 840^\circ\text{C}$) compared to softwood pellets ($\approx 1340^\circ\text{C}$). Low ash melting temperatures may result in agglomeration of ash and inorganic matter at operation temperatures. This may lead to a collapse of the occurring fluidization regime.

Low ash melting behaviours are often linked to high values of alkali metals in combination with silica in the ash. The elementary analysis of the ash (cf. Table 5.3) showed significantly higher amounts for potassium oxide (K_2O) and sodium oxide (Na_2O) in the ash for exhausted olive pomace than measured for softwood pellets. Thus, a high amount of phosphor also influence the ash melting behavior by decreasing the ash melting temperature. The fuel analysis of EOP shows high amounts of all three components compared to wood pellets and sugarcane bagasse. Further information about ash melting behavior can be found in Subsection 2.1.4.

To minimize the negative effects on fluidization behavior caused by low ash melting temperature, different tests with additives were carried out at the test laboratory of the TUW. Therefore EOP was ground and mixed with different shares of additives (CaCO_3 and CaO). As a part of this work, the mixture of EOP powder and additives were reduced to its ash and compared to the ash of raw natural EOP.

Table 5.19: Ash melting behaviour of EOP with different amounts of calcium carbonate and calcium oxide, all percentages are given in wt.-%_{db}

	Unit	Raw natural EOP	EOP + 6% of CaO	EOP + 4% of CaCO_3	EOP + 6% of CaCO_3
Softening temp.	$^\circ\text{C}$	840	740	750 - 850	750 - 890
Spheric temp.	$^\circ\text{C}$	n.a.	1410	>1500	>1500
Hemispheric temp.	$^\circ\text{C}$	n.a.	>1500	>1500	>1500
Flow temp.	$^\circ\text{C}$	1440	>1500	>1500	>1500

n.a. not available

Table 5.19 lists different ash melting temperatures of raw natural EOP, EOP mixed with 6 wt.-%_{db} of CaO , EOP mixed with 4 wt.-%_{db} of CaCO_3 and a mixture of EOP with

6 wt.-%_{db} of CaCO₃. To examine the ash melting behavior a hot stage microscope was applied. Raw EOP show a softening temperature starting at 840°C and a flow temperature occurring at 1440°C. The softening temperature is defined as the temperature, where particles show a first softening phenomena. Unfortunately, no results for the spheric and hemispheric temperatures of raw natural EOP are available but may be in between the softening and flow temperature.

We could not measure a clear temperature for the mixture of EOP with CaCO₃ where a significant softening of the particles occur. A first sinter phenomena may start at a temperature of 750°C, where a strong decrease of the volume of the ash samples occur. This could be explained by the release of CO₂. However, the shape of the ash sample did not change significantly. It can be assumed, that the softening temperature of the mixture of EOP with 6 wt.-%_{db} of CaCO₃ is in the range of 750 to 890°C and slightly decreased for EOP mixed with 4 wt.-%_{db} of CaCO₃.

We measure a softening temperature of EOP mixed with 6 wt.-%_{db} of CaO to be at a temperature of 740°C and a spheric temperature to be at 1410°C. All further softening phenomena could not be measured for EOP mixtures, since the measuring temperature of the hot stage microscope is limited by 1500°C. Therefore, all other temperatures are measured to be greater than 1500°C. Further investigations were carried out using a mixture of EOP with 6 wt.-%_{db} of CaCO₃, since calcium oxide (CaO) exhibit a highly exothermic reaction to calcium hydroxide (Ca(OH)₂) when in contact with water. Thus, the investigation of EOP mixed with 4 wt.-%_{db} of CaCO₃ result in slightly lower softening temperatures.

Figure 5.24 shows the change of the surface of the inspected EOP ash particles at temperatures starting at 550°C up to 1500°C. A significant decrease of the volume of the EOP mixture beginning at 750°C is shown. However, no significant changes in shape occur until 1500°C. Regarding the raw EOP sample, clear softening phenomena are present beginning at a temperature above 840°C. The flow temperature is measured to be above 1440°C.

Based on these analyses further test runs were carried out using EOP mixed with 6 wt.-%_{db} of CaCO₃ as feedstock.

The feedstock was pelletized using raw EOP mixed with a share of 6 wt.-%_{db} calcium carbonate (CaCO₃) and a small amount of water. The same pelletizer was used as already described for the preparation of sugarcane bagasse pellets. To obtain a homogeneous distribution of EOP and calcium carbonate, the pellets were pelletized twice and dried in

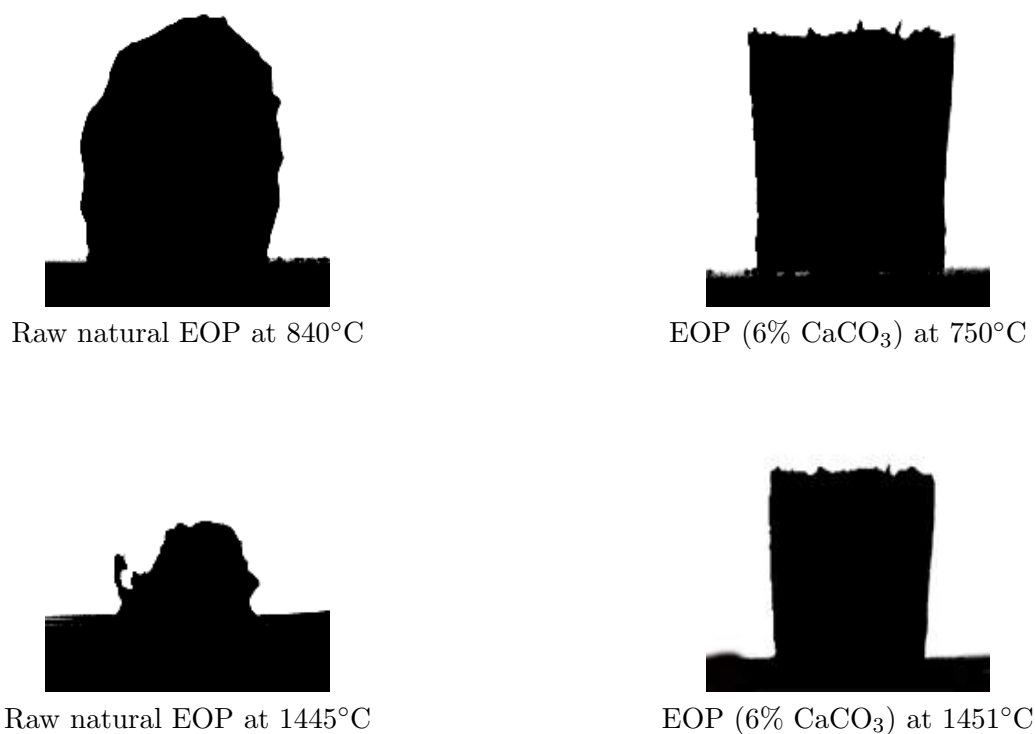


Figure 5.24: Illustration of the ash melting behavior of raw EOP and a mixture of EOP with CaCO₃ using a hot stage microscope

a next step. Since water was added for the preparation, an additional fuel analysis was carried out to determine the water content. A summary of the elementary analysis for exhausted olive pomace pellets used for the investigations can be found in Table 5.3.

For the scheduled test runs 19.8 kg/h of exhausted olive pomace pellets (84 kW) were dosed onto the bubbling bed. Fresh olivine mixed with limestone was used as bed material for the gasification process. The applied materials are listed in Table 5.20. The steam to fuel ratio was set to 1.06. It has to be mentioned that the steam to fuel ratio was calculated based on a water, ash and calcium free feedstock. The gasification temperature in the bubbling bed was set to 737°C at GR3 and 758°C at GR6, in average. The counter-current column was heated up to 861°C at GR16. The temperature in the combustion reactor was close to 872°C at CR4 and 861°C at CR8. To simplify the illustration of the investigation, relevant data are summarized in Table 5.20. Figure 5.25 displays the progress of the relevant gasification and combustion temperatures. Since the softening phenomena shows to start at temperatures below 800°C, gasification and combustion temperatures, especially the gasification temperatures in the bubbling bed, were kept low to avoid unfavourable ash melting phenomena. Therefore, a higher tar content and changes in the product gas composition may be expected.

Table 5.20: Operating parameters and main product gas components for the gasification investigation of EOP. Other gases such as nitrogen were <0.9 vol.-%_{db}

Operation parameter	Unit	Experiment 5 OP1	
General bed material parameter			
Type of bed material	-	fresh olivine & limestone	
Fine olivine inventory	kg	15 (100 - 200 μ m)	
Coarse olivine inventory	kg	50 (200 - 300 μ m)	
Limestone inventory	kg	20 (250 - 600 μ m)	
Total bed material inventory	kg	85	
General bed material parameter			
Feedstock	-	exhausted olive pomace pellets	
Fluidization regime lower GR	-	bubbling bed	
Fluidization regime upper GR	-	turbulent zones	
Fluidization regime in CR	-	fast fluidized bed	
Fuel feeding position in lower GR	-	on-bed feeding	
		Gasification reactor	Combustion reactor
Temperature GR3	$^{\circ}$ C	737 \pm 2	-
Temperature GR6	$^{\circ}$ C	758 \pm 6	-
Temperature GR16	$^{\circ}$ C	861 \pm 3	-
Temperature CR4	$^{\circ}$ C	-	872 \pm 9
Temperature CR8	$^{\circ}$ C	-	861 \pm 2
Fuel input	kg/h	19.8	-
Fuel input	kW	84	54
Steam to fuel ratio	kg _{steam} /kg _{fuel,waf}	1.06	-
Steam to carbon ratio	kg _{steam} /kg _{carbon}	2.05	-
Total fluidization steam input	kg/h	14.2	-
Total air input	Nm ³ /h	-	57.2
H ₂	vol.-% _{db}	47.6 \pm 0.5	
CO	vol.-% _{db}	18.3 \pm 1.4	
CO ₂	vol.-% _{db}	20.4 \pm 0.4	
CH ₄	vol.-% _{db}	6.7 \pm 0.4	
C ₂ H ₄	vol.-% _{db}	2.1 \pm 0.1	
C ₂ H ₆	vol.-% _{db}	0.38	
C ₃ H ₈	vol.-% _{db}	0.01	
Water content	vol.-%	33	
GC-MS tar	g/Nm ³ _{db}	5.0	
Grav. tar	g/Nm ³ _{db}	2.3	
NH ₃	ppm	16260	
H ₂ S	ppm	575	
Dust content	g/Nm ³ _{db}	26.4	
Char content	g/Nm ³ _{db}	3.4	
Water conversion steam X _{H₂O} [79]	kg _{H₂O} /kg _{H₂O}	0.34*	
Water conversion fuel X _{H₂O,fuel} [79]	kg _{H₂O} /kg _{fuel,waf}	0.36*	
Cold gas efficiency η_{cg} [79]	%	99.0*	
Overall cold gas efficiency η_g [79]	%	59.8*	

* calculated with IPSEpro mass & energy balance

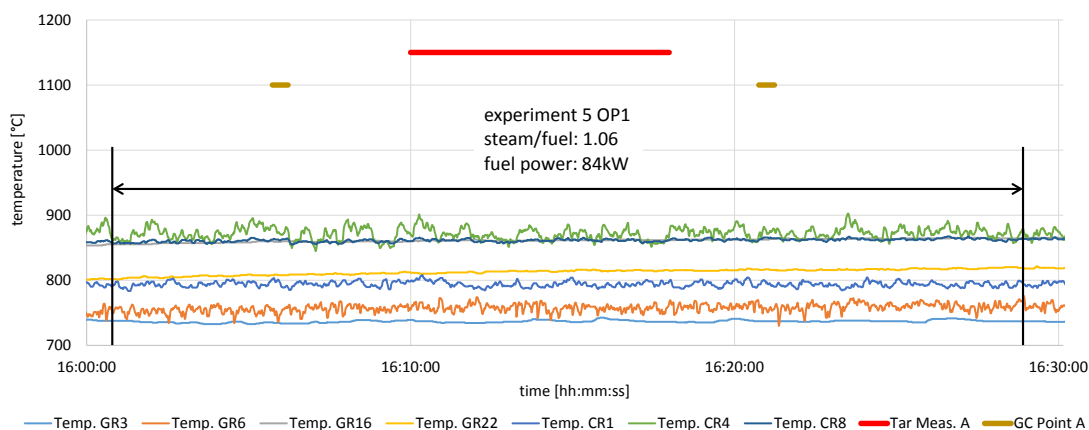


Figure 5.25: Progress of the relevant gasification and combustion temperatures using exhausted olive pomace pellets as feedstock

Although very low gasification temperatures were realized, the product gas composition showed only 5.0 g/Nm^3_{db} GC-MS tar and 2.3 g/Nm^3_{db} gravimetric tar. A hydrogen content of up to 47.6 vol.-%_{db} has been reached, whereas carbon dioxide reached 20.4 vol.-%_{db} . Carbon monoxide and methane showed to be lower at values of 18.3 vol.-%_{db} and 6.7 vol.-%_{db} , respectively. A water content of 33 vol.-% has been measured in the product gas. Additionally, ammonia (16260 ppm) and hydrogen sulphide (575 ppm) were measured.

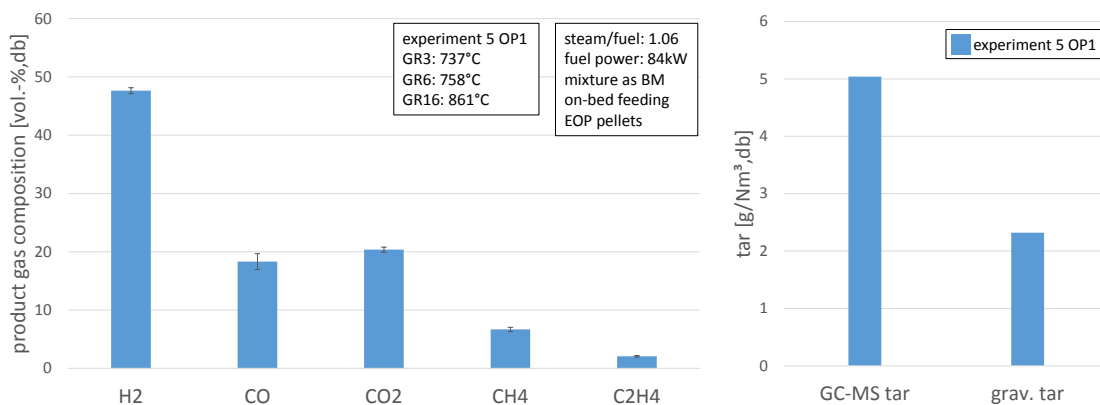


Figure 5.26: Product gas composition (left) and tar measurements, including GC-MS and gravimetric tar (right) using exhausted olive pomace pellets as feedstock

EOP as feedstock could be gasified successfully for a steady state period of 4 hours. A feedstock preparation as mentioned in the beginning of this chapter was needed to inhibit the negative effect of ash melting behavior. To fulfil a save process, low gasification temperatures were set additionally. The novel DFB system enables lower gasification temperatures in bubbling bed without influencing the gasification temperature in the column significantly, where effective tar cracking and steam reforming takes place. These

facts make it possible to gasify exhausted olive pomace pellets with a low tar content in the product gas (compared to other alternative fuel types). EOP resulted in very high contents of hydrogen up to 47.6 vol.-%_{db}. However, what is striking is the fact that the novel system reached a cold gas efficiency of 99.0%. Thus, very high steam related water conversion rates of 0.34 kg_{H₂O}/kg_{H₂O} were reached. An overall cold gas efficiency of 59.8% was measured.

5.9 Evaluation of the Performance of the Novel DFB Test Plant

A comparison of the performance of the classical and the novel DFB pilot plant is given in this section. To meet all requirements for significant assessments, comparable operating points were selected. Gasification test runs using wood pellets as feedstock are compared, since a broad knowledge with wood pellets has been gained in prior investigations.

Table 5.21 lists main operating parameters and results of relevant investigations. The first comparison (abbreviated as comparison A) presents gasification test runs using fresh olivine as bed material. The steam to fuel ratio was in a range of 0.60 - 0.87 and the fuel input was set to 90 - 92kW. The gasification temperature GR6 was set to 835 - 850°C. The second investigation (abbreviated as comparison B) was conducted using different bed materials (mixture of fresh olivine/limestone and used olivine). Steam to fuel ratios were set to 0.86 - 0.87 and the fuel power was set to 97kW. Main gasification temperatures were in similar ranges with GR6 of 848 - 850°C.

It has to be considered that relevant temperatures in both reactors cannot be considered one-by-one due to different geometry and measurement positions. An illustration and description of the measurement positions at the classical DFB pilot plant is shown in Figure 3.3.

Comparison A shows differences in main product gas components and tar species. The counter-current column of the gasification reactor and the higher steam to fuel ratio seems to promote and shift the WGS reaction to the side of products, resulting in higher contents of hydrogen and carbon dioxide. Simultaneously, carbon monoxide decreases. The same applies to tar species measured in the product gas. A significant decrease of GC-MS and gravimetric tar values were reached for the novel DFB pilot plant from 16.8 to 11.2 g/Nm³_{db} for GC-MS tar and from 9.7 to 6.7 g/Nm³_{db} for gravimetric tar. It can be assumed that the increased contact time of solids and fluids and the surplus of steam positively influences tar reduction. Figure 5.27 summaries main product gas compositions and tar values of

Table 5.21: Operating parameters and main product gas components of accomplished test runs on the classical and novel DFB pilot plant. Other gases, mainly nitrogen are $<1.3 \text{ vol.-%}_{db}$

Operation parameter	Unit	Comparison A		Comparison B	
		Kern et al. [33]	Experiment 2 OP2	Wilk et al. [101]	Experiment 3 OP4
Pilot plant	-	classical DFB	novel DFB	classical DFB	novel DFB
General bed material parameter					
Type of bed material	-	fresh olivine		used olivine	mixture
Mean bed material particle size	μm	370	100 - 300	510	100 - 300
Total bed material inventory	kg	100	82	100	97
General bed material parameter					
Feedstock	-	wood pellets			
Fluidization regime lower GR	-	bubbling bed			
Fluidization regime upper GR	-	turbulent zones			
Fluidization regime in CR	-	fast fluidized bed			
Fuel feeding position in lower GR	-	on-bed feeding			
Temperature GR3 ¹	$^{\circ}\text{C}$	-	814 \pm 3	-	828 \pm 4
Temperature GR6 ²	$^{\circ}\text{C}$	850 \pm 2	835 \pm 5	850 \pm 1	848 \pm 5
Temperature GR16 ¹	$^{\circ}\text{C}$	-	950 \pm 7	-	965 \pm 2
Temperature CR4	$^{\circ}\text{C}$	-	978 \pm 4	-	983 \pm 7
Temperature CR8	$^{\circ}\text{C}$	910 \pm 11	952 \pm 6	878 \pm 4	966 \pm 2
Fuel input to GR	kW	90	92	97	97
Fuel input to CR	kW	n.p.	46	n.p.	50
Steam to fuel ratio	$\text{kg}_{\text{steam}}/\text{kg}_{\text{fuel,waf}}$	0.60	0.87	0.86	0.87
Steam to carbon ratio	$\text{kg}_{\text{steam}}/\text{kg}_{\text{carbon}}$	n.p.	1.72	n.p.	1.72
H ₂	vol.-% _{db}	32.8	38.7	43.3	43.6
CO	vol.-% _{db}	34.7	27.1	23.9	21.7
CO ₂	vol.-% _{db}	14.6	18.5	21.5	20.6
CH ₄	vol.-% _{db}	10.3	9.1	8.1	9.1
C ₂ H ₄	vol.-% _{db}	2.7	1.6	2.0	0.8
C ₂ H ₆	vol.-% _{db}	0.2	0.1	0.2	0.05
C ₃ H ₈	vol.-% _{db}	n.p.	0.0	0.3	0.03
Water content	vol.-%	35.8	43.0	39.0	38.0
GC-MS tar	$\text{g}/\text{Nm}_{db}^3$	16.8	11.2	3.4	4.5
Grav. tar	$\text{g}/\text{Nm}_{db}^3$	9.7	6.7	1.4	1.5
Water conversion fuel* $X_{\text{H}_2\text{O},\text{fuel}}$	$\text{kg}_{\text{H}_2\text{O}}/\text{kg}_{\text{fuel,waf}}$	0.14	0.19	0.13**	0.25 [84]
Cold gas efficiency* η_{cg}	%	87.3	90.7	84.5**	88.9 [84]
Carbon conversion in GR*, X_c	$\text{kg}_{c,\text{PG}}/\text{kg}_{c,\text{fuel}}$	0.82	0.87**	0.78**	0.84**
Overall cold gas efficiency* η_g	%	n.p.	60.5**	59.5**	58.7 [84]

* Calculated with IPSEpro mass & energy balance

** Post calculated with IPSEpro mass & energy balance

1 Temperature measurement GR3 & GR16 did not exist at the classical DFB test plant

2 Temperature measurement GR6 was referred to temperature bubbling bed at Wilk and Kern

3 Temperature measurement CR8 was referred to temperature riser at Wilk and Kern

n.p.: not published

comparison A.

The influence of the steam to fuel ratio can be neglected for comparison B, since only minor differences occurred. The product gas composition and the content of gravimetric tar showed to be very similar. However, GC-MS tar were measured to be lower at the classical DFB pilot plant with 3.4 g/Nm^3_{db} and 4.5 g/Nm^3_{db} , respectively. A higher catalytic activity and therefore an enhance tar reforming process can be assumed for the used olivine than for the mixture of fresh olivine and limestone. Figure 5.28 presents the product gas composition and tar species of comparison B.

Both comparisons show significant differences in the performance of the novel and the classical DFB pilot plant in terms of water and carbon conversion in the gasification reactor, as well as, cold gas efficiencies. Both test runs at the classical DFB pilot plant reached fuel related water conversion rates in the range of 0.13 - 0.14. Thus, typical ranges for the cold gas efficiencies were 85 - 87%. The carbon conversion in the GR showed to be in the range of 78 - 82%. Significant better results were reached at the novel DFB pilot plant. Carbon conversion rates in the gasification reactor up to 87% and cold gas efficiencies up to 91% were measured. The biggest difference is shown for the fuel related water conversion, where a conversion of water of up to 25% were reached.

Similar overall cold gas efficiencies were reached for both pilot plants, although higher heat losses for the novel pilot plant are present, influencing the overall cold gas efficiency significantly to lower values. Overall cold gas efficiencies for a 50 MW plant was estimated to be in the range of 70 - 80% [84].

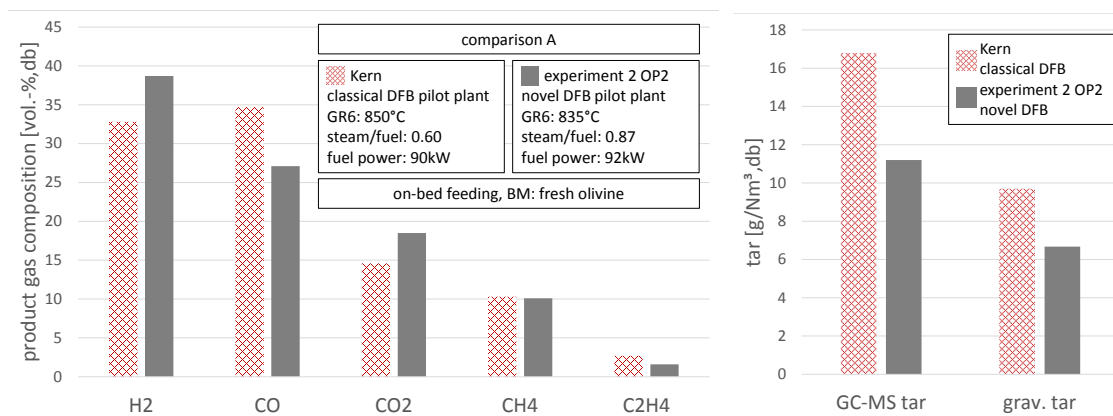


Figure 5.27: Comparison of results conducted at the classical and novel DFB pilot plant. Main product gas components (left) and tar components (right)

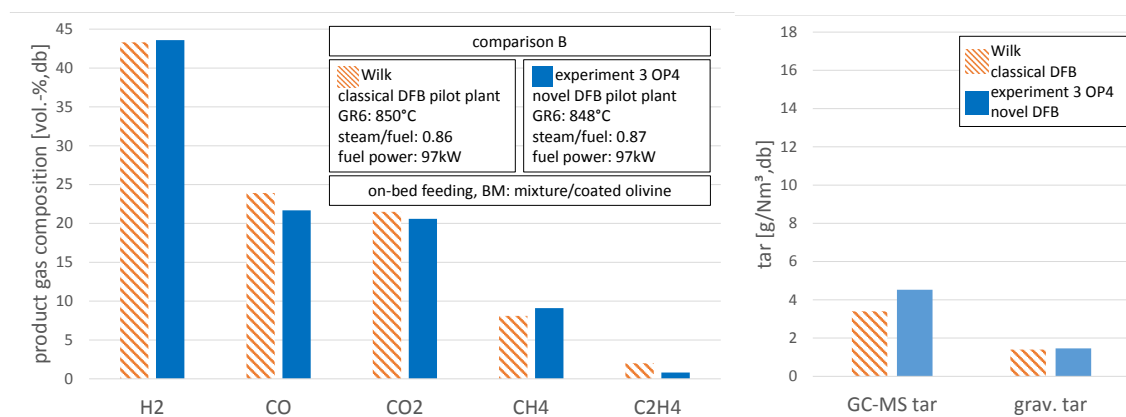


Figure 5.28: Comparison of results conducted at the classical and novel DFB pilot plant. Main product gas components (left) and tar components (right)

5.10 Overview of Experimental Results

In Section 5.10 a detailed overview and discussion of all relevant results conducted at the novel DFB pilot plant is given. Additionally, a comparison of test runs conducted at the novel DFB pilot plant and the classical DFB pilot plant is given.

- Evaluation of the fluid dynamics

The pressure profile of the novel DFB pilot plant shows a very good accordance to the pressure profile of the cold flow model investigation. Higher absolute pressure drops for the gasification process were measured due to differences in density and temperature, see Figure 5.3. The pressure gradient profile shows the expected contribution of solids along the constrictions to fulfil an increased contact time of solids and the gaseous phase (cf. Figure 5.4). Fluidization regimes of main pilot plant sections were examined and showed an excellent match between both investigations and the technical design as presented in Figure 5.5.

- Temperature variation

The temperature variation showed similar results of the product gas composition and tar species to prior investigations at the classical DFB pilot plant. Increasing temperatures led to lower overall tar contents in the product gas. The temperature profile of experiment 2 is depicted, showing the desired temperature gradients in different section of the plant (cf. Figure 5.7).

- Fuel power variation

Fuel power variations did not cause problems for the novel DFB pilot plant. Fast fuel power changes from partial (47kW) to full (92kW) fuel power did not significantly influence the gasification and combustion temperatures, as well as, the product gas composition and tar contents. Steady state conditions could be reached for both operating points without major delays.

- Bed material variation

Already small amounts of limestone as a share of the bed material mixture (10 wt.-%_{db}) resulted in significant differences of the product gas composition. It can be assumed that catalytic active bed material (CaO) promotes the water gas shift (WGS) and steam reforming reactions as already published for prior test runs at the classical DFB pilot plant [34]. Therefore, higher contents of hydrogen and carbon dioxide could be reached. Carbon monoxide showed to decrease using catalytic active bed material. The conversion of methane resulted in minor changes to lower methane contents in the product gas. Kuba et al. [51] examined the reforming of methane during steam gasification. Since low conversion rates of methane (< 1 %) at temperatures up to 860°C were published, the conversion of methane during steam gasification can nearly be neglected. No significant differences are published for fresh and used olivine. Similar findings can be assumed for gasification temperatures up to 965°C. The GC-MS and gravimetric tar contents could be lowered from 11.2 to 4.5 g/Nm³_{db} and 6.7 to 1.5 g/Nm³_{db}, respectively, since a higher activity of the catalytic bed material may promote the WGS and steam reforming reaction.

- Steam to fuel variation

The influence of the steam to fuel ratio on the product gas composition and tar content was already published by several authors [25, 43]. Experiment 3 showed minor differences in the product gas composition to a higher content of hydrogen and lower contents of carbon monoxide, carbon dioxide and methane for a steam to fuel ratio variation of 0.71 - 0.87 kg_{steam}/kg_{fuel,waf}.

Greater differences in the steam to fuel ratio of 0.87 - 1.60 did not show significant differences in the product gas composition. It can be assumed that tar reforming reactions are influenced by a certain amount of steam, but showed a low impact when exceeding a steam to fuel ratios above 0.9 kg_{steam}/kg_{fuel,waf}.

- Tar reforming along the counter-current column

The tar reforming efficiency along the counter-current column of the novel DFB pilot plant was examined. A mixture of fresh olivine and limestone was used as bed material. A significant decrease of the overall tar content was shown along the column of the gasification reactor. However, no significant decrease of multi-ring hydrocarbons (2-4 rings) was observed. Thus, higher PAHs such as anthracene, chrysene, pyrene, fluoranthene, and naphthalene showed a high stability and were not cracked along the column.

High tar reforming efficiency was observed for light aromatic tar with functional groups such as phenol and mesitylene. Light PAHs compounds including oxygen or other functional groups showed great reduction potential. It can be assumed that these compounds most likely convert into benzene or multi-ring (2-3 ring) hydrocarbons, such as naphthalene or acenaphthylene.

- Feedstock variation

Investigation using different feedstock such as wood pellets, sugarcane bagasse pellets and exhausted olive pomace pellets were conducted. Main operating parameter and product gas composition are listed in Table 5.22.

The steam to fuel ratio was in a range of 0.87 - 1.06. Large differences in the gasification temperatures can be observed, since EOP shows very low ash melting temperatures.

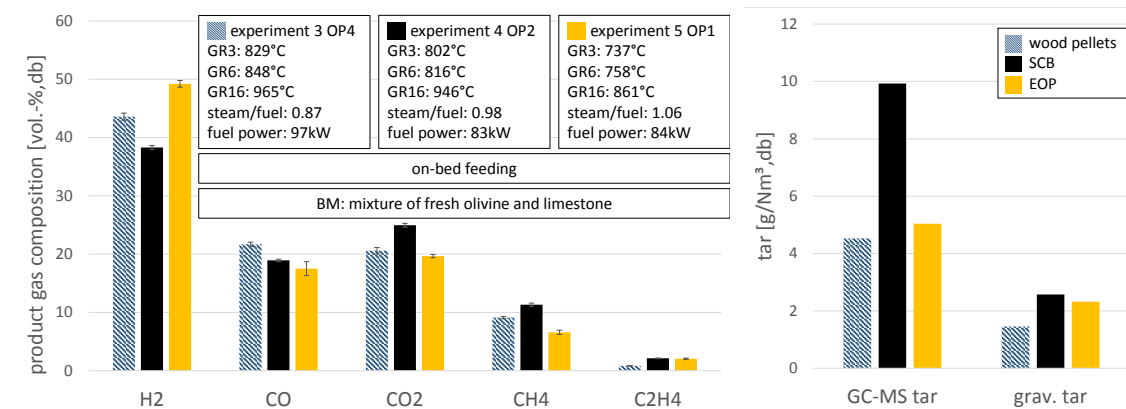


Figure 5.29: Results of accomplished test runs with different feedstock materials

The results illustrated in Figure 5.29 show the applicability of different feedstock materials for the gasification process conducted at the novel DFB pilot plant. Even alternative feedstock materials with very low ash melting temperatures (EOP) did not have a strong impact on the main product gas composition. The novel DFB pilot plant allows low gasification temperatures without major impacts on tar reforming processes in the counter-current column, where effective tar cracking occurs. The novel design allows a

Table 5.22: Operating parameters and main product gas components for gasification of various feedstock. Other gases such as nitrogen were <1.3 vol.-%_{db}

Operation parameter	Unit	Wood pellets	Sugarcane bagasse pellets	EOP pellets
General bed material parameter				
Type of bed material	-	fresh olivine & limestone		
Fine olivine inventory	kg	15 (100 - 200 μ m)	13 (100 - 200 μ m)	15 (100 - 200 μ m)
Coarse olivine inventory	kg	70 (200 - 300 μ m)	58 (200 - 300 μ m)	50 (200 - 300 μ m)
Limestone inventory	kg	10 (250 - 600 μ m)	16 (250 - 600 μ m)	20 (250 - 600 μ m)
Total bed material inventory	kg	97	87	85
General bed material parameter				
Fluidization regime lower GR	-	bubbling bed		
Fluidization regime upper GR	-	turbulent zones		
Fluidization regime in CR	-	fast fluidized bed		
Fuel feeding position in lower GR	-	on-bed feeding		
Temperature GR3	°C	829 \pm 4	802 \pm 10	737 \pm 2
Temperature GR6	°C	848 \pm 5	816 \pm 10	758 \pm 6
Temperature GR16	°C	965 \pm 2	946 \pm 4	861 \pm 3
Temperature CR4	°C	983 \pm 7	973 \pm 8	872 \pm 9
Temperature CR8	°C	966 \pm 3	948 \pm 4	861 \pm 2
Fuel input to GR	kW	97	83	84
Fuel input to CR	kW	50	58	54
Steam to fuel ratio	kg _{steam} /kg _{fuel,waf}	0.87	0.98	1.06
Steam to carbon ratio	kg _{steam} /kg _{carbon}	1.72	2.14	2.05
H ₂	vol.-% _{db}	43.6 \pm 0.2	38.4 \pm 0.3	47.6 \pm 0.5
CO	vol.-% _{db}	21.7 \pm 0.3	18.9 \pm 0.2	18.3 \pm 1.4
CO ₂	vol.-% _{db}	20.6 \pm 0.4	24.9 \pm 0.3	20.4 \pm 0.4
CH ₄	vol.-% _{db}	9.1 \pm 0.2	11.3 \pm 0.3	6.7 \pm 0.4
C ₂ H ₄	vol.-% _{db}	0.8	2.1	2.1
C ₂ H ₆	vol.-% _{db}	0.05	0.13	0.38
C ₃ H ₈	vol.-% _{db}	0.001	0.0	0.01
Water content	vol.-%	38	50	33
GC-MS tar	g/Nm _{db} ³	4.5	9.9	5.0
Grav. tar	g/Nm _{db} ³	1.5	2.6	2.3
Dust content	g/Nm _{db} ³	0.4	17.2	26.4
Char content	g/Nm _{db} ³	1.2	6.8	3.4
Water conversion steam $X_{H_2O,abs}$	kg _{H₂O} /kg _{H₂O}	0.28* [79]	0.21* [81]	0.34* [84]
Water conversion fuel $X_{H_2O,rel}$	kg _{H₂O} /kg _{fuel,waf}	0.25* [79]	0.22* [81]	0.36* [84]
Cold gas efficiency η_{cg}	%	88.9* [79]	95.9* [81]	99.0* [84]
Overall cold gas efficiency η_g	%	58.7* [79]	58.9* [81]	59.8* [84]
Ash melting temperatures				
Softening temp.	°C	1335	1180	750
Spheric temp.	°C	n.m.	1210	> 1500
Hemispheric temp.	°C	n.m.	1260	> 1500
Flow temp.	°C	1438	1330	> 1500

* calculated with IPSEpro mass & energy balance

n.m. not measured

lower gasification temperature in the bubbling bed and a higher gasification temperature in the counter-current column, simultaneously.

Wood pellets and sugarcane bagasse pellets did not cause any serious problems during the gasification process. It was possible to gasify EOP for 4 hours in a steady state gasification process. Agglomeration of bed material and ash particles, however, led to a controlled termination of the test run to avoid any damages of the reactor.

The novel DFB pilot plant reached high water conversion rates for all feedstocks. Especially EOP resulted in a steam related water conversion rate of $0.34 \text{ kg}_{H_2O}/\text{kg}_{H_2O}$. It can be assumed that the high water conversion rate may be partial responsible for the hydrogen content, since water may get split in the novel DFB pilot plant. Furthermore, the low gasification temperature and the limestone as share of the bed material may cause a slight sorption enhanced reforming (SER) process, resulting in higher hydrogen and lower carbon dioxide contents. The cold gas efficiency was measured to be 88.9 - 99.0%. Most of the carbon entering the gasification reactor gets therefore converted and does not slip via LLS into the combustion reactor as residual char. Overall cold gas efficiencies are in similar ranges for all considered feedstock materials of 58.7 - 59.8%.

Although the feedstock was introduced via on-bed feeding into the GR, low overall tar contents were measured. Especially exhausted olive pomace pellets showed very low contents of GC-MS tar ($5.0 \text{ g}/\text{Nm}_{db}^3$) and gravimetric tar ($2.3 \text{ g}/\text{Nm}_{db}^3$) regarding alternative feedstock materials at low gasification temperatures.

- Performance of the Novel DFB Pilot Plant

The comparison of the classical DFB pilot plant to the novel DFB pilot plant resulted in significant differences in the conversion of water and carbon in the gasification reactor. Fuel related water conversion rates in the gasification reactor of the novel DFB pilot plant of up to 25% (cf. 13% for the classical DFB pilot plant) were reached. Thus, the cold gas efficiency was measured to be close to 91% for the novel DFB pilot plant and up to 88% for the classical DFB pilot plant, respectively. Overall cold gas efficiencies were in similar ranges of 60% for both pilot plants. It has be taken into account that heat losses are significant higher for the novel DFB pilot plant and therefore negatively influencing the overall cold gas efficiency. An overall cold gas efficiency of up to 70 - 80 % for a 50 MW pilot plant was estimated for the novel concept.

6 Conclusion and Outlook

Steam gasification of biomass is a proven technology to generate a medium calorific product gas. Prior test runs were conducted at the classical DFB pilot plant at the TU Wien with limitations in tar reductions due to minor residence and contact time of carbonic particles and volatiles with catalytic bed materials. In order to counteract these limitations, a novel design was constructed and assembled at the TU Wien. This thesis deals with the commissioning and the first test runs of a novel dual fluidized bed steam gasification pilot plant. The results should deal to answer the research issue, if the concept of the novel DFB pilot plant shows a better performance compared to the classical DFB pilot plant. The main innovation of the novel DFB pilot plant is the installation of a counter-current column above the bubbling bed of the gasification reactor to improve the interaction of solids and gaseous phase to enhance tar reduction processes. Furthermore, novel separation units were applied to ensure a gentle separation of solids and fluids, since several bed materials (e.g. limestone) have a rather low hardness.

In the course of this work, several test runs were conducted at varying gasification conditions and feedstock materials to examine the performance of the novel concept as follows:

- feedstock flexibility,
- carbon conversion,
- conversion of tar,
- cold gas efficiencies, and
- product gas quality.

Main results obtained throughout this thesis can be summarized as follows:

- the commissioning phase and first test runs at the novel DFB pilot plant were successfully completed without significant technical limitations,

- different variations were carried out at the novel DFB pilot plant and steady state operation was reached over a period of hours. Quick changes in fuel power did not influence the process at all,
- several feedstock materials (wood pellets, sugarcane bagasse and exhausted olive pomace) were able to be gasified and did not cause any significant technical limitations. Only exhausted olive pomace influenced the gasification process after a steady state period of four hours due to its very low ash melting temperature,
- the novel counter-current column of the gasification reactor shows a high potential of tar reduction of heterocyclic aromatics and light PAHs with functional groups. However, no significant reduction could be examined for heavy PAHs,
- the novel DFB pilot plant reached significant higher fuel related water conversion rates and carbon conversion rates compared to the classical DFB pilot plant. Fuel related water conversion rates up to 25% and carbon conversion rates of up to 87% were measured for wood pellets. Overall cold gas efficiencies resulted in similar values of 60%, although significant higher heat losses at the novel DFB pilot plant negatively influence the gas efficiency. Cold gas efficiencies of up to 99% and fuel related water conversion rates up to 36% could be reached for EOP, and
- investigations at the novel DFB pilot plant result in similar product gas compositions compared to the classical DFB pilot plant, regarding main product gas components and tar contents.

Further investigations at the novel DFB pilot plant should include the following:

- several authors (i.a. Kern, Wilk, Koppatz, Kolbitsch) showed a higher tar reduction for in-bed feeding, since the bubbling bed is the active zone for the primary conversion. Therefore, investigations conducted with in-bed feeding of the feedstock should be examined. Tar values may be reduced significantly for in-bed feeding,
- to improve the contact of feedstock and bed material in the bubbling bed of the gasification reactor, a chute below the feeding screw should be integrated. This should improve the intermixing of the feedstock and the bed material,
- several authors examined the performance of several bed material types regarding their conversion of tar compounds. Limestone and used olivine showed favourable results during the gasification process. Therefore, further test runs using pure limestone and used olivine from industrial plants should be considered for further im-

provements of the product gas compositions,

- at future test runs, tar samples should be taken not at the beginning of steady-state performance, but after 30 minutes to minimize the influence on tar and water content measurements. To double check the water content a gas moisture measurement device should be installed,
- the recirculation of fines has been disabled in the first test runs. Future test runs should include both recirculation screw conveyors, since fine particles may enhance the catalytic activity of the bed material. Especially for SER processes, the influence of fines may play a major role, and
- the feasibility of the novel DFB pilot plant is proven. The feedstock flexibility of the new design should be investigated with further challenging feedstock materials and residues, like plastics and sewage sludge.
- at future investigations the product gas quality of the product gas should be examined at reduced steam to fuel ratios.

Nomenclature

Abbreviations

AV	Average
BM	Bed material
BTX	Benzene toluene xylene
C1-C7	Pressure indicators CR classical DFB
CFM	Cold flow model
COP21	21 st Conference of the Parties
CR	Combustion reactor
CR1 - 8	Combustion reactor, position 1 - 8
CRBA	Combustion reactor bottom air
db	dry basis
DFB	Dual Fluidized Bed
ECN	Energy Research Centre of the Netherlands
EOP	Exhausted olive pomace
F	Fuel
FG	Flue gas
fuel	Solid feedstock

g	Gas
G1-G6	Pressure indicators GR classical DFB
GC	Gas chromatograph
GC-MS	Gas chromatograph mass spectrometer
GHG	Greenhouse gases
GR	Gasification reactor
GR1 - 23	Gasification reactor, position 1 - 23
H	Height of the bed
ILS	Internal loop seal
lhv	Lower heating value
LLS	Lower loop seal
MJ	Mega joule
n.m.	Not measured
n.p.	Not published
Nm ³	Gas cubic meter according to standard conditions
OP	Operating point
PAH	Polyaromatic hydrocarbons
PCS	Process control system
PG	Product gas
PhD	Doctor of philosophy
PLC	Programmable logic controller
RME	Rapseedmethylether
S	Steam
SCB	Sugarcane bagasse
SD1	Pressure indicator siphon bottom classical DFB

SER	Sorption enhanced reforming
stp	Standard conditions for temperature and pressure
SU1-2	Pressure indicator siphon up classical DFB
TAP	Temp. primary air classical DFB
TAS	Temp. secondary air classical DFB
TASG	Temp. steam GR classical DFB
TSSD	Temp. steam siphon bottom classical DFB
TSSU	Temp. steam siphon up classical DFB
TUW	TU Wien, Vienna University of Technology
U	Velocity
ULS	Upper loop seal
vol.-% _{db}	volume percent, dry basis
WGS	Water gas shift
wt.-% _{db}	weight percent, dry basis

Symbols

$\dot{m}_{addfuel}$	Mass flow of additional fuel	kg/h
\dot{m}_c	Mass flow of carbon	mol/h
\dot{m}_{fluid}	Mass flow of fluidization agent	kg/h
\dot{m}_{fuel}	Mass flow of fuel	kg/h
\dot{m}_{PG}	Mass flow of product gas	kg/h
A	Cross-sectional area	mm ²
A _c	Cross-sectional area in constrictions	mm ²
Ar	Archimedes number	-

C	Carbon flow	kg/s
d_p	Particle size in diameter	m
d_p^*	Dimensionless particle diameter	-
d_s	Diameter of sphere with same surface as particle	m
d_v	Diameter of sphere with the same volume as particle	m
d_{sv}	Sauter diameter	m
F	Feedstock flow	kg/s
g	Gravity	m/s ²
K_1, K_2	Empirical constants for the calculation of U_{mf}	-
K_p	Equilibrium constant	-
lhv_{fuel}	Lower heating value of solid feedstock	kJ/kg
lhv_{PG}	Lower heating value of product gas	kJ/kg
p_i	Partial pressure of the component i	Pa
Re	Reynolds number	-
Re_{mf}	Reynolds number at minimum fluidization	-
Re_{se}	Reynolds number at U_{se}	-
Re_{sv}	Reynolds number, calculated with d_{sv}	-
S	Particle surface area	m ²
S	Steam flow	kg/s
U	Superficial velocity	m/s
U_c^*	Dimensionless critical velocity	-
U_{mb}^*	Dimensionless minimum bubbling velocity	m/s
U_{mf}^*	Dimensionless minimum fluidization velocity	-
U_{se}^*	Dimensionless U_{se}	-
U_t^*	Dimensionless terminal velocity	-

U^*	Dimensionless velocity	-
U_c	Critical velocity	m/s
U_{mf}	Minimum fluidization velocity	m/s
U_{se}	Superficial velocity where entrainment of solids occur	m/s
U_t	Terminal velocity	m/s
V	Particle volume	m^3
$w_{ash,fuel}$	Ash mass fraction in the fuel	-
$w_{H_2O,fluid}$	Water mass fraction in the fluidization agent	-
$w_{H_2O,fuel}$	Water mass fraction in the fuel	-
X_{cf}	Calorific fuel conversion in GR	kW_{fuel}/kW_{PG}
X_c	Carbon conversion	$kg_{c,PG}/kg_{c,fuel}$
$X_{H_2O,fuel}$	Fuel related water conversion	$kg_{H_2O}/kg_{fuel,waf}$
X_{H_2O}	Steam related water conversion	kg_{H_2O}/kg_{H_2O}

Greek Letters

η_g	Gas efficiency	-
μ	Dynamic gas viscosity	kg/ms
ν	Kinematic gas viscosity	m^2/s
ν	Stoichiometric coefficient	-
ϕ	Sphericity	-
ρ	Density	kg/m^3
ρ_f	Fluid density	kg/m^3
ρ_p	Particle density	kg/m^3
ρ_g	Gas density	kg/m^3

τ	Residence time	-
ε	Volume fraction	-
ε_f	Void particle volume fraction	-
ε_S	Solid particle volume fraction	-

Molecular formula

C_2H_4	Ethylene	-
C_2H_6	Ethane	-
C_3H_8	Propane	-
$Ca(OH)_2$	Calcium hydroxide	-
$CaCO_3$	Calcium carbonate	-
CaO	Calcium oxide	-
CH_4	Methane	-
CO	Carbon monoxide	-
CO_2	Carbon dioxide	-
Cr	Chromium	-
H_2	Hydrogen	-
Ni	Nickel	-

List of Figures

1.1	Progress of emitted carbon dioxide has increased exponentially in the last 70 years [8]	1
1.2	History of primary energy use along the last 170 years until now [61]	2
2.1	Overview of conversion steps for a single particle, adopted from [43]	5
2.2	Schematic description of gasification processes using different gasification agents from [11] based on data from [6]	6
2.3	Illustration of the basic principle of a Dual Fluidized Bed steam gasification System, modified from [84]	6
2.4	Typical GC-MS tar compounds in product gas of biomass gasification, modified from Koppatz [43]	12
2.5	Illustration of main properties of gravimetric tar, from [59]	13
2.6	Scheme of hydrodynamic regimes in a fluidized bed, adapted from [54]	15
2.7	Profile of the fraction of solids along the height of the distributor, adapted from [52]	17
2.8	Geldart classification of particles A - D for air at ambient conditions, modified from [52]	19
2.9	The relation of the pressure drop and the velocity of the fluidization agent [75]	21
2.10	Flow regime map for fluidized beds showing typical ranges for regimes, velocities and Geldart's particle classification for density ratios of $400 < (\rho_p - \rho_g) / \rho_g < 9000$ [78]	24
3.1	Schematic description of the classical Dual Fluidized Bed steam gasifier at the TUW [92], dismantled in February 2013	26

3.2	Flowchart of the classical Dual Fluidized Bed steam gasification pilot plant at the TU Wien, modified from [23]	27
3.3	Technical drawing of the classical DFB test plant on a scale of 1:10 [23]	28
4.1	The cold flow model system is shown. Pressure indicators (blue tubes) and air inlet tubes (white tubes) are illustrated	37
4.2	Pipe and instrumentation design of the cold flow model. Investigations were carried out to examine the fluid dynamic of both reactors, GR and CR [78]	38
4.3	Experimental results at the CFM showing optimal operating points using bronze particles in various sizes [78]	39
4.4	Overview of design values of the mass and energy balance calculated by the use of the simulation software IPSEpro [1]	41
4.5	Basic flow sheet of the overall novel DFB test plant, adapted from [78]	44
4.6	Process control system with flow meters for air (left), steam (middle), and computers to operate the PCS (right)	46
4.7	Schematic illustration of the reactor design of the novel DFB pilot plant at the TU Wien (left), modified from [78] and an illustration of the uninsulated combustion reactor (right)	49
4.8	Basic principle of the Dual Fluidized Bed steam gasification system, modified from [78]	50
4.9	Location plan of measurements along the gasification and combustion reactor at the novel DFB pilot plant, based on [11, 78]	53
4.10	Position of measurements along the bubbling bed of the gasification reactor. GR1, GR2 and GR4 are located along the broadside, whereas GR3 and GR5 to GR9 are shifted by 90 degrees	54
4.11	Arrangement of measurements in the bubbling bed of the GR. The feedstock screw is illustrated on the right picture. The top of the bubbling bed was between GR7 and GR8 for all investigations	54
4.12	Overview of online and offline measuring devices used to determine gas components, [79]	55
4.13	Schematic drawing of the cleaning line for gas analysis [33], modified from [92]	56
4.14	Schematic drawing of the tar sampling line [43, 92]	56

4.15	Schematic design of the sampling box for solids sampling (left) [43] and a picture during investigation at the LLS (right)	57
4.16	Schematic arrangement of the system to remove organic and inorganic matter (left) modified from [43] and a picture during investigation (right) . . .	58
5.1	Presentation of feedstocks used in this work. Milled wood and wood pellets (left), raw EOP and pelletized EOP with CaCO ₃ (middle) and chopped sugarcane bagasse and sugarcane bagasse pellets (right). In order to reach better dosing characteristics and avoid blockages in the fuel dosing system, all feedstocks were pelletized	60
5.2	All bed materials used are shown. Fresh olivine (left), fresh limestone (middle) and a mixture of fresh olivine and fresh limestone (right)	61
5.3	Pressure profile during the cold flow investigation in the novel DFB pilot plant [66, 78] (top) and during gasification process (below)	64
5.4	Pressure gradient profile of the counter-current column of the gasification reactor during gasification process	66
5.5	Operating points of the novel DFB pilot plant for the cold flow investigation and the gasification process modified from Pasteiner [66]. Both axes of the regime map are indicated in logarithmic units [78]	68
5.6	Progress of relevant gasification and combustion temperatures during commissioning test run	69
5.7	Average temperatures of experiment 2 OP2 along the height of both reactors are shown. The blue profile shows the GR, whereas the red profile shows the CR.	72
5.8	The impact of temperature variation on the contents of H ₂ , CO, CO ₂ , CH ₄ , and C ₂ H ₄	73
5.9	Progress of C ₂ H ₄ , GC-MS, and gravimetric tar	74
5.10	Progress of relevant temperatures of both reactors during gasification process. Operating points and sampling times are depicted	76
5.11	Values for main product gas components (left) and for GC-MS and gravimetric tar (right) at varying fuel power and steam to fuel ratio	76

5.12	Values for main product gas components (left) and for GC-MS and gravimetric tar (right) for fresh olivine and a mixture of fresh olivine and fresh limestone as bed material	80
5.13	Progress of main gasification and combustion temperatures during experiment 3 OP3 and OP4	82
5.14	Main product gas components (left) and GC-MS and gravimetric tar (right) at varying steam to fuel ratios given as $\text{kg}_{\text{steam}}/\text{kg}_{\text{fuel,waf}}$	83
5.15	Impinger bottles after tar measurement at sampling point B (left) and sampling point A (right)	85
5.16	Main product gas components (left) and values for tar (right) at different sampling points for on-bed feeding of wood pellets	86
5.17	Overview of all measured GC-MS tar components occurring above the bubbling bed (OP4B) and after the counter-current column (OP4A) in logarithmic scale	89
5.18	Illustration of arising tar components in the product gas after the gasifier of the new design compared to the classical DFB pilot plant. Tar components using fresh olivine as bed material and wood pellets are shown for on-bed feeding in logarithmic scale. Data of Kern are published in [33, 53]	90
5.19	Progress of main gasification and combustion temperatures along steady state operating point OP4 using wood pellets as feedstock	92
5.20	Values of main product gas components (left) and tar measurements, including GC-MS and gravimetric tar (right) for wood pellets at on-bed feeding	94
5.21	Pelletizer manufactured by company Cissonius for feedstock preparation. PP200, 7.5kW, 380V	95
5.22	Progress of main gasification and combustion temperatures along steady state operating point using sugarcane bagasse pellets as feedstock	97
5.23	Values of main product gas components (left) and tar measurements, including GC-MS and gravimetric tar (right) for sugarcane bagasse pellets for on-bed feeding	97
5.24	Illustration of the ash melting behavior of raw EOP and a mixture of EOP with CaCO_3 using a hot stage microscope	100

5.25	Progress of the relevant gasification and combustion temperatures using exhausted olive pomace pellets as feedstock	102
5.26	Product gas composition (left) and tar measurements, including GC-MS and gravimetric tar (right) using exhausted olive pomace pellets as feedstock	102
5.27	Comparison of results conducted at the classical and novel DFB pilot plant. Main product gas components (left) and tar components (right)	105
5.28	Comparison of results conducted at the classical and novel DFB pilot plant. Main product gas components (left) and tar components (right)	106
5.29	Results of accomplished test runs with different feedstock materials	108

List of Tables

2.1	Basic and acidic compounds of primary ash transformation reactions by Bostroem et al. [5]	10
2.2	Survey of secondary ash-forming reactions modified from Bostroem et al. [5]	10
2.3	Tar classification from the Energy Research Centre of the Netherlands (ECN) [12]	14
2.4	Overview of the diameters used for calculation in this work, adapted from [24]	20
3.1	Overview of main operating conditions and the basic geometry of the classical DFB system, modified from [29, 98]	29
3.2	Overview of results conducted at the classical DFB pilot plant using wood pellets as feedstock. Sum of nitrogen and other gas components result in 100 vol.-% _{ab}	30
3.3	Bed material analysis of fresh and used olivine [34]	31
4.1	Main design values for geometric and operating parameters of the reactor system of the novel DFB pilot plant, modified from [84]	43
4.2	Overview of measuring equipment of the classical DFB and novel DFB test plant, modified from [43, 77]	51
5.1	Overview of all conducted test runs and used abbreviations	59
5.2	Overview of all accomplished test runs, related variations, and main operating parameters	60
5.3	Fuel and ash analysis of feedstock used	61
5.4	Bed material analysis of olivine and limestone [84]	62

5.5	Parameter of the test runs operated as cold flow and gasification process, modified from [66]	67
5.6	Overview of operating parameters of the accomplished test run	71
5.7	Comparison of product gas composition at varying gasification temperatures (GR6). All other gases, mainly nitrogen result in less than 2 vol.-% _{db} in total	74
5.8	Summary of main operating parameter for fuel power variation	77
5.9	Comparison of product gas composition at varying fuel load parameters. Other gases, mainly nitrogen show a maximum of 3.0 vol.-% _{db}	77
5.10	Operating parameter of accomplished investigations with different bed materials	79
5.11	Comparison of product gas composition for different bed materials. All samples were measured at sampling position A. Other gases, mainly nitrogen reach maximum values of 1.6 vol.-% _{db}	80
5.12	Operating parameters of the accomplished investigations on steam to fuel ratios	82
5.13	Product gas components at varying steam to fuel ratios. Other gases, mainly nitrogen are < 1.3 vol.-% _{db}	84
5.14	Operating parameter of accomplished investigations to evaluate the performance of tar reduction on the product gas composition of the novel design .	85
5.15	Values of tar and product gas composition at sampling point A and B to evaluate the performance of the counter-current column. Other gases, mainly nitrogen are <1.3 vol.-% _{db} . The dashed lines before sampling point A should present the heat exchanger	87
5.16	Operating parameter of investigation Experiment 2 OP2A and the investigations performed by Kern et al. [33] to demonstrate the tar reduction capability of the novel design	91
5.17	Operating parameters and main product gas components for the gasification of wood pellets. Other gases such as nitrogen were <1.3 vol.-% _{db}	93
5.18	Operating parameters and main product gas components for the gasification investigation with sugarcane bagasse. Other gases such as nitrogen were <1.3 vol.-% _{db}	96

5.19	Ash melting behaviour of EOP with different amounts of calcium carbonate and calcium oxide, all percentages are given in wt.-% _{db}	98
5.20	Operating parameters and main product gas components for the gasification investigation of EOP. Other gases such as nitrogen were <0.9 vol.-% _{db}	101
5.21	Operating parameters and main product gas components of accomplished test runs on the classical and novel DFB pilot plant. Other gases, mainly nitrogen are <1.3 vol.-% _{db}	104
5.22	Operating parameters and main product gas components for gasification of various feedstock. Other gases such as nitrogen were <1.3 vol.-% _{db}	109
1	Detailed analysis of all tar components listed in Chapter 5.7	XXXVIII

Bibliography

- [1] Personal communication between J. C. Schmid, S. Mueller and M. Kolbitsch.
- [2] C. J. Aguiari. *Advanced biofuels from sugarcane residues - an integrated approach*. PhD thesis, TU Wien, to be published.
- [3] A.A. Avidan and J. Yerushalmi. Bed expansion in high velocity fluidization. *Powder Technology*, 32(2):223 – 232, 1982.
- [4] H.T. Bi and J.R. Grace. Flow regime diagrams for gas-solid fluidization and upward transport. *International Journal of Multiphase Flow*, 21(6):1229 – 1236, 1995.
- [5] D. Bostroem, N. Skoglund, A.Grimm, C. Boman, M.Oehman, M. Brostroem, and R.Backman. Ash Transformation Chemistry during Combustion of Biomass. *Energy & Fuels*, 26(dx.doi.org/10.1021/ef201205b):85–93, 2012.
- [6] A. V. Bridgwater, H. Hofbauer, and S. Van Loo. *Thermal Biomass Conversion*. CPL Press, 2009.
- [7] E. Brus, M. Ohman, and A. Nordin. Mechanism of bed agglomeration during fluidized-bed combustion of biomass fuels. *Energy & Fuels*, 19:825–832, 2005.
- [8] Carbon Dioxide Information Analysis Center. Oak Ridge National Laboratory, US Department of Energy, Oak Ridge, Tenn., United States. <http://cdiac.ornl.gov/>, 02 2016.
- [9] CEN/TS. Biomass gasification - Tar and particles in product gas - Sampling and analysis - 15439. Technical report, 2006.
- [10] K. O. Davidsson, L. E. Amand, B. M. Steenari, A. L. Elled, D. Eskilsson, and

- B. Leckner. Countermeasures against alkali-related problems during combustion of biomass in a circulating fluidized bed boiler. *Chemical Engineering Science*, 63:5314–5329, 2008.
- [11] R. Diem. *Design, Construction and Startup of an Advanced 100 kW Dual Fluidized Bed System for Thermal Gasification*. PhD thesis, TU Wien, 2015.
- [12] ECN. Tar Classification System. <http://www.thersites.nl/classification.aspx>, 02 2016.
- [13] Eubionet. Biomass co-firing - an efficient way to reduce green house gas emissions. Technical report, 2003.
- [14] L.S. Fan and C. Zhu. *Principles of gas-solid flows*. Cambridge University Press, Cambridge,UK, 1998.
- [15] F. J. Frandsen. Utilizing biomass and waste for power production - A decade of contributing to the understanding, interpretation and analysis of deposits and corrosion products. *Fuel*, 84(10):1277–1294, 2005.
- [16] J. Fuchs. Ermittlung des Betriebskennfeldes einer innovativen Zweibettwirbelschicht anhand von Kaltmodelluntersuchungen. Master’s thesis, TU Wien and TECON Engineering GmbH, 2013.
- [17] D. Geldart. Types of Gas Fluidization. *Powder Technology*, pages 285–292, 1973.
- [18] J. Good, L. Ventress, H. Knoef, U. Zielke, P. Lyck Hansen, W. van de Kamp, P. de Wild, B. Coda, S. van Paasen, J. Kiel, K. Sjoestroem, T. Liliedahl, Ch. Unger, J. Neeft, M. Suomalainen, and P. Simell. Sampling and analysis of tar and particles in biomass producer gases - Technical Report. CEN BT/TF 143 ”Organic contaminants (”tar”) in biomass producer gases”. Technical report, Verenum and Casella Cre Energy and btg and Danish Technological Institute and ECN and Royal Institute of Technology, KTH and Fraunhofer Institute for Environmental, Safety and Energy Technology UMSICHT and SenterNovem and VTT Processes, 2005.
- [19] J.R. Grace. *Fluidized bed hydrodynamics*. Hemisphere, Washington DC, 1982.

- [20] J.R. Grace. Contacting Modes and Behaviour Classification of Gas-Solid and Other Two-Phase Suspensions. *The Canadian Journal of Chem. Eng.*, 64(3):353–363, 1983.
- [21] A. Grimm, M. Oehman, T. Lindberg, A. Fredriksson, and D. Bostroem. Bed Agglomeration Characteristics in Fluidized-Bed Combustion of Biomass Fuels Using Olivine as Bed Material. *Energy & Fuels*, 26:4550–4559, 2012.
- [22] A. Grimm, N. Skoglund, D. Bostroem, and M. Oehman. Bed Agglomeration Characteristics in Fluidized Quartz Bed Combustion of Phosphorus-Rich Biomass Fuels. *Energy & Fuels*, 25:937–947, 2011.
- [23] E. Hoefftberger. *In-situ CO₂-Adsorption in a Dual Fluidised Bed Biomass Steam Gasifier to Produce a Hydrogen Rich Gas*. PhD thesis, TU Wien, 2005.
- [24] H. Hofbauer. *Wirbelschichttechnik*, volume 5. TU Wien.
- [25] H. Hofbauer and R. Rauch. Stoichiometric Water Consumption of Steam Gasification by the FICFB-Gasification Process. *Progress in Thermochemical Biomass Conversion*, 1:199–208, 2000. ISBN 0-632-05533-2.
- [26] H. Hofbauer, R. Rauch, and I. Siefert. Endbericht Analytik III. Renet. Technical report, 2003.
- [27] M. Hupa. Ash-Related Issues in Fluidized-Bed Combustion of Biomasses: Recent Research Highlights. *Energy & Fuels*, 26(dx.doi.org/10.1021/ef201169k):4–14, 2012.
- [28] M. Kaltschmitt, H. Hartmann, and H. Hofbauer. *Energie aus Biomasse: Grundlagen, Techniken und Verfahren*. Springer, 2001.
- [29] S. J. Kern. *Gasification and Co-gasification of Coal, Biomass and Plastics in a Dual Fluidized Bed System*. PhD thesis, TU Wien, 2013.
- [30] S. J. Kern, C. Pfeifer, and H. Hofbauer. Co-gasification of Polyethylene and Lignite in a Dual Fluidized Bed Gasifier. *Industrial and Engineering Chemistry Research*, 52(11):4360–4371, 2013.
- [31] S. J. Kern, C. Pfeifer, and H. Hofbauer. Co-Gasification of Wood and Lignite in a Dual Fluidized Bed Gasifier. *Energy & Fuels*, 27(2):919–931, 2013.

- [32] S. J. Kern, C. Pfeifer, and H. Hofbauer. Gasification of lignite in a dual fluidized bed gasifier - Influence of bed material particle size and the amount of steam. *Fuel Processing Technology*, 111:1–13, 2013.
- [33] S. J. Kern, C. Pfeifer, and H. Hofbauer. Gasification of wood in a dual fluidized bed gasifier: Influence of fuel feeding on process performance. *Chemical Engineering Science*, 90:284–298, 2013.
- [34] F. Kirnbauer. *The impact of inorganic matter on the performance of dual fluidized bed biomass steam gasification plants*. PhD thesis, TU Wien, Institute of Chemical Engineering, 2013.
- [35] F. Kirnbauer and H. Hofbauer. Investigation of Bed Material Changes in a Dual Fluidized Bed Steam Gasification Plant in Guessing, Austria. *Energy*, 25:3793–3798, 2011.
- [36] F. Kirnbauer and H. Hofbauer. The mechanism of bed material coating in dual fluidized bed biomass steam gasification plants and its impact on plant optimization. *Powder Technology*, 245(DOI:10.1016/j.powtec.2013.04.022):94–104, 2013.
- [37] F. Kirnbauer, M. Koch, R. Koch, C. Aichernig, and H. Hofbauer. Behavior of Inorganic Matter in a Dual Fluidized Steam Gasification Plant. *Energy & Fuels*, (DOI: 10.1021/ef400598h), 2013.
- [38] F. Kirnbauer, V. Wilk, and H. Hofbauer. Performance improvement of dual fluidized bed gasifiers by temperature reduction: The behavior of tar species in the product gas. *Fuel*, 108:534–542, 2012.
- [39] F. Kirnbauer, V. Wilk, H. Kitzner, S. J. Kern, and H. Hofbauer. The positive effects of bed material coating on tar reduction in a dual fluidized bed gasifier. *Fuel*, 95:553–562, 2012.
- [40] H. Knoef. *Handbook Biomass Gasification*. BTG biomass technology group, 2005.
- [41] T. M. Knowlton. Pressure and Temperature Effects in Fluid-Particle Systems. In Wen-Ching Yang, editor, *Fluidization, Solids Handling, and Processing*, pages 111 – 152. William Andrew Publishing, Westwood, NJ, 1998.

- [42] M. Kolbitsch, J. C. Schmid, R. Diem, S. Mueller, and H. Hofbauer. Influence of Fuel Feeding Position on Sorption Enhanced Reforming in a Dual Fluid Gasifier. *in: 11th International Conference on Circulating Fluidized Bed Technology (CGB11), Beijing, China*, pages 693–698, 2014.
- [43] S. Koppatz. *Outlining active bed materials for dual fluidised bed biomass gasification - In-bed catalysts and oxygen/carbonate looping behaviour*. PhD thesis, TU Wien, Institute of Chemical Engineering, 2012.
- [44] S. Koppatz, M. Fuchs, S. Mueller, and J. C. Schmid. Join the research platform FUTURE ENERGY TECHNOLOGY to bring visions to life. Technical report, TU Wien, 2012.
- [45] S. Koppatz, M. Fuchs, S. Mueller, and J. C. Schmid. Future Energy Technology. *TU Wien*, ISBN 978-3-9502754-3-8.
- [46] S. Koppatz, C. Pfeifer, and H. Hofbauer. Application of Fe-olivine as catalytic active bed material in biomass gasification. *in: Proceedings of the International Conference on Polygeneration Strategies (ICPS10), Leipzig, Germany*, 2010.
- [47] S. Koppatz, C. Pfeifer, and H. Hofbauer. Comparison of the performance behaviour of silica sand and olivine in a dual fluidised bed reactor system for steam gasification of biomass at pilot plant scale. *Chemical Engineering Journal*, 175:468–483, 2011.
- [48] S. Koppatz, C. Pfeifer, and H. Hofbauer. Comparison of the performance behaviour of silica sand and olivine in a dual fluidised bed reactor system for steam gasification of biomass at pilot scale. *Chemical Engineering Journal*, 175:468–483, 2011.
- [49] S. Koppatz, C. Pfeifer, A. Kreuzeder, G. Soukup, and H. Hofbauer. Application of CaO-Based Bed Material for Dual Fluidized Bed Steam Biomass Gasification. *in: Proceedings of the 20th International Conference on Fluidized Bed Combustion Conference, Xi'an, China*, II:712–718, 2009.
- [50] M. Kraussler, M. Binder, and H. Hofbauer. Behaviour of GCMS tar components in a water gas shift unit operated with tar-rich product gas from an industrial scale dual fluidized bed biomass steam gasification plant. *Biomass Conversion and Biorefinery*,

- pages 1–11, 2016.
- [51] M. Kuba, F. Kirnbauer, and H. Hofbauer. Influence of coated olivine on the conversion of intermediate products from decomposition of biomass tars by steam reforming. *Biomass Conversion and Biorefinery*, 2016.
- [52] D. Kunii and O. Levenspiel. *Fluidization Engineering*. Butterworth-Heinemann series in chemical engineering. Butterworth-Heinemann, 1991.
- [53] Test laboratory of the Vienna University of Technology. Kurzbericht, Auftragsnummer: PL-12065-M. Technical report, TU Wien, 2012.
- [54] K.S. Lim, J.X. Zhu, and J.R. Grace. Hydrodynamics of gas-solid fluidization. *International Journal of Multiphase Flow*, 21, Supplement(0):141 – 193, 1995. Annual Reviews in Multiphase Flow 1995.
- [55] M. Llorente and J. Garcia. Comparing methods for predicting the sintering of biomass ash in combustion. *Fuel*, 84:1893–1900, 2005.
- [56] D. Martinovic. Kaltmodellversuche und MSR-Konzept einer Zweibett-Wirbelschicht-Vergasungsanlage. Master’s thesis, TU Wien, 2013.
- [57] T. R. Miles, L. L. Baxter, R. W. Bryers, B. M. Jenkins, and L. L. Oden. Boiler deposits from firing biomass fuels. *Biomass and Bioenergy*, 10:125–138, 1996.
- [58] T.A. Milne, R.J. Evans, and N. Abatzoglou. Biomass Gasifier ”Tars”: Their Nature, Formation and Conversion. Technical report, National Renewable Energy Laboratory, Golden, Colorado, 1998.
- [59] P. O. Morf. *Secondary reactions of tar during thermochemical biomass conversion*. PhD thesis, ETH Zuerich, 2001.
- [60] S. Mueller. *Hydrogen from Biomass for Industry - Industrial Application of Hydrogen Production Based on Dual Fluid Gasification*, ISBN: 978-3-9502754-5-2. PhD thesis, TU Wien, 2013.
- [61] N. Nakicenovic, T. B. Johansson, A. Patwardhan, and L. Gomez-Echeverri. *Global Energy Assessment (GEA) - Toward a Sustainable Future*. CAMBRIDGE UNI-

- VERSITY PRESS Cambridge UK and New York, NY, USA and the International Institute for Applied Systems Analysis, Laxenburg, Austria, 2012.
- [62] J.P.A. Neeft, H.A.M. Knoef, G.J. Buffinga, U. Zielke, K. Sjoestroem, C. Brage, P. Hasler, P.A. Simell, M. Suomalainen, M.A. Dorrington, and C. Greil. Guideline for sampling and analysis of tars and particles in biomass producer gases. *Progress in Thermochemical Biomass Conversion*, A.Bridgwater, pages 162–175, 2001.
- [63] H.P. Nielsen, F.J. Frandsen, K. Dam-Johansen, and L.L. Baxter. The implications of chlorine-associated corrosion on the operation of biomass-fired boilers. *Energy and Combustion Science*, 26:283–298, 2000.
- [64] M. Oehman, D. Bostroem, and A. Nordin. Effect of Kaolin and Limestone Addition on Slag Formation during Combustion of Wood Fuels. *Energy & Fuels*, 18:1370–1376, 2004.
- [65] M. Oehman, A. Nordin, B. Skrifvars, R. Backman, and M. Hupa. Bed agglomeration characteristics during fluidized bed combustion of biomass fuels. *Energy & Fuels*, 14:169–178, 2000.
- [66] H. Pasteiner. Cold Flow Investigations on a Novel Dual Fluidised Bed Steam Gasification Test Plant. Master’s thesis, TU Wien, 2015.
- [67] C. Pfeifer, S. Koppatz, and H. Hofbauer. Catalysts for dual fluidised bed biomass gasification - an experimental study at the pilot plant scale. *Biomass Conversion and Biorefinery*, Springer Verlag, Berlin, 1:63–74, 2011.
- [68] C. Pfeifer, J. C. Schmid, T. Proell, and H. Hofbauer. Next Generation Biomass Gasifier. In *Proc. in the 19th European Biomass Conference and Exhibition, Berlin, Germany*, 2011.
- [69] P. Plaza, A. J. Griffiths, N. Syred, and T. Rees-Gralton. Use of a Predictive Model for the Impact of Cofiring Coal/Biomass Blends on Slagging and Fouling Propensity. *Energy & Fuels*, 23:3437–3445, 2012.
- [70] T. Proell. *Potenziale der Wirbelschichtdampfergasung fester Biomasse - Modellierung und Simulation auf Basis der Betriebserfahrungen am Biomassekraftwerk*

- Guessing*. PhD thesis, TU Wien, 2004.
- [71] T. Proell, J. C. Schmid, C. Pfeifer, and H. Hofbauer. Verbessertes Wirbelschichtreaktorsystem, AT509586A4 and AT509586B1/B8 and W2011/153568A1, 2011.
- [72] M. Pronobis. The influence of biomass co-combustion on boiler fouling and efficiency. *Fuel*, 85:474–480, 2006.
- [73] L. Reh. *Das Wirbeln von körnigem Gut im schlanken Diffusor als Grenzzustand zwischen Wirbelschicht und pneumatischer Förderung*. PhD thesis, Technische Hochschule Karlsruhe Fakultät für Maschinenwesen, 1961.
- [74] L. Rosendahl. *Biomass Combustion Science, Technology and Engineering*. Woodhead Publishing, 2013.
- [75] D. Sau, S. Mohanty, and K. Biswal. Minimal fluidization velocities and maximum bed pressure drops for gas-solid tapered fluidized beds. *Chemical Engineering Journal*, 132(1-3):151–175, 2007.
- [76] S.C. Saxena and G.J. Vogel. Measurement of Incipient Fluidisation Velocities in a Bed of Coarse Dolomite at Temperature and Pressure. *Trans Inst Chem Eng*, 55(3):184–189, 1977. cited By (since 1996)41.
- [77] M. Schmalzl. Implementierung der MSR-Technik einer 100 kW DUAL FLUID Versuchsanlage zur Vergasung von Festbrennstoffen. Master’s thesis, TU Wien, 2014.
- [78] J. C. Schmid. *Development of a novel dual fluidized bed gasification system for increased fuel flexibility*. PhD thesis, TU Wien, Institute of Chemical Engineering, 2014.
- [79] J. C. Schmid, M. Kolbitsch, J. Fuchs, S. Mueller F. Benedikt, and H. Hofbauer. Technical Report of Scientific Experimental Research for the EU project PHENOLIVE. Steam gasification of EXHAUSTED OLIVE POMACE with the dual fluidized bed pilot plant. Technical report, TU Wien, 2016.
- [80] J. C. Schmid and S. Mueller. Technical Report of Scientific Experimental Research. Technical report, TU Wien, 2016.

- [81] J. C. Schmid, S. Mueller, J. Fuchs, and H. Hofbauer. "SCB 2 GAS" Dual fluidized bed steam gasification of sugar cane bagasse with the novel pilot plant at TU Wien, technical report for Fitroleum Biochemicals GmbH. Technical report, TU Wien, Institute of Chemical Engineering, 2016.
- [82] J. C. Schmid, S. Mueller, and H. Hofbauer. A Novel Dual Fluid Gasifier at Vienna University of Technology. In *Proceedings of the 1st International Conference on Renewable Energy Gas Technology (REGATEC), Malmoe, Schweden*, 2014.
- [83] J. C. Schmid, S. Mueller, and H. Hofbauer. Test Plant Engineering and Construction of a Dual Circulating Fluidized Bed System for the Conversion of Solid Fuels. In *Proc. of the 4th International Symposium on Gasification and its Applications (iSGA-4), Vienna, Austria*, 2014.
- [84] J. C. Schmid, S. Mueller, and H. Hofbauer. Dual fluidized bed steam gasification of wood with the novel pilot plant at TU Wien, technical report for the Department of Chemical Engineering - Lund Univers. Technical report, TU Wien, Institut of Chemical Engineering, 2016.
- [85] J. C. Schmid, C. Pfeifer, H. Kitzler, T. Proell, and H. Hofbauer. A new Dual Fluidized Bed Gasifier Design for Improved in Situ Conversion of Hydrocarbons. In *Proceedings of the International Conference on Polygeneration Strategies (ICPS11), Vienna, Austria*, 2011.
- [86] J. C. Schmid, C. Pfeifer, T. Proell, H. Kitzler, and H. Hofbauer. Wirbelschichtreaktorsystem, AT510228A1, Wo2012/009737A1, 2012.
- [87] J. C. Schmid, T. Proell, I. Diaz, C. Hafner, K. Joerg, C. Pfeifer, and H. Hofbauer. G-VOLUTION: Biomasse-Dampfvergasung der zweiten Generation. Technical report, Neue Energien 2020, publizierter Endbericht, Klima und Energiefonds managed by FFG, TU Wien, TECON Engineering GmbH, 2011.
- [88] J. C. Schmid, T. Proell, and H. Hofbauer. Wirbelschichtreaktorsystem, AT513490A4 and AT513490B1 and WO2014/071436A1, 2014.
- [89] J. C. Schmid, T. Proell, H. Kitzler, C. Pfeifer, and H. Hofbauer. Cold flow model

- investigations of the countercurrent flow of a dual circulating fluidized bed gasifier. *Biomass Conversion and Biorefinery*, 2(3)(doi:10.1007/s13399-012-0035-5):229–244, 2012.
- [90] J. C. Schmid, T. Proell, C. Pfeifer, and H. Hofbauer. Improvement of Gas-Solid Interaction in Dual Circulating Fluidized Bed System. In *Proc. 9th European Conference on Industrial Furnaces and Boilers (INFUB), Estoria, Portugal, 2011*.
- [91] J. C. Schmid, T. Proell, R. Rauch, and H. Hofbauer. Cold flow model investigation on a modified riser with enhanced gas-solid contact - Locating the regions of operation in a fluidization regime map. In *Proceedings of the 21st International Conference on Fluidized Bed Combustion (FBC), Naples, Italy, p.80-87*, number ISBN 978-88-89677-83-4, 2012.
- [92] J. C. Schmid, U. Wolfesberger, S. Koppatz, C. Pfeifer, and H. Hofbauer. Variation of feedstock in a dual fluidized bed steam gasifier - Influence on product gas, tar content and composition. *Environmental Progress & Sustainable Energy*, 31(2)(Wiley, doi:10.1002/ep.11607):205–2015, July 2012.
- [93] P. Stephan. *Thermodynamik*. Springer-Lehrbuch. Springer, 2009.
- [94] P. Teixeira, H. Lopes, I. Gulyurtlu, N. Lapa, and P. Abelha. Evaluation of slagging and fouling tendency during biomass co-firing with coal in a fluidized bed. *Biomass and Bio*, 39:192–203, 2012.
- [95] C.Y. Wen and Y.H. Yu. A generalized method for predicting the minimum fluidization velocity. *AIChE Journal*, 12:610, 1966.
- [96] V. Wilk. *Extending the range of feedstock of the dual fluidized bed gasification process towards residues and waste*. PhD thesis, TU Wien, 2013.
- [97] V. Wilk, C. Aichernig, and H. Hofbauer. Waste wood gasification: Distribution of nitrogen, sulphur and chlorine in a dual fluidised bed steam gasifier. In *Pugsley, T. et al, editors, Proceedings of the International Conference on Circulating Fluidized Bed Technology (CFB10), Sunriver, Oregon, USA, pages 209–216, 2011*.
- [98] V. Wilk and H. Hofbauer. Co-gasification of biomass and plastics in a dual fluidized

- bed steam gasifier. *Energy & Fuels*, 27(6):3261–3273, 2013.
- [99] V. Wilk and H. Hofbauer. Conversion of fuel nitrogen in a dual fluidized bed steam gasifier. *Fuel*, 106:793–801, 2013.
- [100] V. Wilk and H. Hofbauer. Influence of fuel particle size on gasification in a dual fluidized bed steam gasifier. *Fuel Processing Technology*, 115:139 – 151, 2013.
- [101] V. Wilk, J. C. Schmid, and H. Hofbauer. Influence of fuel feeding positions on gasification in dual fluidized bed gasifiers. *Biomass and Bioenergy*, 54:46–58, 2013.
- [102] U. Wolfesberger, I. Aigner, and H. Hofbauer. Tar content and composition in producer gas of fluidized bed gasification of wood - influence of temperature and pressure. *Environmental Progress & Sustainable Energy*, pages 372–379, 2009.
- [103] U. Wolfesberger, S. Koppatz, C. Pfeifer, and H. Hofbauer. Effect on iron supported olivine on the distribution of tar compounds derived by steam gasification biomass. *in: Proceedings of the International Conference on Polygeneration Strategies (ICPS11), Vienna, Austria*, 2011.
- [104] CBCNEWS World. 5 key points in Paris Agreement on climate change. <http://www.cbc.ca/news/world/paris-agreement-key-climate-points-1.3362500>, 12 2015.

Appendix A

Table 1 lists an detail analysis of tar compounds measured at both sample points for several test runs.

Table 1: Detailed analysis of all tar components listed in Chapter 5.7

Tar components	Unit	Experiment 3 OP4B_mixture	Experiment 3 OP4A_mixture	Experiment 3 OP2A_fresh olivine	Kern [33, 53] fresh olivine
Phenylacetylene	mg/Nm ³	180	0	33	97
Styrene	mg/Nm ³	1600	73	210	603
Mesitylene	mg/Nm ³	17	0	0	0
Phenol	mg/Nm ³	2745	0	0	183
Benzofuran	mg/Nm ³	479	0	0	76
1H-Indene	mg/Nm ³	2551	113	437	1657
2-Methylphenol	mg/Nm ³	301	0	0	0
4-Methylphenol	mg/Nm ³	797	0	0	23
2-Methylbenzofuran	mg/Nm ³	67	0	0	0
2,5 and 2,4-Dimethylphenol	mg/Nm ³	91	0	0	0
3,5-Dimethylphenol	mg/Nm ³	84	0	0	0
2,3-Dimethylphenol	mg/Nm ³	96	0	0	0
Naphthalene	mg/Nm ³	3106	2438	4696	5177
2-Methylnaphthaline	mg/Nm ³	567	0	48	179
1-Methylnaphthaline	mg/Nm ³	381	0	28	97
1-Indanone	mg/Nm ³	31	0	0	0
Indole	mg/Nm ³	58	0	0	2
Biphenyl	mg/Nm ³	212	55	112	221
Acenaphylene	mg/Nm ³	1301	664	1803	2589
Acenaphtene	mg/Nm ³	64	16	26	29
Dibenzofuran	mg/Nm ³	190	27	222	351
Fluorene	mg/Nm ³	367	27	219	707
Anthracene	mg/Nm ³	482	449	1153	1362
Phenanthrene	mg/Nm ³	171	103	290	474
4,5-Methylphenanthrene	mg/Nm ³	130	23	129	247
Flouranthene	mg/Nm ³	187	219	639	783
Pyrene	mg/Nm ³	171	177	554	699
Benzo(a)anthracene	mg/Nm ³	82	40	116	141
Chrysene	mg/Nm ³	71	57	139	189
Benzo(b)flouranthene	mg/Nm ³	37	0	94	96
Benzo(k)flouranthene	mg/Nm ³	0	0	69	70
Benzo(a)pyrene	mg/Nm ³	45	0	146	175
Benzo(g,h,i)perylene	mg/Nm ³	0	0	63	97
Indeno(1,2,3-cd)pyrene	mg/Nm ³	0	0	74	97